MODELING A RUN-AROUND HEAT AND MOISTURE RECOVERY SYSTEM

A Thesis Submitted to the College of

Graduate Studies and Research

in Partial Fulfillment of the Requirements

for the Degree of Master of Science

in the Department of Mechanical Engineering

University of Saskatchewan

Saskatoon

By

Haisheng Fan

PERMISSION TO USE

In presenting this thesis in partial fulfilment of the requirements for a Postgraduate degree from the University of Saskatchewan, I agree that the Libraries of this University may make it freely available for inspection. I further agree that permission for copying of this thesis in any manner, in whole or in part, for scholarly purposes may be granted by the professor or professors who supervised my thesis work or, in their absence, by the Head of the Department or the Dean of the College in which my thesis work was done. It is understood that any copying or publication or use of this thesis or parts thereof for financial gain shall not be allowed without my written permission. It is also understood that due recognition shall be given to me and to the University of Saskatchewan in any scholarly use which may be made of any material in my thesis.

Requests for permission to copy or to make other use of material in this thesis in whole or part should be addressed to:

Head of the Department of Mechanical Engineering

University of Saskatchewan

Saskatoon, Saskatchewan S7N 5A9

ABSTRACT

Run-around energy recovery systems are one of the several ways for transferring energy between two air streams. Compared with other air-to-air energy recovery systems, run-around systems are very reliable and flexible, especially in retro-fit applications. Previous research in this area has mainly dealt with sensible run-around heat recovery system. However, an ideal air-to-air energy recovery device should be able to recover moisture as well as sensible heat. It is the objective of this research project to simulate a run-around system that exchanges both moisture and sensible heat, and to do a performance analysis to find the design characteristics of such a system.

The first step in the study was to develop a numerical model for a run-around system with two sensible heat exchangers and validate the model using data from the published literature. Following this, a mathematical/numerical model of a heat and moisture exchanger and the run-around heat and moisture recovery system was developed using only basic physical and chemical principles, component properties and operating conditions. With this model, the position dependent temperature and moisture content properties of both a single exchanger and a run-around system were simulated for steady state operating conditions. This simulation enables the study of the performance of the exchanger and the run-around system. In the investigation, the $\varepsilon - NTU$ method was employed to characterize the performance of a single exchanger and a run-around system and two new independent parameters, the number of mass transfer units, NTU_m, and mass flow rate ratio, M_{Salt} / M_{Air}, were introduced.

The results show that, for the sensible run-around heat recovery system with a specified *NTU*, the maximum effectiveness occurs approximately at a heat capacity ratio

$C_{Sol}/C_{Air}=1$, but for the run-around system with both heat and moisture exchange, the maximum effectiveness occurs approximately at heat capacity ratio $C_{Sol}/C_{Air}=3$ for ARI summer and winter test conditions and the maximum effectiveness varies with NTU. The analysis of the run-around system with both heat and moisture exchange with NTU_m and M_{Salt}/M_{Air} as independent parameters shows that the maximum effectiveness occurs approximately when $M_{Salt}/M_{Air}=1$. As well, the value of maximum effectiveness was found to be different when different coupling salt solutions were used.

ACKNOWLEDGEMENTS

A sincere thanks is firstly extended to Professor R.W. Besant and Professor C. J. Simonson. Thank you for your guidance and support throughout this research, and also for providing the opportunity to study and work in this area. I am also grateful to Dr. W. Shang and Mr. Manfred Gerber for their advice and support during my research. I would also like to thank my family for their love and support, without which I wouldn't have finished this project.

Financial assistance from the Natural Science and Engineering Research Council of Canada (NSERC) and Venmar CES, Saskatoon is also acknowledged and appreciated.

DEDICATION

I dedicate this thesis to my parents, Zhenying Jia and Jinlong Fan, and my wife, Cheng Zhu. Thank you very much for your love and support throughout this work.

TABLE OF CONTENTS

LIST OF TABLES

LIST OF FIGURES

NOMENCLATURE

ACRONYMS

ARI	Air-conditioning and Refrigeration Institute
ASHRAE	American Society of Heating, Refrigerating and Air-Conditioning Engineers
HVAC	Heating, Ventilation and Air-Conditioning
LCC	Life-Cycle Cost
RH	Relative Humidity

ENGLISH SYMBOLS

C	Heat capacity [J / K]
C_G	Equilibrium composition of G in dilute solution
Cp	Specific heat [$J /(kg \cdot K)$]
Cr	Heat capacity ratio
C_{Salt}	Concentration of salt solution
d	Channel dimension [mm]
D_h	Hydraulic diameter [m]
G	A component of a mixture
h	Convective heat transfer coefficient [$W /(m^2 \cdot K)$]
h_m	Convective mass transfer coefficient [$kg /(m^2 \cdot s)$]
h_{fg}	Heat of vaporization [J / kg]

H	Enthalpy [J / kg]
H_e	Henry's law constant
H^*	Operating condition factor
I	Ionic strength [mol / kg]
k	Thermal conductivity [$W /(m \cdot K)$]
k_m	Mass diffusion coefficient [$kg /(m \cdot s)$]
K	Electrolyte parameter
Le	Lewis number
m	Mass flow rate [kg/s]
$\dot{m}$	Rate of phase change per unit width of flow [$kg /(m \cdot s)$]
M	Mass flow rate per unit width of flow [$kg /(m \cdot s)$]
M_S	Molecular weight of solvent
NTU	Number of transfer units
NTU_m	Number of mass transfer units
Nu	Nusselt number
p	Partial pressure [Pa]
P	Total pressure [Pa]
Pe	Peclet number
Pr	Prandtl number
q	Heat transfer rate [W]
Re	Reynolds number
Sh	Sherwood number
T	Temperature [K]

t	Temperature [$^{\circ}C$]
U	Overall heat transfer coefficient [$W/(m^2 \cdot K)$]
U_m	Overall mass transfer coefficient [$kg/(m^2 \cdot s)$]
v_+	Number of moles of cation
v_-	Number of moles of anion
V	Variance
W	Humidity ratio [*kgw/kga*]
X	Ratio of water mass to desiccant mass [*kgw/kgd*]
x	Coordinates [*m*]
y	Coordinates [*m*]
z	Coordinates [*m*]
x^*	Dimensionless coordinates
y^*	Dimensionless coordinates
z^*	Dimensionless coordinates
Z_+	Valency of cation
Z_-	Valency of anion

GREEK SYMBOLS

θ	Dimensionless temperature difference
δ	Thickness of the membrane [*mm*]
μ	Viscosity [$Pa \cdot s$]
ρ	Density [kg/m^3]
ε	Effectiveness

SUBSCRIPT

A	Air side
Air	Air side
AS	Supply side air
AE	Exhaust side air
E	Exhaust side
f	Fluid flow
G	Component of a mixture
in	Inlet
l	Latent
L	Liquid side
LS	Supply side liquid
LE	Exhaust side liquid
m	Mass transfer
out	Outlet
s	Sensible
S	Supply side
Salt	Pure salt
Sol	Solution side
w	Water
0	Overall

Chapter 1

INTRODUCTION

1.1 Overview

Providing a comfortable and healthy indoor environment for building occupants is the primary concern of HVAC engineers. Adequate outdoor air ventilation rate is one of the key requirements for a comfortable and healthy indoor environment, especially for commercial and institutional buildings. The minimum requirement for the outdoor air ventilation rate in buildings has been modified over the years. ASHRAE Standard 62-1989 recommended 9.4 L/s (20 cfm) of outdoor air per person in office buildings, whereas only 2.4 L/s (5 cfm) per person was recommended previously in ASHRAE Standard 62-1981. The new ASHRAE Standard 62-2003 now requires modified calculations of ventilation air flow rates that result in values somewhat similar to Standard 62-1989, but the calculated rate depends on both the type of occupied space and the number of people. Most often, increased ventilation air flow rates result in increased heating, ventilating, and air-conditioning (HVAC) equipment capacities and building operating costs. One way to reduce the cost of conditioning ventilation is to transfer heat and moisture between exhaust and supply air streams when it is cost

effective. That is, use an air-to air energy recovery device to partly condition the supply air.

Energy is stored in air due to its molecular kinetic energy (i.e. sensible energy) and its chemical composition (i.e., water vapour concentration). Energy transfers occur in air when the sensible energy (determined by its temperature) or its water vapour concentration or humidity ratio is changed. This latter form of energy is most often referred to as latent energy because liquid water would most likely be evaporated into the air to increase the humidity ratio and condensed or absorbed out of the air to decrease the humidity ratio—both implying a latent energy change. Energy can be exchanged between the supply and exhaust air streams in its sensible (temperature only) and/or latent (moisture) form. Units that recover sensible energy only are called sensible heat exchangers, or when packaged in a single HVAC unit, heat recovery ventilators. Devices that transfer both heat and moisture are known as energy or enthalpy devices or energy recovery ventilators (ASHRAE, 2004). There are several types of existing air-to-air energy recovery devices including compact air-to-air cross-flow heat exchangers that are often called plate heat exchangers, air-to-air cross flow enthalpy or energy exchangers, energy or enthalpy wheels, run-around heat recovery systems, heat pipes, and twin-tower enthalpy recovery loops. Performance of an energy recovery system is characterized by its effectiveness to account for each type of energy transfer, the pressure drop to account for the fan power required for moving air through the exchanger, the recovery energy ratio or coefficient of performance to account for the auxiliary power need for pumping liquids or rotating a wheel, cross flow or outside air correction factor to account for air leakage from the supply to the exhaust streams, and

the exhaust air transfer ratio to account for cross contamination from the exhaust to the supply air (ASHRAE Std 84-91R and ARI Std 1060-2003).

An ideal air-to-air energy exchanger (ASHRAE, 2004):

- allows temperature-driven heat transfer between participating airstreams,
- allows partial-pressure-driven moisture transfer between the two streams, and
- minimizes cross-stream transfer of air, other gases (e.g. pollutants), biological contaminants, and particulates.

According to these criteria, all of the currently available air-to-air energy recovery devices have some disadvantages. Cross-flow heat exchangers and heat pipes do not transfer moisture and they must be installed with the supply and exhaust air ducts side-by-side, which makes them susceptible to cross-stream transfer of contaminants. The run-around heat recovery system does not require the supply and exhaust air ducts to be side-by-side, but it does not transfer moisture. Energy wheels and cross flow enthalpy plate exchangers do transfer moisture between the supply and exhaust air streams, but they require the air ducts to be side-by-side. In addition, energy wheels have moving parts and can have some cross contamination. Twin-tower enthalpy recovery loops may avoid most of these problems but they are usually not cost effective and their performance has only been moderate. These loops can exchange moisture between remote supply and exhaust air streams and do not cause cross contamination. They, like run-around heat exchangers, do not require the air ducts to be installed side-by-side. But since they are open systems, the installation and maintenance costs have been very high.

A newly proposed run-around system using two cross-flow semi-permeable plate exchangers with a salt solution coupling liquid pumped between the exchangers provides

a method for heat and moisture exchange in a closed system. This system, shown schematically in Figure 1.1, allows heat and water vapour to be exchanged between the exhaust and supply air flows by pumping a desiccant liquid in a closed loop between two exchangers that are coupled to the flowing air streams. According to the characteristics of an ideal air-to-air energy exchanger listed previously, this system could be an ideal air-to-air energy recovery device. It can recover both sensible and latent energy and has no direct cross contamination. The supply and exhaust air ducts are not restricted to side-by-side installation. This will give it an advantage over other energy recovery devices, especially in retrofit applications. Except for the pump, the system has no moving parts. Therefore the operating cost for such a system should be low.

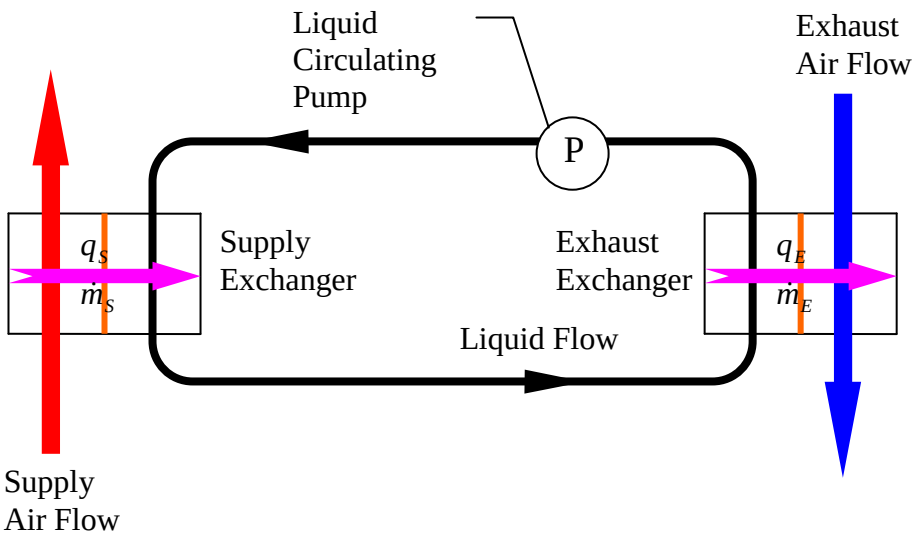

Figure 1.1 *Run-around heat and moisture recovery system*

The general purpose of this thesis is to investigate this new run-around system for exchanging heat and moisture between two air streams using plate exchangers in each air streams. The research is limited to a numerical study. The aims are to develop a

numerical model for this new energy recovery system, to verify its validity and accuracy using information from the literature, and investigate the overall effectiveness of this run-around heat and moisture recovery system subject to a range of operating conditions.

1.2 Literature Review

Many research papers have been published on flat-plate heat exchangers, enthalpy exchangers, and run-around heat recovery systems. A brief review of the recent literature for these devices follows.

Cross flow plate heat exchangers and enthalpy exchangers

Cross-flow plate heat exchangers have been used in applications for many years. A lot of research work has been done on this type of exchanger. The first analytical solution on the properties and performance of cross-flow heat exchangers was presented by Mason (1955) who obtained a closed form solution which is in the form of an infinite series obtained using Laplace transforms. This exact solution converges more rapidly than previous solutions. Correlations for the effectiveness of cross-flow plate heat exchangers were deduced from this solution by Kays and London (1984) who also summarized the correlations and design procedure for all types of heat exchangers.

Luo and Roetzel (1998) developed an axial dispersion analytical model for cross-flow plate heat exchangers using Laplace transforms. This solution also takes entrance region maldistributions and backmixing into account. Analytical solutions for the effectiveness and temperature distributions in cross-flow heat exchangers were presented. These results show that the influence of axial dispersion on the sensible energy effectiveness is only significant for small Peclet numbers (i.e. $Pe < 20$), especially when heat capacity ratio is close to one (i.e. $Cr \approx 1$). The influence of axial dispersion

increases with the increase of number of transfer units (*NTU*). Above $Pe = 20$, dispersion need not be included in the model.

Mishra et al. (2004) investigated the transient behaviour of cross-flow heat exchangers with longitudinal conduction and axial dispersion. A mathematical model was developed for determining the transient behaviour of cross-flow exchangers and was solved using a finite difference method. The dynamic performance of the heat exchanger was studied in response to step, ramp, and exponential excitations of the inlet temperature of the hot fluid. The results show that the fluid exit temperature reaches steady state faster at low Peclet numbers. In addition, longitudinal heat conduction in the wall of the heat exchanger influences the performance of the heat exchanger during the transient period. They showed that the combined effects of longitudinal conduction and axial dispersion are complex. In the hot fluid side, the presence of axial dispersion with longitudinal heat conduction gives somewhat similar effects on the effectiveness, but axial dispersion in the cold steam diminishes the net effect of longitudinal heat conduction.

Enthalpy, or heat and moisture plate exchangers, plate exchangers constructed with water vapour permeable surfaces are a more recent invention and only a few research papers have been published. Niu and Zhang (2001) studied the coupled heat and moisture transfer in a cross-flow air-to-air enthalpy exchanger with hydrophilic membrane cores. They developed a mathematical model which was solved using the finite difference method. Variations of sensible, latent and enthalpy effectiveness with various operating parameters were presented. It was found that latent effectiveness is influenced by both the membrane material selected and the operating conditions. To account for these influences, a coefficient of moisture diffusion was defined. Zhang and

Niu (2002) furthered their study by developing a correlation for the effectiveness of heat and moisture transfer in an enthalpy exchanger. The latent effectiveness was given as a function of the number of mass transfer units, NTU_m.

There appears to be no analytical or numerical research on heat and moisture exchangers using fluids other than air and none on run-around heat and moisture recovery systems.

Run-around heat recovery systems

The run-around heat recovery system, also called liquid-coupled indirect-transfer-type exchanger system, has been used in industry for many decades. Because of its high reliability and flexibility in HVAC design and retrofit, it became an active research area. Perhaps the first study of such a system was published by Kays and London (1951). They found that the optimum condition of operation for the system is the heat capacity rate (or product of mass flow rate and specific heat) of the coupling liquid equals the heat capacity rate of the air.

Forsyth and Besant (1988a, 1988b) studied the procedure for analyzing and optimizing the design of a run-around heat recovery system with two coils for a given set of inlet operating conditions of airflow, temperature and humidity. A numerical optimization technique was used to solve the run-around system design problem. The simulated system and the measured system performed similarly for variations in the design parameters, but they didn't have comparable output for a given design. This was believed to be caused by the different geometry of the coils used. For the system design optimization, Forsyth and Besant proposed that many design parameters should be taken into account rather than only overall effectiveness. A more realistic design performance measurement is the total system cost. The results imply that fully developed turbulent

flow in the coil tubes is essential if the maximum overall effectiveness is to be realized and too high a concentration of ethylene-glycol can result in a 50% drop in system effectiveness under some conditions.

Zeng et al. (1992) furthered the research of Forsyth and Besant by studying the temperature dependent properties for a run-around system using a numerical simulation. In this numerical model, the heat exchanger coil was subdivided into a number of elements across which heat flows between the aqueous glycol and air. Based on the energy balances on each exchanger and the inlet temperature match, a matrix of the temperatures at a finite number of nodes in the exchanger was solved, giving the temperature distribution in the exchanger. The results show that temperature dependent properties of aqueous-glycol coupling fluids must be included in the analysis of run-around heat recovery systems when the temperature difference between inlet supply and exhaust air is large and the Reynolds number is low for the coupling fluid in the coil tubes. Compared to a system with only averaged properties and for turbulent flow and large temperature swings in the coupling fluid, errors of up to 25% for overall effectiveness were simulated, when low coil-tube Reynolds numbers are used.

Bennett et al. (1994a, 1994b) improved Forsyth and Besant's (1988a, 1988b) work by simulating the geometry effects of wavy fins, which are used on the air side of coil and fin exchanger, and liquid bypassing, which is often used to control the heat rate of the run-around system. An upgraded numerical model of Forsyth and Besant, including liquid bypass, thermal contact resistance between the fins and coils, wavy-fin coil geometry, and hourly weather data for performing yearly simulation was developed and verified using measured data. A life-cycle cost design procedure was developed consisting of doing a cost optimization study for 17 independent coil and pumping rate

design variables. Results were presented and illustrated for a typical run-around heat recovery system. It was found that through the use of life-cycle cost (LCC) optimized design, the performance of a run-around heat recovery system could be greatly enhanced. The effectiveness for the optimum system could be increased from less than 50% to more than 66%. For the large run-around system investigated in this study, the payback period could be less than three years. The life-cycle net savings were expected to increase by more than 45% in the optimized system compared to the installed system.

Johnson et al. (1995) studied the design of multi-coil run-around heat recovery systems and did LCC analyses for systems. A thermal model of a multiple-coil heat recovery system was developed to simulate any number of supply and exhaust coils in the run-around heat recovery system. This simulation enabled the rating of a run-around system based on the known physical parameters of each coil, the supply and exhaust airflow rates, inlet supply and exhaust air conditions. It was found that the effectiveness of an optimized system with two coils was nearly the same as the performance of a four-coil optimized run-around system with the same total airflows as the two-coil system at 62% compared to the installed effectiveness at 44% at the design operating condition. A variable-speed pump for heat rate control was also simulated. The results show that a variable-speed pump control can be more cost effective than liquid bypass control through a control valve because the operating cost is reduced.

The previous research only dealt with sensible energy exchange in run-around heat recovery systems with coil type heat exchangers. There has been no research on run-around heat recovery systems using flat-plate exchangers in a run-around system that can exchange both heat and moisture.

1.3 Objectives

It is the general purpose of this study to investigate the feasibility of a run-around heat and moisture recovery system through the study of its design characteristics and performance.

The explicit objectives of this research are as listed below:

1. Using only the fundamental equations of energy and mass transfer and empirical property values, develop a numerical simulation for a run-around heat and water vapour transfer system which includes two plate-type, cross-flow, air-to-liquid exchangers and a coupling solution of aqueous desiccant (LiBr and LiCl).
2. Using the literature on plate-type cross-flow heat exchangers and run-around heat recovery systems, verify the accuracy of the simulation model for the case of no mass transfer (i.e. only heat transfer).
3. Investigate the exchanger design characteristics and the coupling fluid flow rate to allow a designer to optimize the performance factors for the case of no water vapour transfer as in objective 2.
4. With both heat and moisture transfer in each exchanger, identify the exchanger design characteristics and the fluid flow rate and salt concentrations of the coupling fluid that will allow the designer to optimize the performance factors for the system.
5. To include in the above study for objective 4 a full discussion and presentation of suitable performance factors that can be used to characterize the performance of run-around systems that transfer both heat and water vapour.
6. Verify the numerical model as far as practical through a sensitivity study.

In this thesis, both the single exchanger and a coupled run-around system were investigated using numerical methods. The operating conditions of the exchanger and the system are ARI summer and winter test conditions (ANSI/ARI Standard 1060, 2001) and only steady state conditions are considered.

1.4 Thesis Overview

A mathematical/numerical model of a sensible flat-plate heat exchanger and run-around heat recovery system is developed in Chapter 2. This numerical model is steady state and one dimensional and is formulated using the finite difference method (Fan et al. 2005). With this model, a complete investigation of the performance of a single heat exchanger and a run-around heat recovery system is also carried out in this chapter. The model is validated by comparison with well known analytical correlations.

In Chapter 3, a mathematical/numerical model of a heat and moisture exchanger is developed and the design characteristics of the exchanger are studied. The numerical model for a run-around heat and moisture recovery system is presented in Chapter 4, and a discussion and analysis of suitable dimensionless performance factors of the system are also given in this chapter.

The final objective of this research is to partially verify the model of the run-around heat and moisture recovery system through sensitivity studies and these sensitivity studies are presented in Chapter 5.

Chapter 2

RUN-AROUND HEAT RECOVERY SYSTEM

2.1 Introduction

A run-around heat recovery system is comprised of two or more liquid-to-air heat exchangers that are coupled by a liquid circuit as shown in Figure 2.1 with each exchanger transferring only sensible heat (i.e. no moisture transfer). In this chapter, the performance of a run-around heat recovery system with cross-flow flat-plate heat exchangers will be investigated using a LiBr solution as the coupling fluid. The same type of system will be used for the coupled heat and moisture exchange study in Chapters 3 to 5, except that the polyethylene plastic heat exchange surfaces will be replaced by water vapour permeable surfaces in the later chapters.

Cross-flow flat-plate heat exchangers, made using low-cost plastics, could reduce the pay back period and increase life-cycle savings of flat-plate run-around systems compared to coil run-around system, and are proposed to be used in this research.

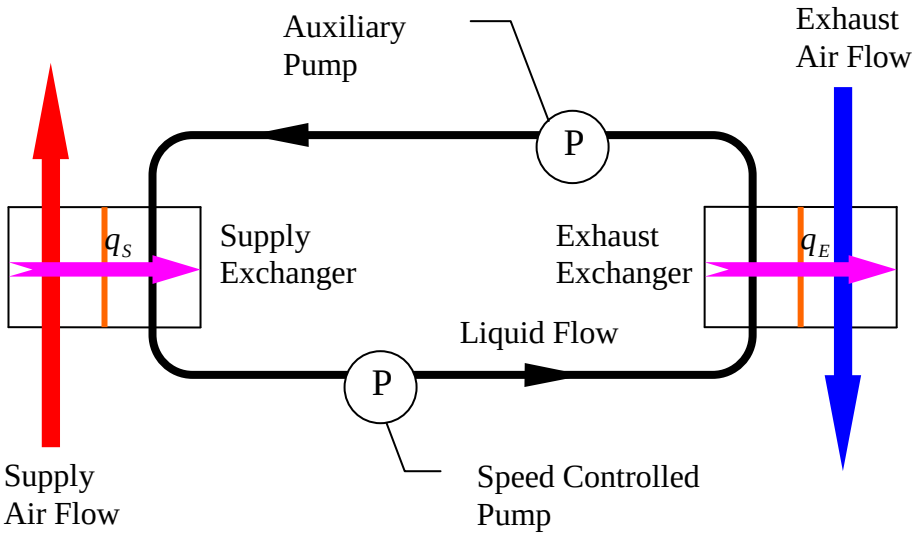

Figure 2.1 *Schematic diagram of a run-around heat recovery system*

2.2 Theoretical Model of the Single Cross-Flow Heat Exchanger

The geometry of one pair of flow channels for a cross-flow flat plate heat exchanger and the coordinate system used for the mathematical model are shown in Figure 2.2. Flow channels adjacent to these two shown are assumed to be identical, implying that only one exchange surface need be modelled. The channel sizes of the air side (d_A) and liquid side (d_L) are not necessarily the same.

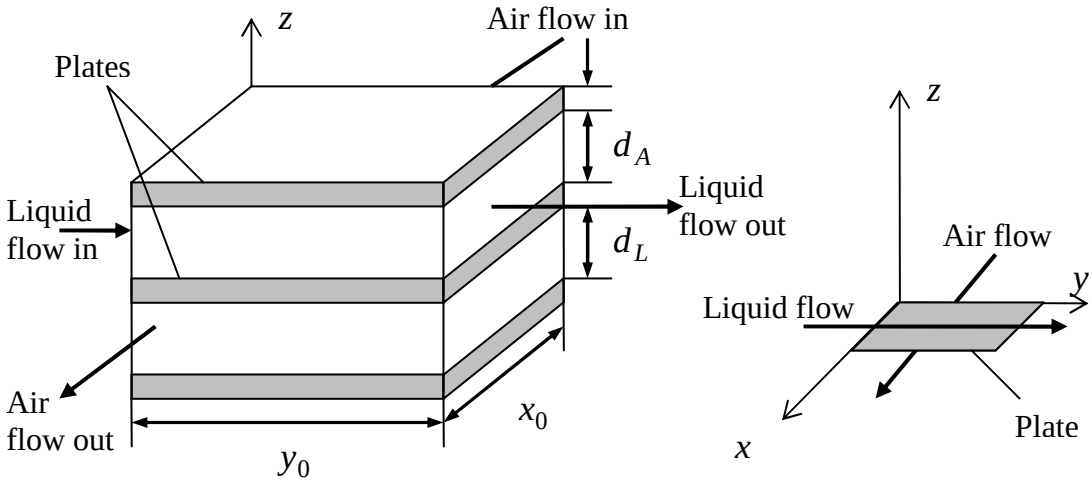

(a) One pair of flow channels (b) The coordinate system

Figure 2.2 *Schematic of a cross-flow flat-plate heat exchanger showing three membranes separating one liquid and one air channel*

2.2.1 Assumptions and Governing Equations

Assumptions

The major assumptions in the formulation of the mathematical model are as listed below:

1. Conduction heat transfer is steady state and equal for each membrane, and only in the z direction normal to each membrane.

2. The flow and heat transfer processes are fully developed in each flow channel.

3. The air flow and liquid flow are fully developed and unmixed when they go through the channels of the heat exchanger.

These assumptions will be accurate for most typical flat-plate exchanger geometries and inlet operating conditions. Sensitivity studies will be presented in Chapter 5 to demonstrate the validity of these assumptions.

Governing equations

Two coupled governing energy balance equations are needed to analyze the heat transfer through the membrane at any point (x, y) on the surface one for the air flow through the exchanger and the other for the liquid solution flow.

Air side

At any point (x, y) in the exchanger in Figure 2.2, the steady state heat flux through the membrane is balanced by the heat gain/loss in the air:

$$\frac{2U \cdot y_0}{C_A}\left(T_A - T_L\right) = -\frac{\partial T_A}{\partial x} \tag{2.1}$$

where T_A and T_L are the bulk mean temperatures at (x, y) in the air and liquid solution respectively, C_A is the heat capacity rate of the air (i.e. $C_A = m_A \cdot Cp_A$), and m_A is the mass flow rate of the dry air through a single channel. The overall heat transfer coefficient (U) between the air and the liquid is

$$U = \left[\frac{1}{h_L} + \frac{\delta}{k} + \frac{1}{h_A}\right]^{-1}. \tag{2.2}$$

The convective heat transfer coefficients in the air stream, h_A, and liquid solution, h_L, are assumed to be constant, therefore U will be independent of position in the exchanger.

Liquid side

At any point (x, y) in the exchanger, the heat flux through the membrane surface is balanced by the net heat gain/loss in the liquid:

$$\frac{2U \cdot x_0}{C_L}\left(T_A - T_L\right) = \frac{\partial T_L}{\partial y}, \tag{2.3}$$

where C_L is the heat capacity rate of the salt solution (i.e., $C_L = m_L \cdot Cp_L$, the determination of Cp_L is presented in Appendix A), and m_L is the mass flow rate of the liquid through a single channel.

Rewriting the above governing equations to include the dimensionless groups for heat transfer (see Table 2.1), gives, for the air side:

$$NTU_A\left(T_A - T_L\right) = -\frac{\partial T_A}{\partial x^*}, \tag{2.4}$$

and the liquid side:

$$NTU_L\left(T_A - T_L\right) = \frac{\partial T_L}{\partial y^*}. \tag{2.5}$$

Where:

$$x^* = \frac{x}{x_0}, \tag{2.6}$$

$$y^* = \frac{y}{y_0}, \tag{2.7}$$

$$NTU_A = \frac{2 \cdot U \cdot x_0 \cdot y_0}{C_A}, \text{ and} \tag{2.8}$$

$$NTU_L = \frac{2 \cdot U \cdot x_0 \cdot y_0}{C_L}. \tag{2.9}$$

The number of heat transfer units for a single exchanger is defined as:

$$NTU = \frac{2 \cdot U \cdot x_0 \cdot y_0}{\min\{C_A, C_L\}} = \max\{NTU_A, NTU_L\}. \tag{2.10}$$

Table 2.1 *Dimensionless variables and parameters for the governing equations of a heat exchanger*

x^*	y^*	NTU_A	NTU_L	NTU
$\frac{x}{x_0}$	$\frac{y}{y_0}$	$\frac{2 \cdot U \cdot x_0 \cdot y_0}{C_A}$	$\frac{2 \cdot U \cdot x_0 \cdot y_0}{C_L}$	$\max\{NTU_A, NTU_L\}$

The detailed development of the governing equations is given in Appendix B.

The overall heat transfer coefficient, *U*

The overall heat transfer coefficient, *U*, can be calculated from equation (2.2). In this equation, *k* is the conductivity of the plate of the heat exchanger and is determined by the material used for the plate. In this chapter, the plate is polyethylene plastic with $k = 0.334\, W/(m \cdot K)$. The performance of the heat exchanger is not very sensitive to *k*

and simulation results show that effectiveness changes less than *1%* with k varying from $3.34\,W/(m\cdot K)$ to $0.0334\,W/(m\cdot K)$ (see Section 5.1).

The convection heat transfer coefficients have a greater impact on *U*. Convection heat transfer coefficients can be obtained experimentally and correlated with an algebraic expression of the form (Incropera and DeWitt, 1996)

$$Nu = C\cdot \mathrm{Re}^{m}\,\mathrm{Pr}^{n} \tag{2.11}$$

for turbulent flow in a channel and Reynolds number (Re) greater than 10^4 and Prandtl number (Pr) greater than 0.07, where *Nu* is the Nusselt number defined by $Nu = \dfrac{h\cdot D_h}{k}$.

For moderate Reynolds numbers ($3{,}000 < \mathrm{Re} < 5\times 10^6$), a better correlation (Incropera and DeWitt, 1996) is:

$$Nu = \frac{(f/8)\cdot(\mathrm{Re}-1000)\cdot \mathrm{Pr}}{1+12.7\cdot(f/8)^{1/2}\cdot(\mathrm{Pr}^{2/3}-1)}, \tag{2.12}$$

where $f = [0.79\ln(\mathrm{Re})-1.64]^{-2}$ is the friction factor for smooth walled tubes.

For fully developed laminar flow with $\mathrm{Re} \le 2{,}300$, the Nusselt number can be predicted analytically when property variations are negligible, which is

$$Nu = const. = \frac{h\cdot D_h}{k_f}, \tag{2.13}$$

where k_f is the thermal conductivity of the fluid flow.

In this study, $Nu = 8.24$ (Kays and Crawford, 1990) is selected for equation (2.13) which is the case of fully developed heat transfer between infinite rectangular plates with a uniform surface heat flux.

2.2.2 Boundary Conditions

The appropriate boundary conditions for the governing equations can be summarized as shown in Figure 2.3 and are stated in the following equations.

Air side (inlet) ($x^* = 0, y^*$):

$$T_A \mid_{x^*=0} = T_{A,in} . \tag{2.14}$$

Liquid side (inlet) ($x^*, y^* = 0$):

$$T_L \mid_{y^*=0} = T_{L,in} . \tag{2.15}$$

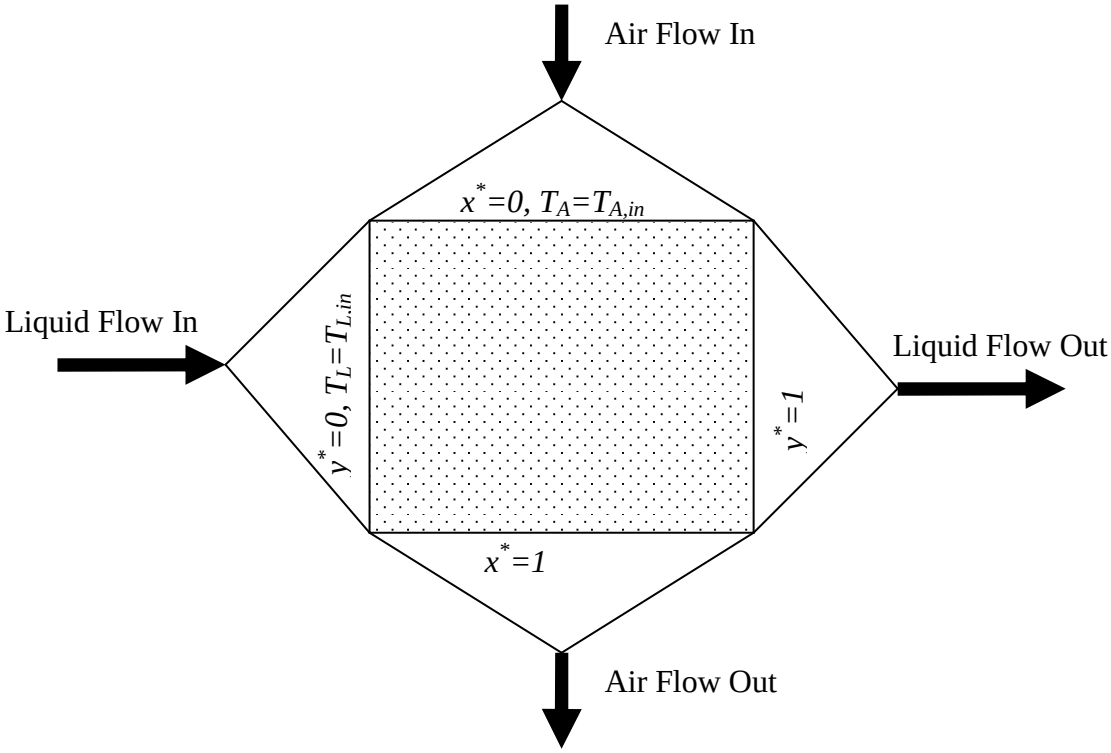

Figure 2.3 *Boundary conditions for the heat exchangers*

2.3 Theoretical Model of the Run-Around System

The theoretical model for the run-around system (as shown in Figure 2.4) uses the same governing equations as presented in Section 2.2 for a single heat exchanger. Additional equations are needed to couple the two heat exchangers in a run-around loop and these are presented in this section together with the numerical algorithm used to determine the steady state solution.

Under steady-state operating conditions for a run-around system with no interactions with the ambient air other than the pump which is assumed to add no heat to the liquid, the total heat transfer rate on the exhaust air side must equal the total heat

transfer rate on the supply side. In practice the small amount of pumping power required to circulate the coupling fluid is much less than the heat transfer rate at design conditions. The assumptions used for single heat exchangers in this analysis are the same as for the individual exchangers in each air stream. Also, it is assumed that:

1. No heat transfer occurs except within each exchanger (i.e., there is no heat transfer between the exchanger and ambient air or between the piping loop and the surrounding air); and

2. Steady state operating conditions.

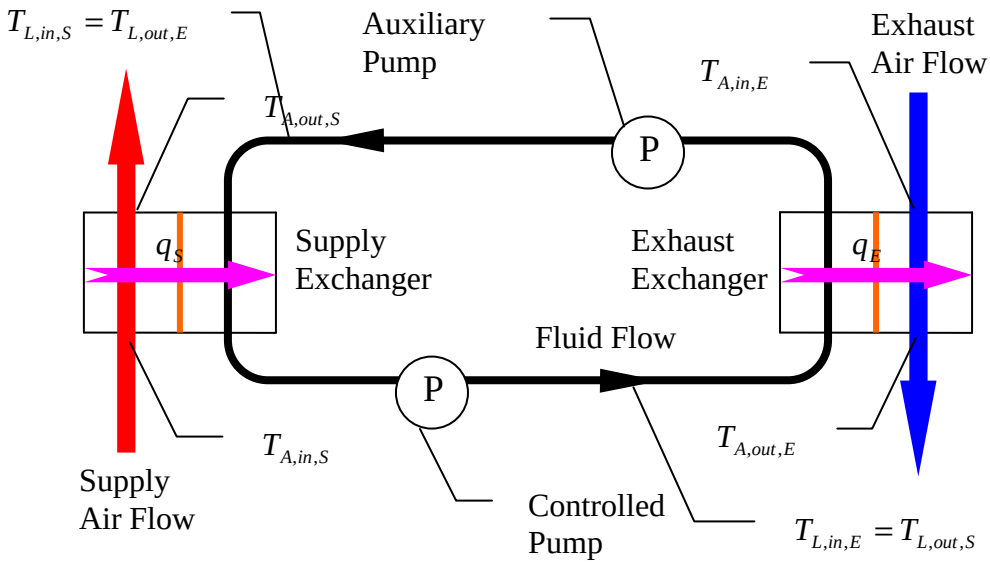

Figure 2.4 *Thermal circuit of the run-around system with cross-flow heat exchangers*

For the run-around system shown in Figure 2.4, it is assumed that the inlet air temperatures of the supply and exhaust side air, $T_{A,in,S}$ and $T_{A,in,E}$, are known and constant. The total heat transfer rate in the supply exchanger (q_S) is:

$$q_S = C_{A,S} \cdot (T_{A,in,S} - T_{A,out,S}) = C_L \cdot (T_{L,out,S} - T_{L,in,S}), \tag{2.16}$$

and in the exhaust exchanger is:

$$q_E = C_{A,E} \cdot (T_{A,out,E} - T_{A,in,E}) = C_L \cdot (T_{L,in,E} - T_{L,out,E}). \tag{2.17}$$

For no heat and mass gain/loss in the connecting pipes, the liquid inlet temperature of the supply exchanger is equal to the liquid outlet temperature of the exhaust exchanger. Therefore

$$T_{L,in,S} = T_{L,out,E}, \text{ and} \tag{2.18}$$

$$T_{L,in,E} = T_{L,out,S}. \tag{2.19}$$

The heat capacity rate of the air at different conditions is calculated using the equation:

$$C_A = m_A \cdot Cp_A = m_A \cdot (Cp_{air} + W \cdot Cp_v). \tag{2.20}$$

The outlet bulk mean outlet temperatures of the air and the solution fluid are calculated using the following equations:

$$T_{A,out} = \frac{1}{m_A Cp_A} \cdot \int_y M_A Cp_A T_A dy \text{ , and} \tag{2.21}$$

$$T_{L,out} = \frac{1}{m_L Cp_L} \cdot \int_x M_L Cp_L T_L dx \text{ .} \tag{2.22}$$

where M_A and M_L are the mass flow rate of the air and liquid per unit width of the channel. The steady state inlet and outlet conditions allow the determination of the overall effectiveness of the system.

To start the simulation, an arbitrary inlet condition of the supply side liquid, $T_{L,in,S}$ is chosen. Then using the programming algorithm to start iterating the properties, all the parameters of the inlet and outlet conditions for each exchanger are calculated and the imbalance of heat flows in the run-around system is determined. For subsequent iterations, new inlet conditions based on the previous iteration values are adopted and the outlet conditions are calculated. Based on the energy balance, that is $q_S = q_E$, the steady state inlet and outlet conditions of the liquid in the run-around system can be reached by iterating on the liquid temperature and other properties.

The effectiveness of any type of a heat exchanger, including a run-around system, can be expressed as:

$$\varepsilon = \frac{Actual\ heat\ transfer\ rate}{Maximum\ possible\ heat\ transfer\ rate\ of\ an\ exchanger\ with\ an\ infinite\ heat\ transfer\ area\ and\ the\ same\ operating\ conditions} \tag{2.23}$$

Using this definition, the sensible effectiveness of the run-around system with cross-flow heat exchangers (inlet conditions shown in Figure 2.5) is

$$\varepsilon_0 = \frac{C_{A,S} \cdot (T_{A,in,S} - T_{A,out,S})}{C_{\min} \cdot (T_{A,in,S} - T_{A,in,E})} = \frac{C_{A,E} \cdot (T_{A,out,E} - T_{A,in,E})}{C_{\min} \cdot (T_{A,in,S} - T_{A,in,E})}, \tag{2.24}$$

where $C_{\min} = \min(C_{A,S}, C_{A,E})$.

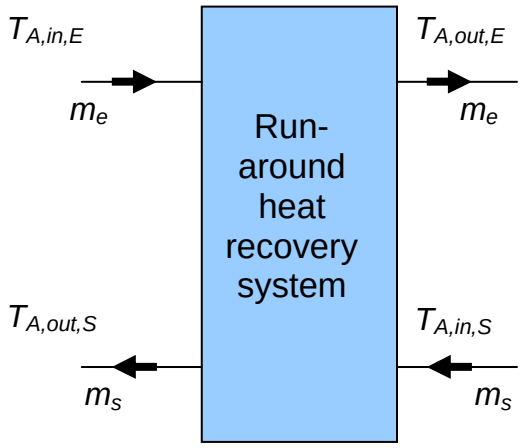

Figure 2.5 *Schematic of the inlet-outlet conditions of the run-around heat recovery system*

2.4 Numerical Solution Method and Results

2.4.1 Single Cross-Flow Heat Exchanger

In the numerical model the governing equations are discretized using the finite difference method with first order accuracy for the spatial nodes (see Appendix B for more details). Spatial derivatives are all performed using the backward scheme. The under relaxation iteration scheme is used to provide a stable solution and the solution is

considered converged when the change in the dimensionless temperature difference is less than 10^{-12}. The details of the algorithm used are given in Appendix C.

The problem was solved with 100×100 spatial nodes which gave a stable solution and increasing the number of nodes had negligible effect on the solution. Increasing the number of nodes by a factor 10 increased computation time by a factor of 100, but changed the effective of the exchanger by less than 0.01%. This scheme also gave good agreement between analytical and numerical results as will be shown in Section 2.5. The physical properties of the heat exchanger that is modeled in this section are shown in Table 2.2.

Table 2.2 *Some parameters and properties of the enthalpy exchangers*

Name	Symbol	Value
Size of the exchanger	$x_0 \times y_0 \times z_0$	$0.3\,m \times 0.3\,m \times 0.3\,m$
Channel thickness of air side	d_A	2mm
Channel thickness of liquid side	d_L	0.3mm
Membrane thickness	δ	0.5mm
Heat conductivity of the membrane	k	$0.334\,W/(m \cdot K)$,

The ARI summer test condition (ANSI/ARI Standard 1060, 2001) ($T_{A,in} = 308.15\,K\ (35^{\circ}C), W_{A,in} = 17.5\,g/kg$) was selected for the air to determine the performance of one cross-flow exchanger (Table 2.3). The operating condition for the solution is: $T_{L,in} = 297.15\,K\ (24^{\circ}C), X_{L,in} = 1.5\,kg(water)/kg(salt)$, implying that the concentration of salt in the solution is 40% $(C_{Salt} = 40\%)$.

Table 2.3 *Operating conditions of the single exchanger modeled in Chapter 2*

Inlet temperature of the air stream ($T_{A,in}$)	308.15 K ($35^{\circ}C$)
Inlet humidity ratio of the air stream ($W_{A,in}$)	17.5 g/kg
Inlet temperature of the liquid stream ($T_{L,in}$)	297.15 K ($24^{\circ}C$)
Inlet concentration of the liquid stream ($X_{L,in}$)	1.5 kg/kg (C_{Salt} = 40%)

Graphical results are presented for the temperature distribution in the exchanger and are presented in Figure 2.6 and Figure 2.7 for the air and liquid sides for two cases—one for *NTU=1* and *Cr=1*, and the other for *NTU*=10 and *Cr=1*.

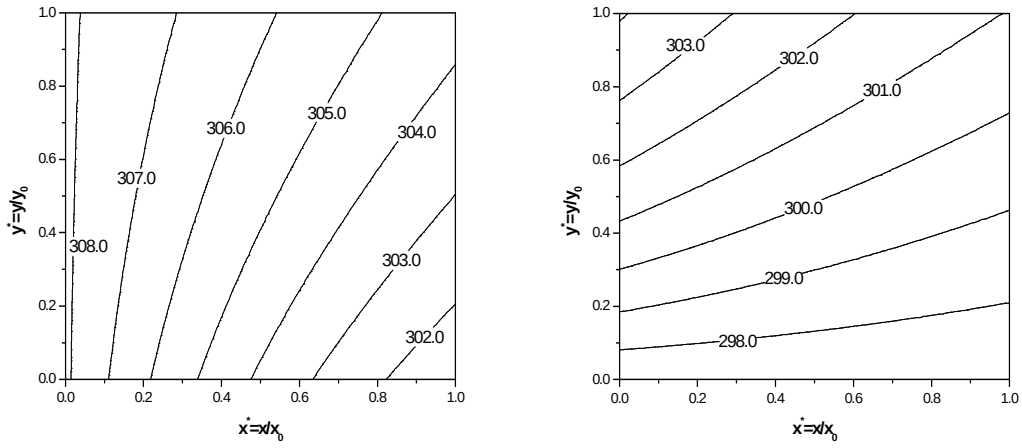

a. $T_A(x^*, y^*)$ (K), air side b. $T_L(x^*, y^*)$ (K), liquid side

Figure 2.6 *Temperature distributions in one exchanger for NTU=1 and Cr=1 (air flow in the positive x-direction and liquid flow in the positive y-direction).*

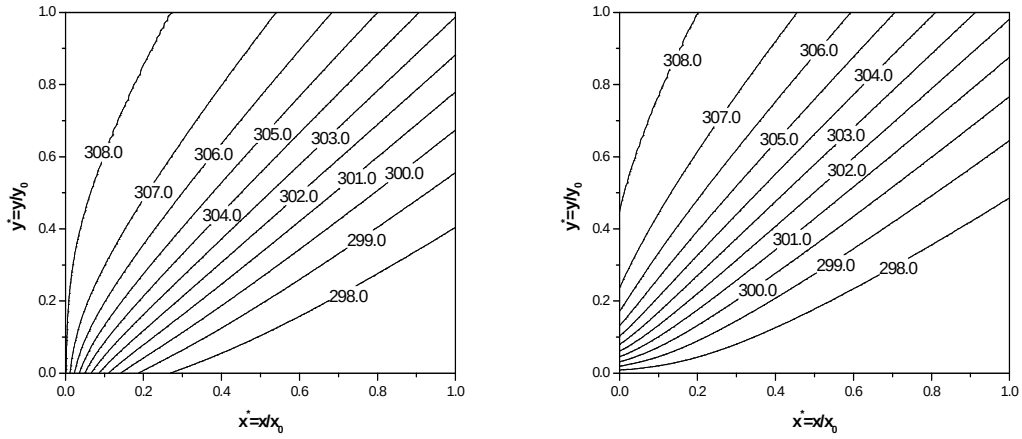

a. $T_A(x^*, y^*)$ (K), air side b. $T_L(x^*, y^*)$ (K), liquid side

Figure 2.7 *Temperature distributions in one exchanger for NTU=10 and Cr=1(air flow in the positive x-direction and liquid flow in the positive y-direction).*

Figure 2.6 and Figure 2.7 show that the number of heat transfer unit, *NTU*, has a significant impact on the contours of the temperature in the exchanger. With *NTU=1*, the isothermal lines on the air side and the liquid side indicate smaller temperature gradients in each exchanger in the flow direction at each point (x^*, y^*) compared to the case of *NTU=10*. These results imply that the heat exchanger transfers heat at a greater rate with a higher *NTU* for the same inlet conditions. As well, a higher *NTU* will result a higher effectiveness as indicated by calculated effectiveness, which are 47.6% for *NTU*=1 and 81.7% for *NTU*=10 with *Cr*=1.

With this model, it is possible to compare heat exchangers with the same *NTU* but different values of *Cr*. Graphical results are presented for the cases of (*NTU*=6,

Cr=1), (NTU=6, Cr=0.1 for C_A<C_L) and (NTU=6, Cr=0.1 for C_A>C_L) in Figure 2.8, Figure 2.9 and Figure 2.10.

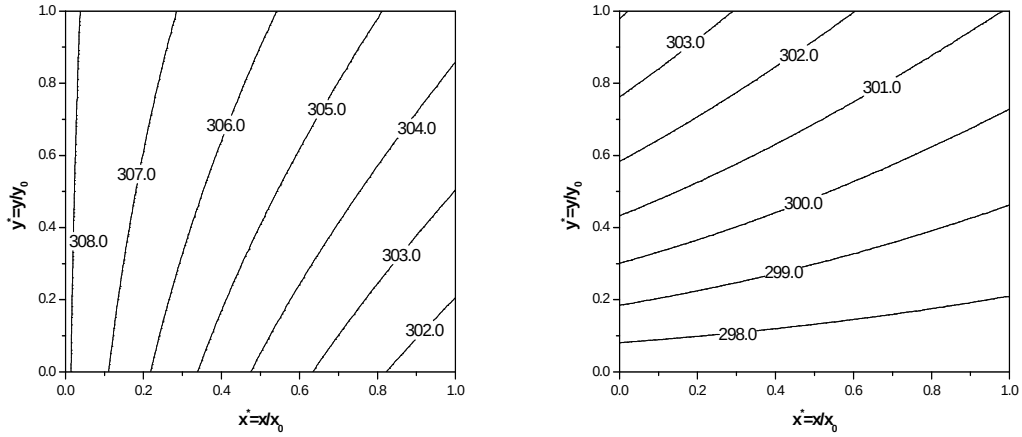

a. $T_A(x^*, y^*)$(K), air side b. $T_L(x^*, y^*)$(K), liquid side

Figure 2.8 *Temperature distributions in one exchanger for NTU=6 and Cr=1(air flow in the positive x-direction and liquid flow in the positive y-direction).*

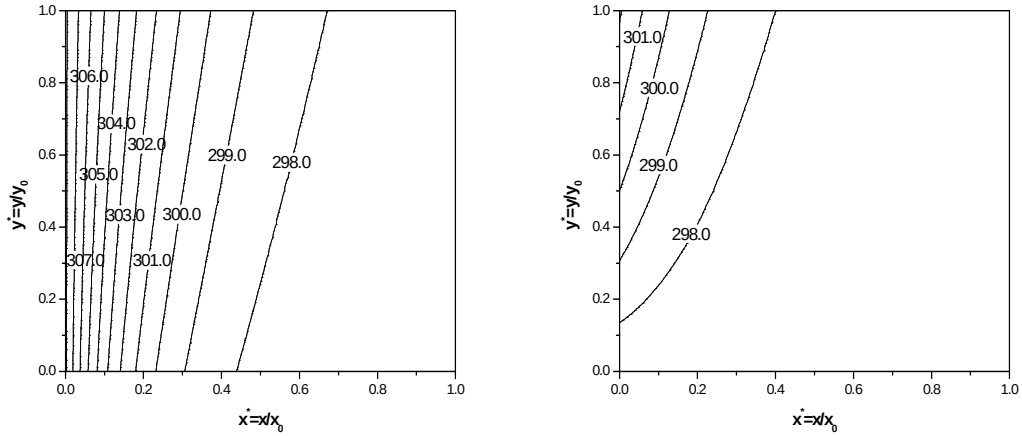

a. $T_A(x^*, y^*)$(K), air side b. $T_L(x^*, y^*)$(K), liquid side

Figure 2.9 *Temperature distributions in one exchanger for NTU=6 and Cr=0.1(C_A<C_L, air flow in the positive x-direction and liquid flow in the positive y-direction).*

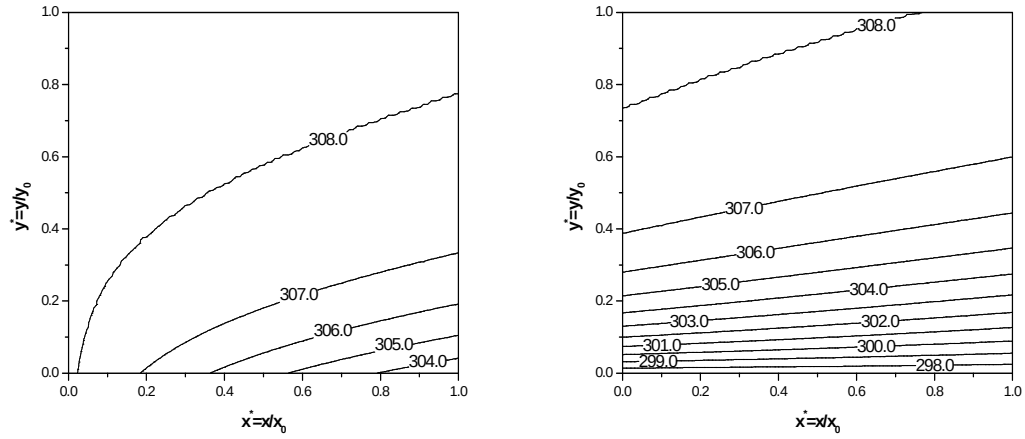

a. $T_A(x^*, y^*)$ (K), air side

b. $T_L(x^*, y^*)$ (K), liquid side

Figure 2.10 *Temperature distributions in one exchanger for NTU=6 and Cr=0.1 (C_A>C_L, air flow in the positive x-direction and liquid flow in the positive y-direction).*

From Figures 2.8 to 2.10, it can be seen that the gradient of the isotherms in the flow direction are equally distributed on the air side and the liquid side for the case of *Cr=1*. But for *Cr=0.1*, the isotherms are distributed unequally on the air side and the liquid side. The distribution of the isotherms is related to the gradient of the temperature. The gradient of temperature, ∇T, can be related to the heat transfer rate at any point in the exchanger using equations (2.1) and (2.3), and

$$\hat{j} \cdot \nabla T = \frac{\partial T}{\partial y} \text{ and } \hat{i} \cdot \nabla T = \frac{\partial T}{\partial x} \tag{2.25}$$

where $\hat{j}$ is the unit vector in the *y*-direction and $\hat{i}$ is the unit vector in the *x*-direction. The heat transfer rate per unit area (or heat flux) between the air and the liquid at any point in the heat exchanger is determined with:

$$-\frac{1}{x_0 \cdot y_0} \cdot C_A \cdot \frac{\partial T_A}{\partial x} = -q(z)_A(x,y) = q(z)_L(x,y) = \frac{1}{x_0 \cdot y_0} \cdot C_L \cdot \frac{\partial T_L}{\partial y}. \qquad (2.26)$$

Where $q(z)_A(x,y)$ is the heat flux from the air to the liquid at any point and $q(z)_L(x,y)$ is the heat flux from the liquid to the air at any point. In an exchanger, the total heat transfer to the air has to equal the total heat transfer from the liquid for an energy balance, that is

$$(\int_0^{y_0}\int_0^{x_0} q(z)_A(x,y)dxdy)_{Air} = -(\int_0^{x_0}\int_0^{y_0} q(z)_L(x,y)dydx)_{Liq}. \qquad (2.27)$$

Equation (2.26) shows that $\left|\frac{\partial T_A}{\partial x}\right| = \left|\frac{\partial T_L}{\partial y}\right|$ when $C_A = C_L$, but $\left|\frac{\partial T_A}{\partial x}\right| \neq \left|\frac{\partial T_L}{\partial y}\right|$ when $C_A \neq C_L$. Therefore, the value of the heat capacity ratio, *Cr*, has great impact on the gradients of the temperatures in the air and liquid and on the distribution of the isotherms of the air and liquid. For the same value of *Cr*, the values of C_A and C_L determine the isotherms of the air and liquid. For the case of *Cr*=0.1 (as shown in Figures 2.9 and 2.10), the distributions of the isothermal lines are different for $C_A > C_L$ and $C_A < C_L$. For $C_A < C_L$ (Figure 2.9), equation (2.26) indicates that the gradient in the air will be greater than the gradient in the liquid and thus the isothermal lines are closer together in the air than in the liquid. On the other hand for $C_A > C_L$, equation (2.26) and Figure 2.10 show that the isothermal lines are much closer in the liquid than in the air.

The temperature profiles presented in Figures 2.6 and 2.10 indicate that the model could be used to study the condensation and frosting in heat exchangers under some operating conditions. That is, with these temperature contours known for the air

and liquid side, it is possible to calculate the exchanger surface temperature distribution (Appendix D) and determine which part of the exchanger will experience condensation and/or frosting during cold weather. Such investigations will be left to future studies. The temperature profile of the air (and liquid) within a single flow channel may be of interest for future studies on frosting and the effect of variable properties (Zeng et al., 1992). Appendix D provides an expression for the temperature distribution within a flow channel but these effects are not investigated further in this thesis.

With this model, the effectiveness of the single exchanger can be determined by calculating the average outlet conditions on the air side and the liquid side. The results are presented in Figure 2.11.

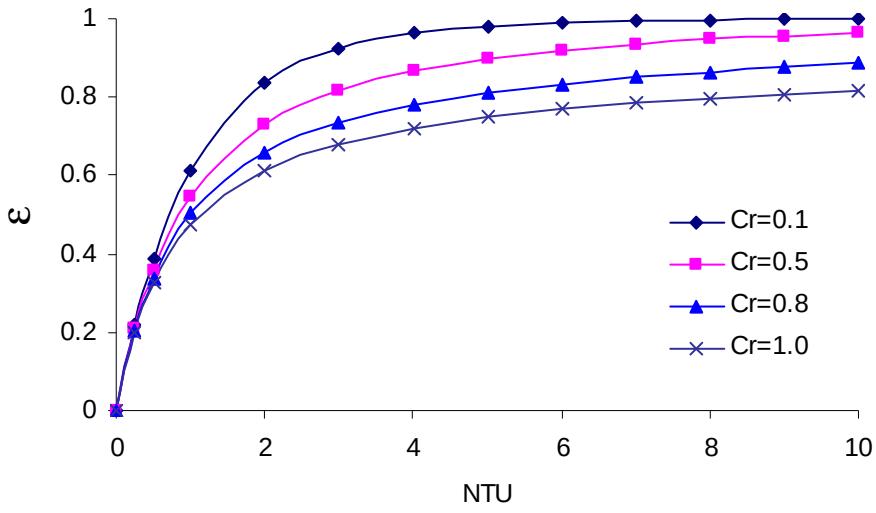

Figure 2.11 *Effectiveness of a single heat exchanger for various values of NTU and Cr.*

Figure 2.11 shows that the effectiveness of the single exchanger increases with increasing *NTU*, but decreases with increasing *Cr*. These results, which are very similar

to the correlation results shown in (Incropera and Dewitt, 1996), do not imply that the heat rate will be increased if *Cr* is chosen to be small because the definition of effectiveness in equation (2.24) requires that the heat rate is calculated by the product of and $C_{\min}$ and $(T_{A,in,S} - T_{A,in,E})$.

2.4.2 Run-Around System

In this section, the run-around heat recovery system is assumed to be composed of two cross-flow flat-plate heat exchangers of the same parameters and properties as the heat exchanger described in Table 2.2—one as the supply side exchanger and the other the exhaust side exchanger. The inlet conditions of supply and exhaust air correspond to the ARI Summer testing condition (as shown in Table 2.4). The initial conditions for the coupling liquid are $(T_{L,in} = 297.15\ K\ (24^{\circ}C)$, $X_{L,in} = 1.5\ kg/kg(C_{Salt} = 40\%))$, but are not critical because only the steady state solution will be presented.

Table 2.4 *Operating conditions of the run-around system modeled in Chapter 2.*

Inlet temperature of the supply air stream ($T_{A,in,S}$)	$308.15\ K\ (35^{\circ}C)$
Inlet humidity ratio of the supply air stream ($W_{A,in,S}$)	$17.5\ g/kg$
Inlet temperature of the exhaust air stream ($T_{A,in,E}$)	$297.15\ K\ (24^{\circ}C)$
Inlet humidity ratio of the exhaust air stream ($W_{A,in,E}$)	$9.3\ g/kg$
The initial inlet temperature of the liquid stream ($T_{L,in}$)	$297.15\ K\ (24^{\circ}C)$
The initial inlet concentration of the liquid stream ($X_{L,in}$)	$1.5\ kg/kg(C_{Salt} = 40\%)$

As mentioned in Section 2.3, the numerical solution method for the run-around heat recovery system is based on the balance of the heat transferred in the two

exchangers. An initial inlet operating condition of the coupling liquid is selected, and the program is iterated until the heat is balanced. The solution is considered converged when the difference in heat rate, q, is less than 10^{-4}, that is

$$\frac{q_S - q_E}{(q_S + q_E)/2} < 10^{-4}. \tag{2.28}$$

The overall effectiveness, ε_0, is presented in Figure 2.12 and Figure 2.13 for the case of equal exhaust (E) and supply (S) air mass flow rates so that $C_A = C_{A,E} = C_{A,S}$, while the flow rate of the liquid coupling fluid can have any value and C_L may and may not equal C_A. For each exchanger, $Cr = C_{\min} / C_{\max}$ where $C_{\min} = \min[C_A, C_L]$ and $C_{\max} = \max[C_A, C_L]$. The results in Figure 2.12 and Figure 2.13 are for the case when $NTU = NTU_S = NTU_E$. Thus both Cr and NTU are for individual exchangers while ε_0 is for the overall run-around system.

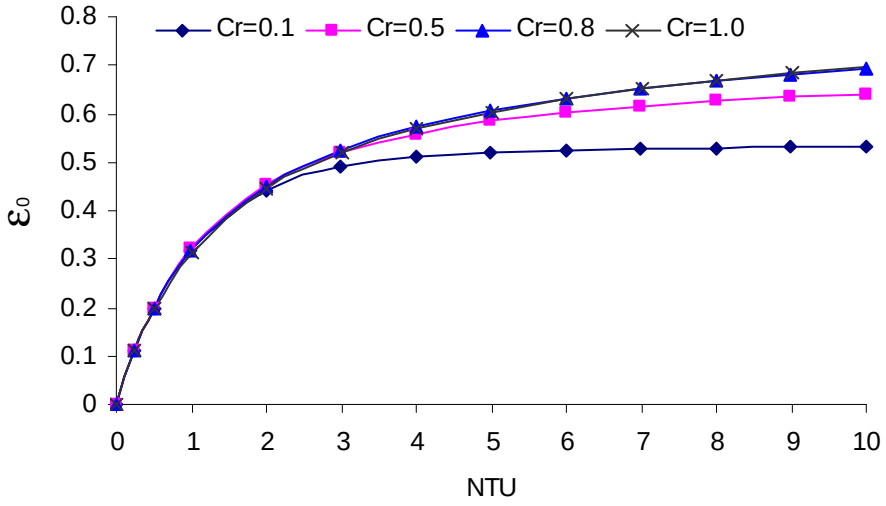

Figure 2.12 *Overall system effectiveness of the run-around system, ε_0, as the function of the number of transfer units, NTU, and capacity ratio, Cr , for each exchanger with $C_A < C_L$.*

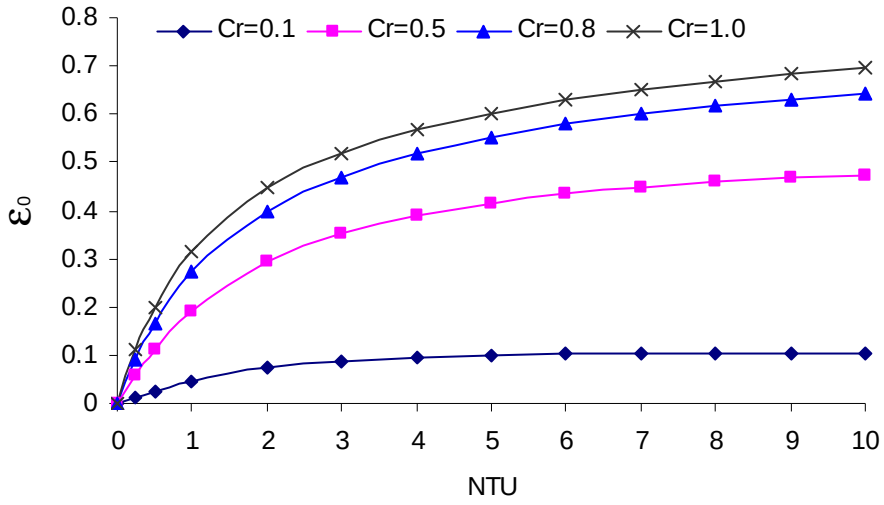

Figure 2.13 *Overall system effectiveness of the run-around system, ε_0, as the function of the number of transfer units, NTU, and capacity ratio, Cr , for each exchanger with $C_A > C_L$.*

Figures 2.12 and 2.13 show that the overall effectiveness of the run-around heat recovery system with cross-flow flat-plate heat exchangers increases with an increase of *NTU* for the same *Cr*. For both cases, when *NTU*>3 the overall effectiveness of the run-around system depends strongly on *Cr* and is a maximum when *Cr* approaches 1. In contrast, a single cross-flow flat-plate heat exchanger has a minimum effectiveness when *Cr*=1 as shown in Figure 2.11. The overall effectiveness of the system varies dramatically with *NTU* for *NTU*<3, but is nearly constant for *NTU*>6. Low *NTU* values result in a very low effectiveness which indicates that a large *NTU* should be sought when designing a run-around system with cross-flow flat-plate heat exchangers. The

total effectiveness of the run-around system is more sensitive to Cr for the case of $C_A > C_L$ than the case of $C_A < C_L$.

The overall effectiveness of the run-around system as a function of Cr was also investigated and the results are shown in Figure 2.14 and Figure 2.15.

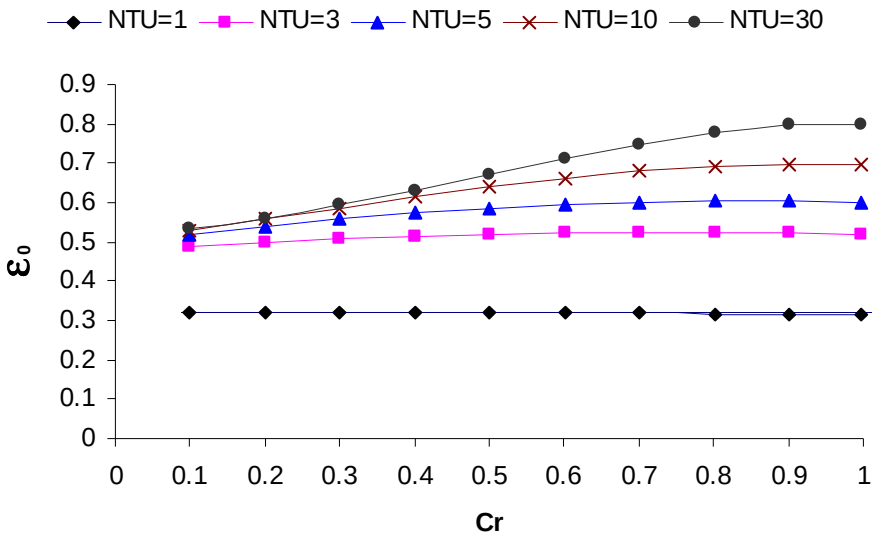

Figure 2.14 *Overall system effectiveness of the run-around system, ε_0, as a function of the heat capacity ratio, Cr, with $C_A < C_L$*

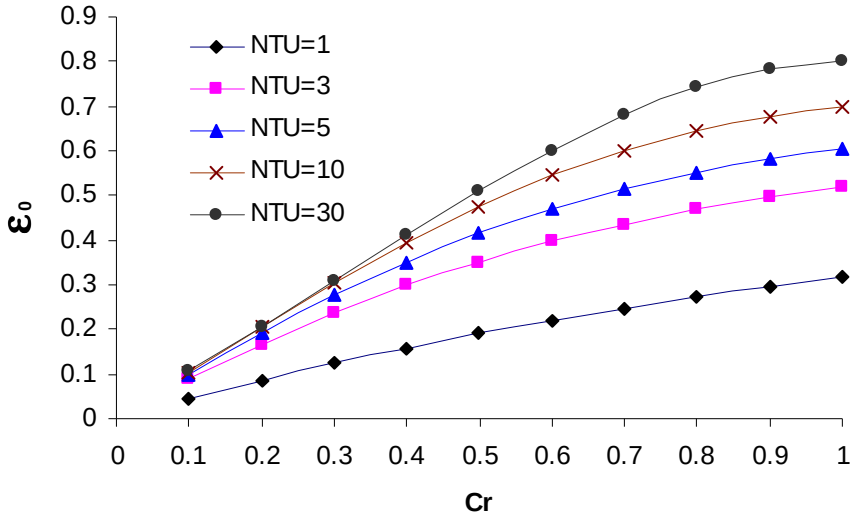

Figure 2.15 *Overall system effectiveness of the run-around system, ε_0, as a function of the heat capacity ratio, Cr, with $C_A > C_L$.*

From Figure 2.14 and 2.15, which show the overall effectiveness, ε_0, versus Cr, it can be seen that for any NTU, the overall effectiveness of the run-around system reaches its maximum at $Cr = 1$ for the case of $C_A > C_L$. But for the case of $C_A < C_L$, the overall effectiveness is maximum at $Cr = 1$ only for high NTU (e.g. $NTU \geq 10$, and it is nearly independent of Cr for small value of NTU (e.g. $NTU \leq 1$) . The maximum effectiveness is at various value of Cr for intermediate NTU (e.g. $3 \leq NTU \leq 10$). But for both cases, there is little change in the overall effectiveness for $0.7 \leq Cr \leq 1$.

In order to analyze the effect of varying the heat capacity rate of the liquid salt solution, C_L, on the overall effectiveness of the run-around systems, the ratio C_L / C_A is varied between 0 and 10 as shown in Figure 2.16.

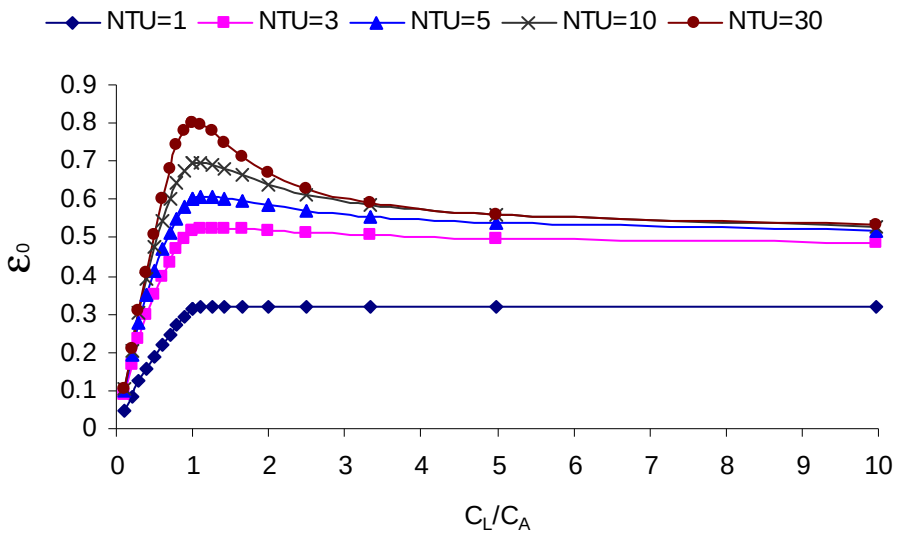

Figure 2.16 *Overall effectiveness of the run-around system as a function of* C_L / C_A *for various values of NTU.*

Figure 2.16 shows that the maximum overall effectiveness of a run-around system occurs at approximately $C_L / C_A = 1$ for high values of *NTU* (e.g. $NTU \geq 10$). For low values of *NTU* (e.g. $NTU \leq 1$), the effectiveness is nearly independent of C_L / C_A for $C_L / C_A > 1$. For $3 \leq NTU \leq 10$, the maximum effectiveness occurs at $C_L / C_A > 1$, but the effectiveness doesn't change so much for $0.8 \leq C_L / C_A \leq 1.2$. This means the heat capacity of the LiBr solution, C_L, should be kept in the range of $(0.8C_A < C_L < 1.2C_A)$ for the designing peak load condition of a run-around system for maximum heat rate.

It is noted that these findings for the optimum heat rate when $C_L / C_A \approx 1$ differ from the findings of Bennett et al. (1994) and Johnson et al. (1995) for run-around systems using finned-tube coils because they were dealing with designs where both the air and the liquid sides of the exchangers had turbulent flows. In this study, using low-

cost, plastic, cross-flow heat exchangers, laminar flow is used on both the air and liquid sides—so the best design conditions are quite different.

When the heat transfer rate between the supply and exhaust air streams of this run-around system exceeds that which is required (i.e. during moderate outdoor air temperature conditions), the system heat transfer rate can be controlled for part load conditions by reducing the value of C_L / C_A. This can be realized by reducing the mass flow of liquid (i.e. the pumping rate of the coupling fluid). Of course, as C_L / C_A is decreased, *NTU* will increase—so the trajectory of this control on Figure 2.16 will not be on a constant *NTU* line. Chapter 5 presents the sensitivity of effectiveness and heat transfer rate to the mass flow rate of the liquid.

2.5 Validation of the Model

2.5.1 Single Cross-Flow Heat Exchanger

The numerical model developed as outlined above, is quite general and it can be used to investigate variable fluid properties and exchanger operating conditions, but its accuracy needs to be demonstrated. In this section, the numerical solution is compared to analytical solutions for the temperature distribution in a single exchanger and effectiveness correlations from the literature.

Analytical solution of the simplified theoretical model of one heat exchanger

For a cross-flow flat-plate heat exchanger with both fluids unmixed and constant properties across the surface of the exchanger, Mason (1955) obtained an analytical

solution of the distribution of the dimensionless temperature difference between the two flows presented in (Kern and Kraus, 1972). The exact solution for the dimensionless temperature with constant fluid and convective properties is (see Appendix E for detailed development of the equation):

$$\theta(x,y) = e^{-(NTU_1)y-(NTU_2)x} \sum_{n=0}^{\infty} \left[\frac{(NTU_1)(NTU_2)xy}{(n!)^2} \right]^n \tag{2.29}$$

where:

$\theta = \frac{T_1 - T_2}{T_{1,in} - T_{2,in}}$ is the local dimensionless temperature difference at any point (x, y) on the heat exchanger surface.

$NTU_1 = \frac{U \cdot A}{C_1}$: the number of heat transfer units for flow channel 1 (e.g. the air side).

$NTU_2 = \frac{U \cdot A}{C_2}$: the number of heat transfer units for flow channel 2 (e.g. the liquid side).

This solution can be used to validate the numerical model presented in this chapter. The comparison of the analytical and numerical solutions of the distribution of the dimensionless temperature difference (θ) across the exchanger at any point (x, y) is shown in Figure 2.17. The actual temperature difference at each point is found by multiplying θ by ($T_{1,in} - T_{2,in}$).

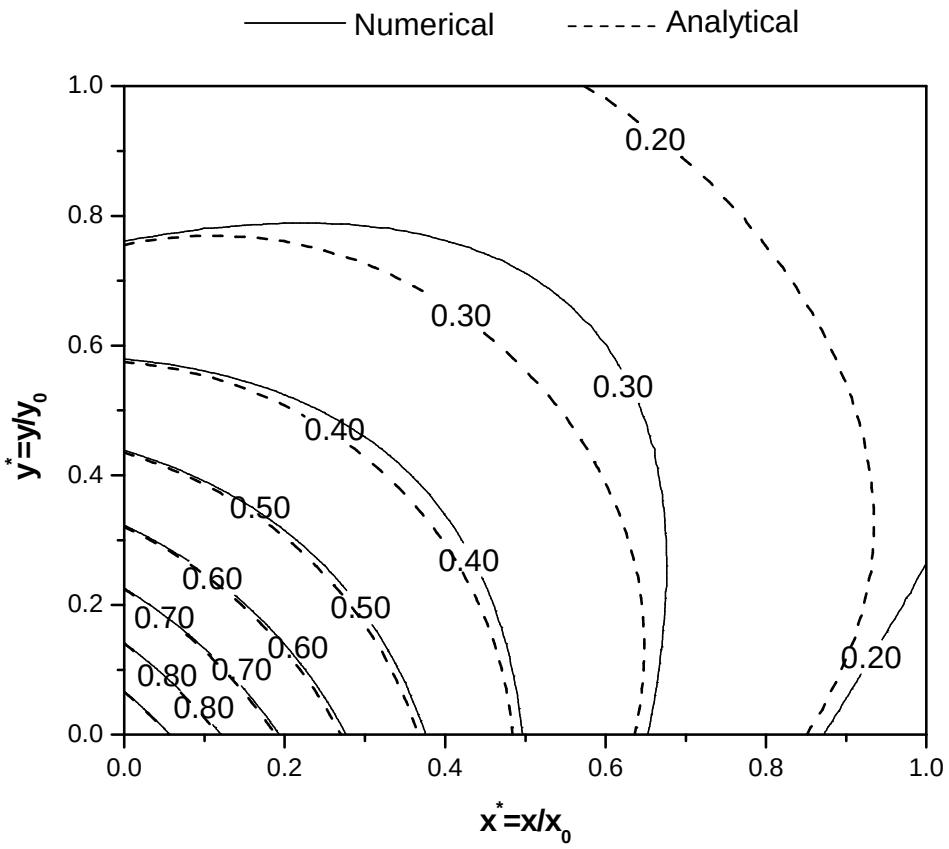

Figure 2.17 *Comparison of the dimensionless temperature difference(θ) distribution in one exchanger for the numerical result and analytical result with equation (2.29).*

From the Figure 2.17, it can be seen that the numerical solution using a grid of 100×100 nodes is very close to the analytical solution at every node except in the corner of the exchanger where the temperature gradient is the lowest. In spite of this apparent graphical contour discrepancy between the analytical and numerical solution, the actual temperature differences at any node are very small. The largest difference occurs at x^*=1 and y^*=1 where the difference is 0.08, which corresponds to $0.8^\circ C$ for a typical $10^\circ C$ temperature difference in energy recovery devices in HVAC applications. The average variance for all nodes is

$$V(\theta) = \frac{\sum_{1}^{N} \left(\theta_{analytical} - \theta_{numerical}\right)^2}{N} = 5.63 \times 10^{-5}, \tag{2.30}$$

The maximum variance at one node is $V_{\max}(\theta) = \max\{D(\theta)\ at\ any\ node\} = 4.74 \times 10^{-3}$.

This very close agreement with the analytical solution implies that the conduction/convection heat transfer model that has been developed gives excellent agreement with the exact analytical solution for a single cross-flow flat-plate exchanger. It should be noted that both the analytical and numerical models used similar assumptions; namely, constant wall heat flux and fully developed flows and heat transfer.

Analytical calculation of the effectiveness of the cross-flow flat-plate exchanger

For any heat exchanger it can be shown that (Inropera and Dewitt, 1996):

$$\varepsilon = f(NTU, Cr,\ flow\ arrangement) \tag{2.31}$$

where $NTU = \frac{U \cdot A}{C_{\min}}$ is the number of heat transfer units and $Cr = \frac{C_{\min}}{C_{\max}}$ is the heat capacity ratio of the two fluids.

For a cross-flow exchanger with both fluids unmixed the effectiveness can be determined using the analytical correlation (Incropera and Dewitt, 1996):

$$\varepsilon = 1 - \exp\left[\left(\frac{1}{C_r}\right)(NTU)^{0.22}\left\{\exp\left[-C_r(NTU)^{0.78}\right] - 1\right\}\right] \tag{2.32}$$

Using analytical correlation (2.32), the effectiveness of the cross-flow flat-plate heat exchanger can be compared with the effectiveness from the numerical model as shown in Figure 2.18.

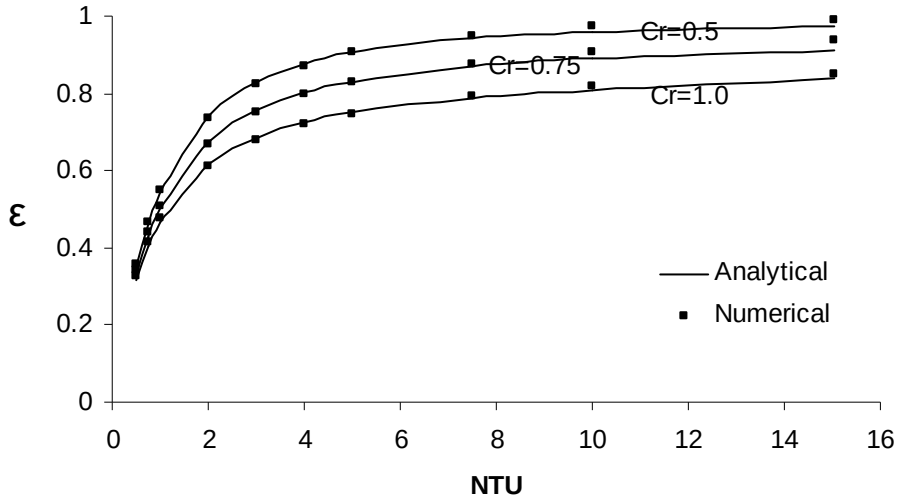

Figure 2.18 *Comparison of the numerical and analytical effectiveness for a cross-flow flat-plate heat exchanger.*

Figure 2.18 shows that effectiveness calculated with the numerical model agrees well with the correlation for a cross-flow flat-plate heat exchanger for $NTU<8$ and differs by a small amount for $10<NTU<15$. The maximum difference between the effectiveness calculated from the correlation and the model is 2.7% at $NTU=15$ and $Cr=0.75$. The average difference is only 1.1%. This comparison implies that the numerical model can predict the performance of a single heat exchanger accurately.

2.5.2 Run-Around System

Zeng (1990) showed that the overall effectiveness of the run-around heat recovery system, ε_0, is only a function of the number of transfer units, *NTU*, for each exchanger and thermal capacity rate ratio, *Cr* ($Cr = C_{\min} / C_{\max}$), for each exchanger and the thermal capacity ratio between the air and liquid solution flow. This relationship can be written in the form:

$$\frac{1}{\varepsilon_0} = \frac{C_{\min,A}}{\varepsilon_E \cdot C_{\min,E}} + \frac{C_{\min,A}}{\varepsilon_S \cdot C_{\min,S}} - \frac{C_{\min,A}}{C_L}. \tag{2.33}$$

For the case of equal heat capacity ratios for both the supply and exhaust air flows ($Cr_S = Cr_E$) and $NTU_S = NTU_E$ (i.e. equal surface area A_S and A_E), equation (2.33) can be simplified:

for $C_A \le C_L$:

$$\frac{1}{\varepsilon_0} = \frac{1}{\varepsilon_E} + \frac{1}{\varepsilon_S} - Cr, \tag{2.34}$$

where $Cr = C_A / C_L$,

and for $C_A > C_L$:

$$\frac{1}{\varepsilon_0} = \frac{1}{Cr} \cdot (\frac{1}{\varepsilon_E} + \frac{1}{\varepsilon_S} - 1), \tag{2.35}$$

where $Cr = C_L / C_A$.

This latter case (equation (2.35)) is of greatest interest for heat recovery in this study because for part load control $C_A > C_L$ (i.e., the heat transfer will be controlled by reducing the flow rate of the coupling fluid). With equations (2.33)-(2.35) and correlation equation (2.32), the overall effectiveness of the run-around system can be calculated and compared with simulation data. Figure 2.19 and Figure 2.20 present the comparison between analytical and numerical data for the case of equal exhaust and supply air mass flow rates and $NTU_S = NTU_E$.

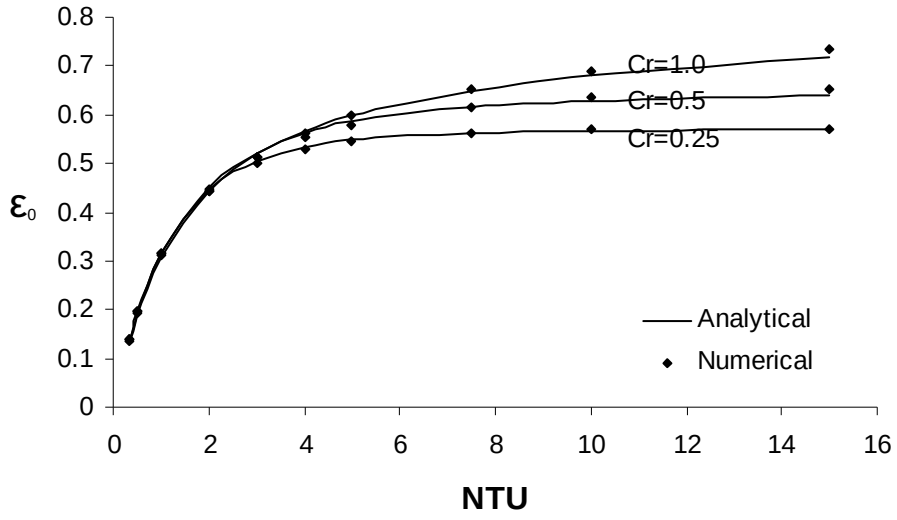

Figure 2.19 *Comparison of the analytical and numerical overall system effectiveness of the run-around system,* ε_0*, for* $C_A < C_L$.

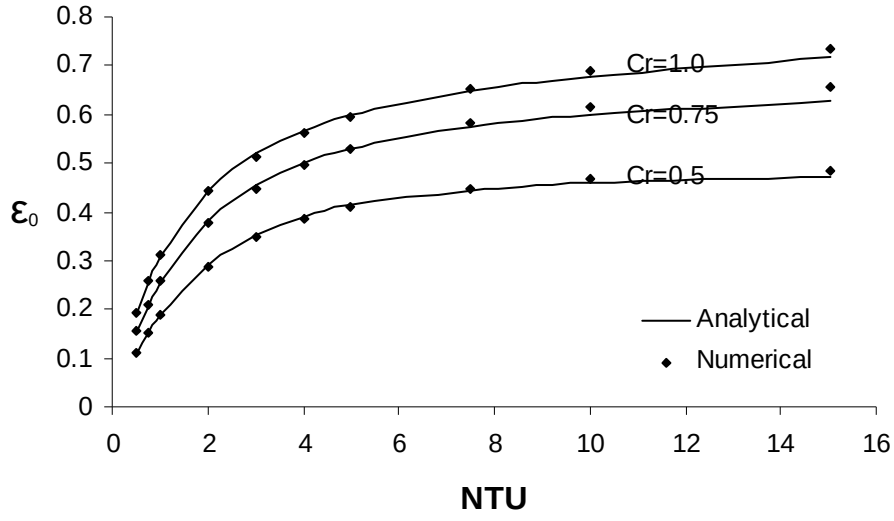

Figure 2.20 *Comparison of the analytical and numerical overall system effectiveness of the run-around system,* ε_0*, for* $C_A > C_L$.

Figures 2.19 and 2.20 show that the numerical results agree well with the analytical-correlation results, except when $NTU \geq 10$. This slight difference is thought to be caused by the correlation equation (2.32), which is less accurate when *NTU* is larger. The maximum difference between the effectiveness calculated from the correlation and the model is 2.1% at *NTU*=15 and *Cr*=1. The average difference is only 0.9%. This comparison implies that the numerical model can predict the performance of the run-around heat recovery system accurately.

Chapter 3

SINGLE HEAT AND MOISTURE EXCHANGER

3.1 Introduction

Consideration of both the heat transfer rates between the fluids and the mechanical pumping power expended to overcome fluid friction and move the fluids through the heat exchanger should be included in any heat exchanger design. Besides these two factors, the moisture transfer rates must also be considered in the design of exchangers that transfer heat and moisture. For exchangers operating with fluids with different phases (i.e., gas and liquid), the heat and moisture transfer will be coupled by phase changes. This research project will only deal with the heat and moisture transfer problem. The fluid friction problem which is usually a less difficult problem will be left to the future research.

The methodology of arriving at an optimum heat and moisture exchanger design is a complex one, not only because of the calculations required, but more particularly because of the many qualitative judgements that must be introduced. Kays and London (1984) provided a procedure for design of a heat exchanger as shown in Figure 3.1. This procedure is also applicable to the design of heat and moisture exchangers.

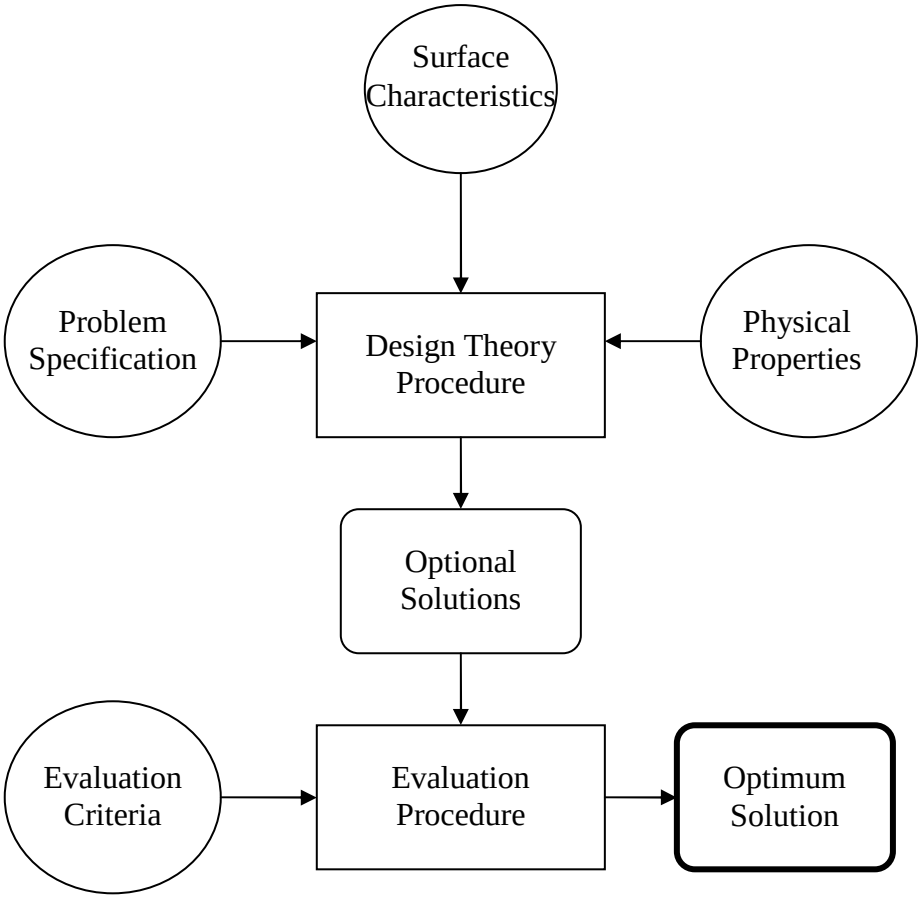

Figure 3.1 *Methodology of heat exchanger design*

It is the purpose of this chapter to investigate the thermal or heat transfer and moisture transfer design characteristics of a cross-flow plate exchanger using a numerical model. In this chapter, a theoretical model of the heat and moisture exchanger is developed which is then solved numerically. As in Chapter 2, the $\varepsilon - NTU$ method is employed to study the performance of the exchanger. For the moisture transfer in the exchanger, the number of mass transfer units, NTU_m, is introduced as follows:

$$NTU_m = \frac{U_m \cdot A}{M_{\min}}, \tag{3.1}$$

where U_m is the overall mass transfer coefficient and $M_{\min}$ is the minimum mass flow rate of the pure salt and dry air.

3.2 Theoretical Model

The geometry of one pair of flow channels for the cross-flow heat and moisture exchanger and the coordinate system for the mathematical model is shown in Figure 3.2. In this exchanger, it is assumed that water vapour can diffuse through each flat-plate semi-permeable membrane but liquid water and air will not be transferred. Other major assumptions in the formulation of the mathematical model are as follows:

1. The heat and mass transfer processes are in steady state and only in the z direction normal to each membrane.

2. The channel flow and the heat and mass transfer processes are fully developed throughout the exchanger.

3. Heat gain or loss due to the latent heat from the phase change of water at the membrane occurs only in the liquid component.

Assumptions 1 and 2 can be shown to be accurate for most typical geometries and operating conditions using sensitivity studies. These assumptions imply there are only two independent variables, *x* and *y*. The third assumption requires a separate analytical study to show that it is correct (Simonson and Besant, 1997). However,

assuming that the phase change energy is delivered only to the liquid desiccant is likely very close to the reality of phase change between an air stream and a liquid stream because phase change will occur at the air-liquid interface inside the membrane and the liquid side convective heat transfer coefficient is higher than the air side coefficient. In the exchangers studied in this thesis, the convection coefficient on the liquid desiccant side is typically 9 to 10 times greater than the convection heat transfer coefficient on the air side.

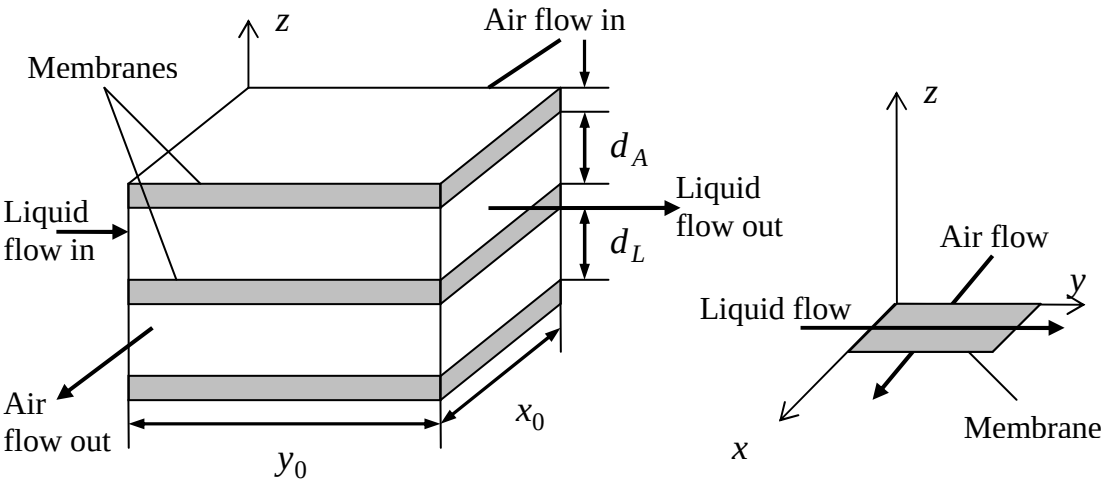

(a) One pair of flow channels (b) The coordinate system

Figure 3.2 *Schematic of a cross-flow enthalpy exchanger showing three semi-permeable membranes separating one liquid and one air channel.*

3.1.1 Dimensional Governing Equations

The governing mass balance and energy balance equations for analyzing the coupled heat and moisture transfer through the permeable membrane at any point (x, y) on the surface are:

Air side

At any point (x, y) in the exchanger, the water vapour flux through the membrane surface is balanced by the mass gain/loss in the air:

$$\frac{2U_m \cdot y_0}{m_{Air}}(W_{Air} - W_{Sol}) = -\frac{\partial W_{Air}}{\partial x}, \tag{3.2}$$

where the humidity ratios W_{Air} and W_{Sol} are the bulk mean values across the air and liquid channels at the same point (x, y), and the overall mass transfer coefficient for water mass flux between the air and salt solution is

$$U_m = \left[\frac{1}{h_{m,Sol}} + \frac{\delta}{k_m} + \frac{1}{h_{m,Air}}\right]^{-1}. \tag{3.3}$$

At any point (x, y) in the exchanger, the heat flux through the membrane surface is balanced by the heat gain/loss in the air:

$$\frac{2U \cdot y_0}{C_{Air}}(T_{Air} - T_{Sol}) = -\frac{\partial T_{Air}}{\partial x}, \tag{3.4}$$

where T_{Air} and T_{Sol} are the bulk mean temperatures at (x, y) in each fluid, and the overall heat transfer coefficient between the air and salt solution is

$$U = \left[\frac{1}{h_{Sol}} + \frac{\delta}{k} + \frac{1}{h_{Air}}\right]^{-1}. \tag{3.5}$$

The heat capacity rate of the air is

$$C_{Air} = m_{Air}(Cp_{Air} + W_{Air} \cdot Cp_{Vapor}), \tag{3.6}$$

where m_{Air} is the mass flow rate of the air through a single channel.

Liquid side

At any point (x, y) in the exchanger, the water flux through the membrane surface is balanced by the mass gain/loss in the liquid:

$$\frac{2U_m \cdot x_0}{m_{Salt}}(W_{Air} - W_{Sol}) = \frac{\partial X_{Sol}}{\partial y}, \tag{3.7}$$

where m_{salt} is the mass flow rate of the pure salt through a single channel. W_{Sol} is the equilibrium humidity ratio for air in contact with the salt solution (i.e., it is the humidity ratio that air would reach when left in contact with the salt solution for a long time). This equilibrium humidity ratio depends on the temperature and concentration of the salt solution:

$$W_{Sol} = f(X_{Sol}, T_{Sol}), \tag{3.8}$$

where

$$X_{Sol} = \frac{Mass\ of\ H_2O}{Mass\ of\ Salt}, \tag{3.9}$$

and the relationship will be presented in Section 3.1.4.

At any point (x, y) in the exchanger, the heat flux through the membrane surface is balanced by the net heat gain/loss by the liquid solution and the phase change at the membrane surface:

$$\frac{2U \cdot x_0}{C_{Sol}}\left(T_{Air} - T_{Sol}\right) = \frac{\partial T_{Sol}}{\partial y} - \frac{2U_m \cdot x_0}{C_{Sol}}(W_{Air} - W_{Sol}) \cdot h_{fg}\,, \tag{3.10}$$

and the heat capacity of the solution is:

$$C_{Sol} = m_{Sol} \cdot Cp_{Sol}\,, \tag{3.11}$$

where the mass flow rate of the salt solution is:

$$m_{Sol} = m_{Salt} \cdot (1 + X_{Sol})\,. \tag{3.12}$$

It is also assumed that $h_{m,Air}$ and $h_{m,Sol}$ are constant, therefore U_m will be independent of position in the exchanger which is similar to the assumption in Chapter 2 that h_{Air}, h_{Sol} and U are constant.

3.1.2 Dimensionless Governing Equations

Following the method presented in (Shah, 1981) and (Simonson and Besant, 1999), the governing equations can be arranged to highlight the governing dimensionless group (given in Table 3.1) for heat and mass transfer. These dimensionless groups are the number of transfer units for heat and mass transfer NTU and NTU_m. The equations for the air side are:

$$NTU_{m,Air}(W_{Air} - W_{Sol}) = -\frac{\partial W_{Air}}{\partial x^*}\,, \tag{3.13}$$

$$NTU_{Air}\left(T_{Air} - T_{Sol}\right) = -\frac{\partial T_{Air}}{\partial x^*}\,, \tag{3.14}$$

and the liquid side:

$$NTU_{m,Sol}(W_{Air} - W_{Sol}) = \frac{\partial X_{Sol}}{\partial y^*}, \tag{3.15}$$

$$NTU_{Sol}(T_{Air} - T_{Sol}) = \frac{\partial T_{Sol}}{\partial y^*} - \frac{2U_m x_0 y_0}{C_{Sol}}(W_{Air} - W_{Sol}) \cdot h_{fg}. \tag{3.16}$$

Where:

$$x^* = \frac{x}{x_0}, \tag{3.17}$$

$$y^* = \frac{y}{y_0}, \tag{3.18}$$

$$NTU_{Air} = 2 \cdot \frac{U \cdot x_0 \cdot y_0}{C_{Air}}, \tag{3.19}$$

$$NTU_{m,Air} = 2 \cdot \frac{U_m \cdot x_0 \cdot y_0}{m_{Air}}, \tag{3.20}$$

$$NTU_{Sol} = 2 \cdot \frac{U \cdot x_0 \cdot y_0}{C_{Sol}}, \tag{3.21}$$

$$NTU_{m,Sol} = 2 \cdot \frac{U_m \cdot x_0 \cdot y_0}{m_{Sol}} \tag{3.22}$$

Table 3.1 *Dimensionless Variables and Parameters for governing equations of a heat and moisture exchanger*

x^*	y^*	NTU_{Air}	$NTU_{m,Air}$	NTU_{Sol}	$NTU_{m,Sol}$
$\frac{x}{x_0}$	$\frac{y}{y_0}$	$2\cdot\frac{U\cdot x_0\cdot y_0}{C_{Air}}$	$2\cdot\frac{U_m\cdot x_0\cdot y_0}{m_{Air}}$	$2\cdot\frac{U\cdot x_0\cdot y_0}{C_{Sol}}$	$2\cdot\frac{U_m\cdot x_0\cdot y_0}{m_{Sol}}$

Since the heat and moisture transfer are coupled in the heat and moisture exchanger, the equilibrium vapour pressure correlations for the salt solution has to be employed for the closure of the governing equations. This will be discussed in Section 3.1.4. The detailed development of the governing equations is given in Appendix B.

3.1.3 Overall Heat and Mass Transfer Coefficients

As shown in equations (3.3) and (3.5), the overall heat and mass transfer coefficients depend on the convection coefficients (h and h_m) and the membrane conductivities (k and k_m). The convection heat transfer coefficients can be obtained as described in Chapter 2 and the convection mass transfer coefficients can be obtained using an analogy between the heat and mass transfer. The Chilton-Colburn analogy (Welty et al., 2001):

$$Sh = Nu \cdot Le^{-2/3} \tag{3.23}$$

gives an equation relating the mass transfer coefficient (h_m) to the heat transfer coefficient (h) as follows:

$$h_m = \frac{h}{Cp} Le^{-2/3}. \tag{2.24}$$

For the semi-permeable membrane, the heat and mass flow conductivities (k and k_m) depend on the material chosen. Polytetrafluoroethylene (PTFE) is used in this research, and the typical values of the heat and mass flow conductivities are $k = 0.334\, W/(m \cdot K)$ and $k_m = 3.91 \times 10^{-5}\ kg/(m \cdot s)$.

3.1.4 Equilibrium Humidity Ratio of Aqueous Desiccant Solutions

In order to solve equation (3.7) and determine the moisture transfer through the membrane, the equilibrium humidity ratio of the salt solution is required. Figure 3.3 illustrates an equilibrium curve which shows the relationship between the concentration of the solute in the liquid phase and the partial pressure of the solute in the gas phase (Welty et al., 2001). Equations relating the equilibrium concentrations in the two phases have been developed and are presented in many thermodynamic textbooks. In the case of an ideal gas and dilute liquid mixtures, the relations are very simple. Raoult's law for dilute liquid mixtures is:

$$p_G = x_G P_G , \tag{3.25}$$

where p_G is the equilibrium partial pressure of a component *G* in the vapour phase above the liquid phase, x_G is the mole fraction of *G* in the liquid mixture, and P_G is the vapour pressure of pure *G* at the equilibrium temperature.

When the gas phase is an ideal gas, Dalton's law for mixtures of ideal gases is obeyed. This is:

$$p_G = y_G P , \tag{3.26}$$

where y_G is the mole fraction of *G* in the gas phase and *P* is the total pressure of the system. When both phases are ideal, the two equations may be combined to obtain a relation between the concentration terms, x_G and y_G , at constant pressure and temperature, the combined Raoult-Dalton equilibrium law stipulates

$$y_G P = x_G P_G \,. \tag{3.27}$$

For equilibrium conditions between gas and liquid phases in dilute solutions, Henry's law for the partial vapour pressure of simple mixtures applies,

$$p_G = H_e \cdot C_G \,, \tag{3.28}$$

where H_e is the Henry's law constant and C_G is the equilibrium composition of *G* in the dilute liquid phase.

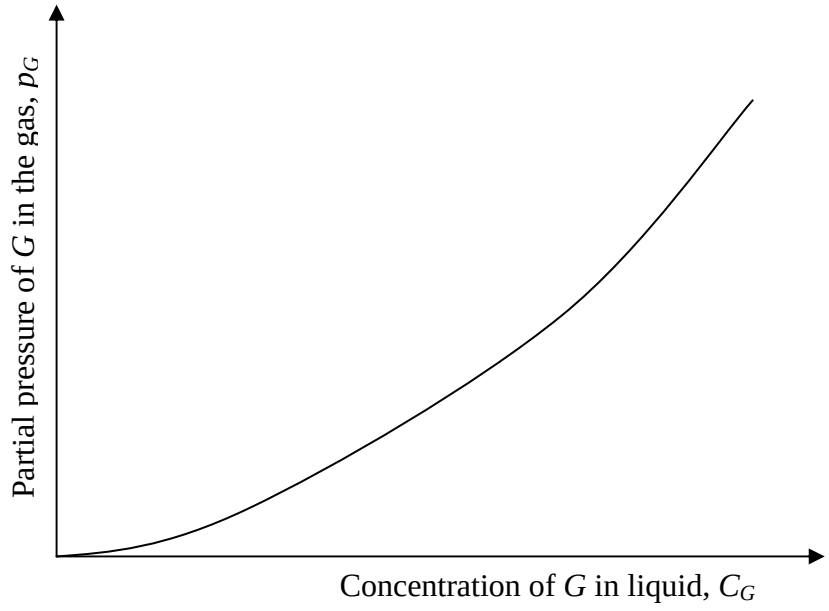

Figure 3.3 *Equilibrium distribution of solute G between a gas a liquid phase at one temperature.*

For the cases of non-ideal gas and liquid phases, empirical equations are required to relate the equilibrium values of the two phases. In this research, the correlations developed by Cisternas and Lam (1991) are used:

$$\log p_v = KI[A - B/(T - E_s)] + [C - D/(T - E_s)], \tag{3.29}$$

where

$$A = A_s + 3.60591e^{-4} \cdot I + M_s / 2303, \tag{3.30}$$

$$B = B_s + 1.382982 \cdot I - 0.031185 \cdot I^2, \tag{3.31}$$

$$C = C_s - 3.99334e - 1.11614e^{-4} \cdot I^2 + M_s \cdot I \cdot (1 - \chi) / 2303, \tag{3.32}$$

$$D = D_s - 0.138481 \cdot I + 0.027511 \cdot I^2 - 1.79277e^{-3} \cdot I^3, \text{ and} \tag{3.33}$$

$$\chi = 2 \cdot (v_+ + v_-) / (v_+ \cdot Z_+^2 + v_- \cdot Z_-^2). \tag{3.34}$$

Where A_s, B_s, C_s, D_s, and E_s are constants, T is the temperature of the salt solution (K), I is the ionic strength (mol/kg), M_s is the molecular weight of solvent (i.e. water), K is an electrolyte parameter, v_+ is the number of moles of cation and v_- is the number of moles of anion produced by the dissociation of one mole of the electrolyte, and Z_+ denotes the valency of cation and Z_- the valency of anion. These constants are listed in Table 3.2.

Table 3.2 *Constants for LiBr and LiCl solutions used in the correlations for equilibrium vapour pressure(Cisternas and Lam, 1991)*

	A_s	B_s	C_s	D_s	E_s	K
LiBr	-0.021302	-5.390915	7.192959	1730.2857	39.53	1.0
LiCl	-0.021302	-5.390915	7.192959	1730.2857	39.53	0.72567

The equilibrium humidity ratio of the solution (W_{Sol}) can be determined by knowing the partial pressure of the water vapour, p_w and the total pressure, P, (ASHRAE, 2001).

$$W_{Sol} = 0.62198 \frac{p_v}{P - p_v} \tag{3.35}$$

With equations (3.29)-(3.35) we can generate equilibrium concentration lines for the LiBr and LiCl solutions and superimpose these on the psychrometric chart as shown in Figure 3.4 and Figure 3.5, where C_{Salt} is the salt concentration at equilibrium and

$$C_{Salt} = \frac{1}{1 + X_{Sol}}. \tag{3.36}$$

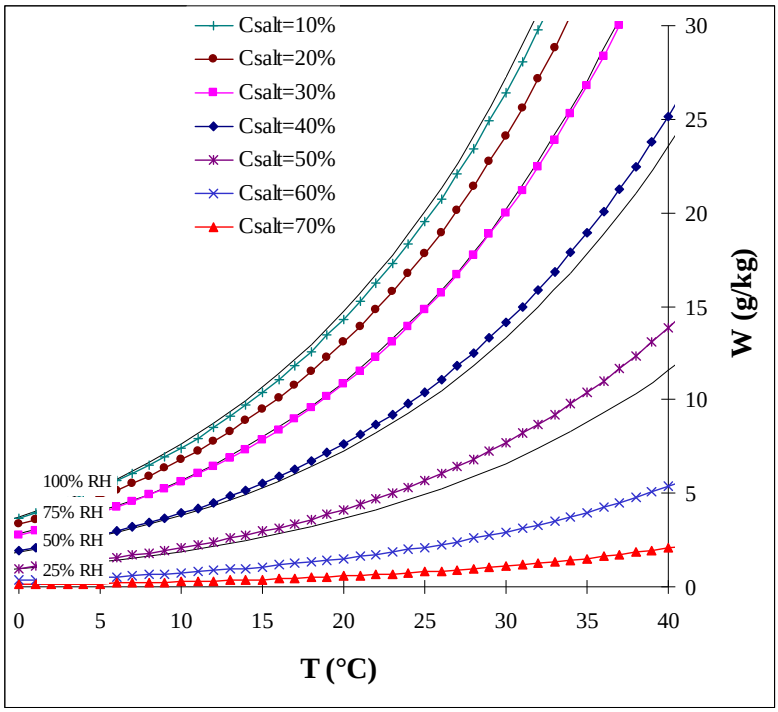

Figure 3.4 *Equilibrium concentration lines of the LiBr solution superimposed on the psychrometric chart*

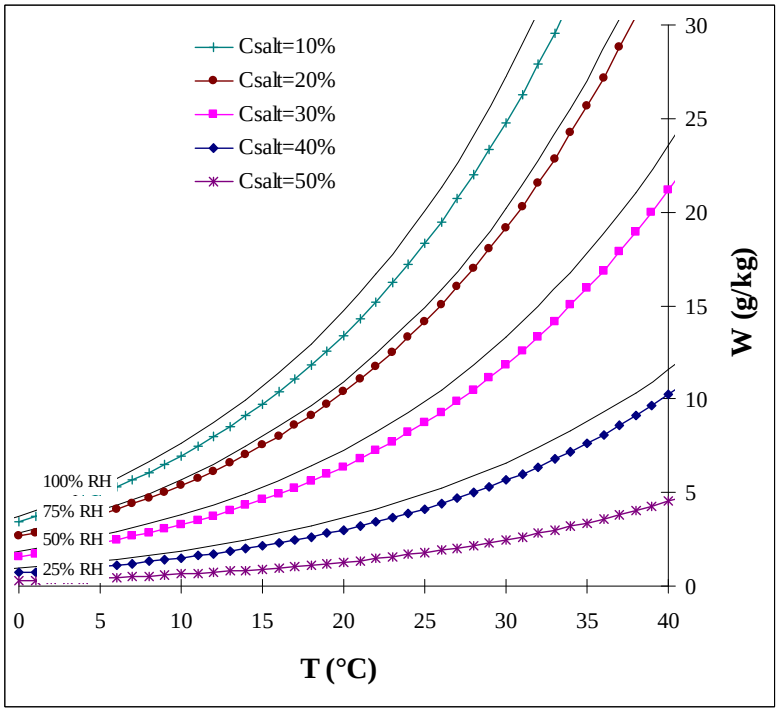

Figure 3.5 *Equilibrium concentration lines of the LiCl solution superimposed on the psychrometric chart*

From Figure 3.4 and Figure 3.5 it can be seen that the equilibrium concentration lines of these two salt solutions are very similar to the constant relative humidity lines on the psychrometric chart.

3.1.5 Boundary Conditions

The required boundary conditions are the temperature and humidity ratio of the air at the inlet of the exchanger at the air side. They are assumed to be uniform and constant.

Air side (inlet) ($x^* = 0, y^*$):

$$T_{Air}\,|_{x^*=0} = T_{Air,in}\text{, and} \tag{3.37}$$

$$W_{Air}\,|_{x^*=0} = W_{Air,in}\,. \tag{3.38}$$

Similarly, the temperature and mass fraction of water in the salt solution are the required boundary conditions on the liquid side. Liquid side (inlet) ($x^*, y^* = 0$):

$$T_{Sol}\,|_{y^*=0} = T_{Sol,in}\text{, and} \tag{3.39}$$

$$X_{Sol}\,|_{y^*=0} = X_{Sol,in}\,. \tag{3.40}$$

The appropriate boundary conditions for the governing equations can be summarized as shown in Figure 3.6.

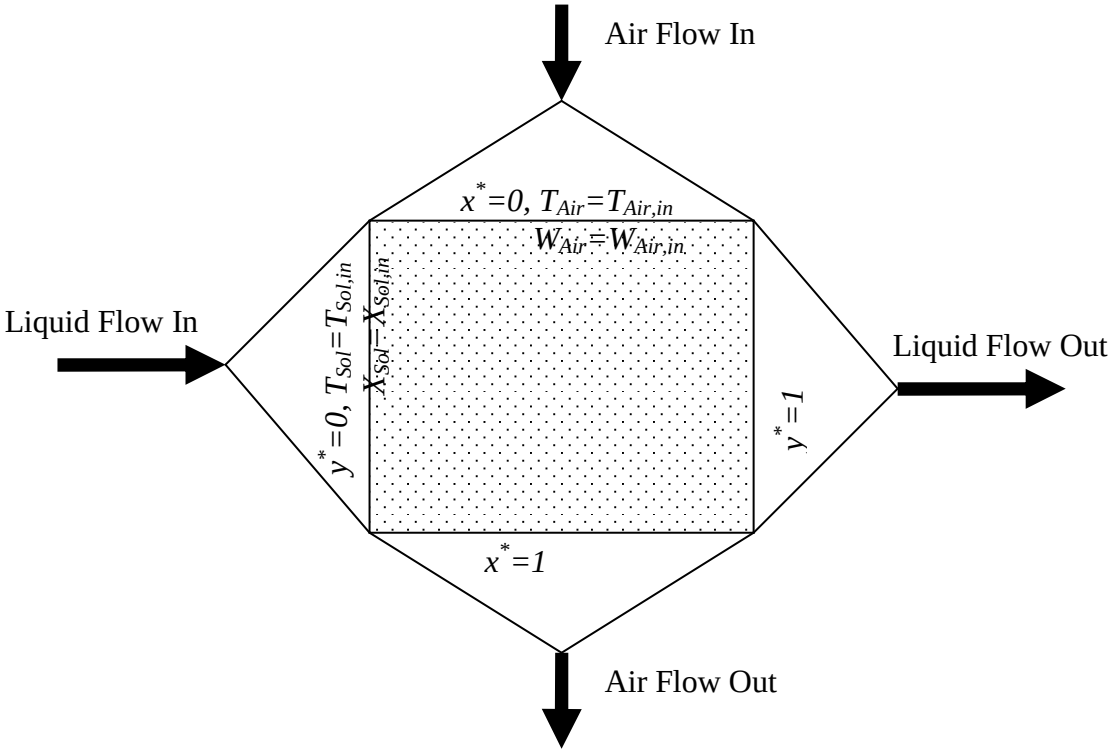

Figure 3.6 *Boundary conditions for the heat and moisture exchangers*

3.1.6 Effectiveness Definition for a Single Heat and Moisture Exchanger:

The sensible effectiveness of a single heat and moisture exchanger is relatively straightforward and easy to define. As presented in Chapter 2, the sensible effectiveness of the single exchanger is:

$$\varepsilon_s = \frac{C_{Air} \cdot (T_{Air,in} - T_{Air,out})}{C_{\min} \cdot (T_{Air,in} - T_{Sol,in})}, \tag{3.41}$$

where $C_{\min} = \min(C_{Air}, C_{Sol})$ and the inlet parameters are shown in Figure 3.7.

On the other hand, the latent and total effectiveness of the exchanger are not so straightforward to define because the maximum moisture or energy transfer is difficult

to define for coupled heat and moisture transfer between a liquid and air. A definition of the maximum possible moisture transfer is required because latent effectiveness is the ratio of the actual moisture transfer to the maximum possible moisture transfer:

$$\varepsilon_l = \frac{m_{Air} \cdot (W_{Air,in} - W_{Air,out})}{Maximum\ Possible\ Moisture\ Transfer}. \tag{3.42}$$

The maximum possible moisture transfer would occur in an ideal exchanger that had an infinite moisture transfer surface area. With this ideal exchanger two possibilities could exist, depending on the mass flow rate of the air and salt solution: (1) the outlet conditions on the air side ($W_{Air,out}$) would be in equilibrium with the inlet salt solution ($X_{Sol,in}$), or (2) the outlet conditions on the liquid side ($X_{Sol,out}$) would be in equilibrium with the inlet air conditions ($W_{Air,in}$). Since the moisture transfer on the air side and liquid side must be equal at steady state, the maximum possible moisture transfer can be calculated with:

Maximum Possible Moisture Transfer

$$= \min\{m_{Air} \cdot (W_{Air,in} - W_{Sol,in}), m_{Salt} \cdot (X_{Air,in} - X_{Sol,in})\}, \tag{3.43}$$

where $W_{Sol,in}$ is the humidity ratio for air in equilibrium with the inlet salt solution,

$$W_{Sol,in} = f(X_{Sol,in}, T_{Sol,in}), \tag{3.44}$$

and $X_{Air,in}$ is the mass faction of water for the liquid desiccant in equilibrium with the inlet air,

$$X_{Air,in} = f^{-1}(W_{Air,in}, T_{Air,in}). \tag{3.45}$$

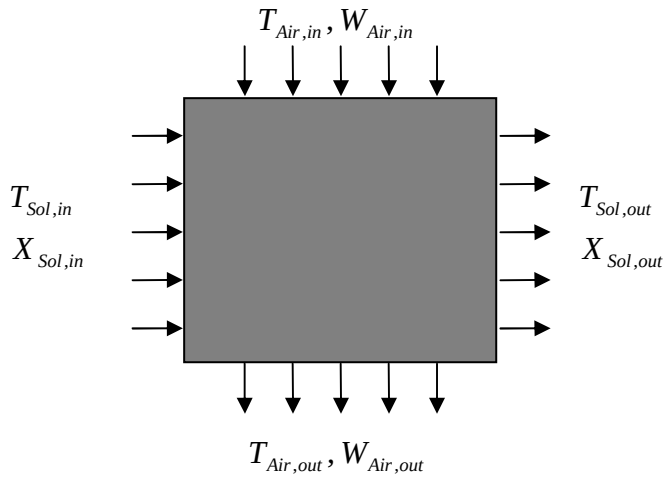

Figure 3.7 *Schematic of a cross-flow heat and moisture exchanger*

With the sensible effectiveness and the latent effectiveness of a single exchanger, the total effectiveness of the single exchanger can be estimated with following correlation (Simonson, 1998):

$$\varepsilon_t = \frac{\varepsilon_s + \varepsilon_l \cdot H^*}{1 + H^*} \tag{3.46}$$

where $H^* \approx 2500 \frac{\Delta W}{\Delta T}$ is the operating condition factor. ΔW is the inlet humidity ratio difference of the air and salt solution and ΔT is the inlet temperature difference of the air and salt solution.

3.3 Numerical Solution Method and Results

The numerical solution scheme for the heat and moisture exchanger is similar to that for the sensible heat exchanger (see Appendix B for more details). The under relaxation iteration scheme is used to provide a stable solution and the solution is

considered converged when the change in both T and W is less than 10^{-12}. The results in this chapter are obtained with 100×100 spatial nodes which give a stable solution and increasing the number of nodes has little effect on the solution. The details of the algorithm for the exchanger are given in Appendix C. The parameters of the heat and moisture exchanger used to generate the results in this chapter are shown in Table 3.3 and the operating conditions are in Table 3.4.

Table 3.3 *Parameters and properties of the heat and moisture exchanger used to generate the numerical results in Chapter 3.*

Name	Symbol	Value
Size of the exchanger	$x_0 \times y_0 \times z_0$	$0.3\,m \times 0.3\,m \times 0.3\,m$
Channel thickness of the air side	d_A	2 mm
Channel thickness of the liquid side	d_L	0.3mm
Membrane thickness	δ	0.5 mm
Heat conductivity of the membrane	k	$0.334\,W/(m \cdot K)$,
Mass conductivity of the membrane	k_m	$3.91 \times 10^{-5}\ kg/(m \cdot s)$

Table 3.4 *Operating conditions of the single exchanger in Chapter 3*

Inlet temperature of the air stream ($T_{Air,in}$)	$306\,K\ (32.85\ ^{\circ}C)$
Inlet humidity ratio of the air stream ($W_{Air,in}$)	$16\,g/kg$
Inlet temperature of the liquid stream ($T_{Sol,in}$)	$287\,K\ (13.85\ ^{\circ}C)$
Inlet concentration of the liquid stream (,$X_{Sol,\,in}$)	$1.15\,kg/kg\,(46.51\%)$
Mass flow rate of the air stream	$0.3\,kg/s$
Mass flow rate of the liquid stream	$0.2\,kg/s$

Graphical results are presented for the temperature and the moisture contents and are compared with two extreme cases—one without moisture transfer and one without heat transfer. Comparisons of the temperature and moisture content distribution in the exchanger are shown in Figure 3.8 and Figure 3.9 with and without moisture or heat transfer.

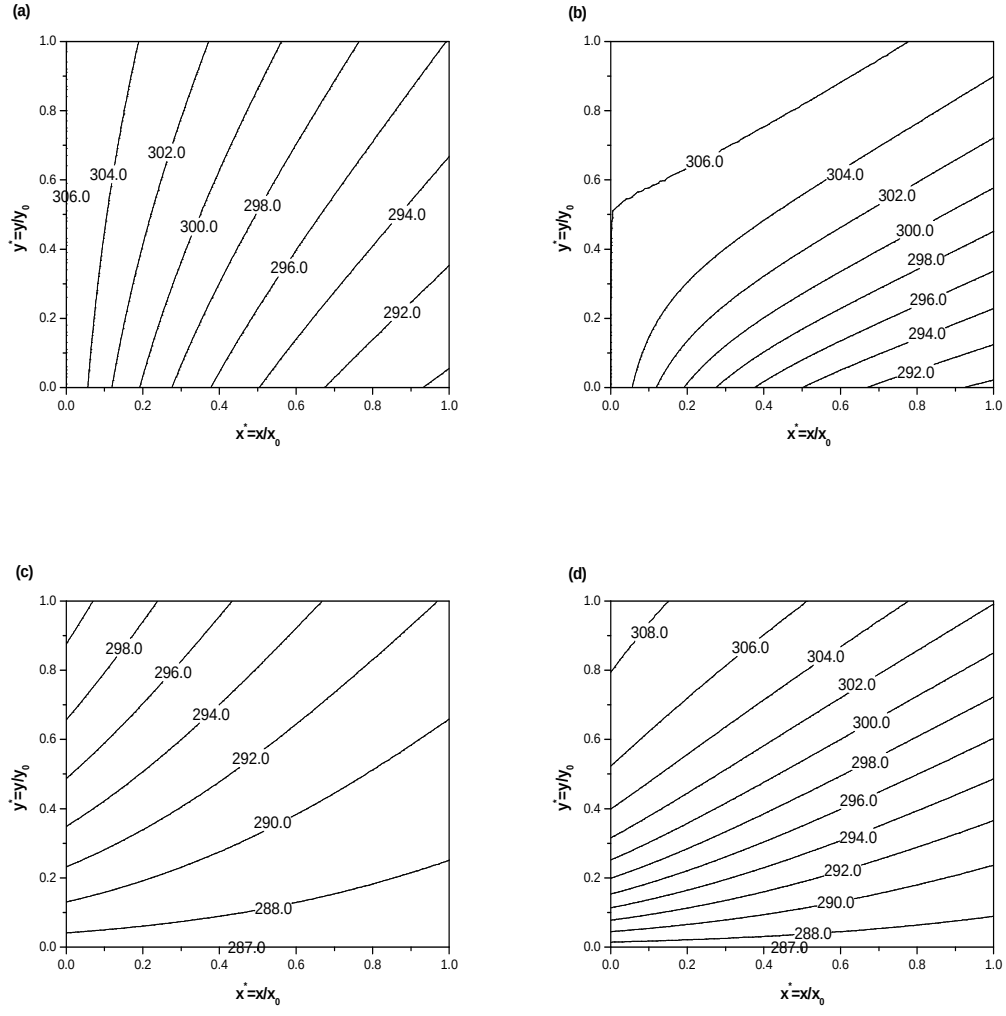

Figure 3.8 *Temperature distributions in one exchanger for air (in positive x-direction) (a) without moisture transfer and (b) with moisture transfer, and LiBr salt solution (in positive y-direction) (c) without moisture transfer and (d) with moisture transfer*

Figure 3.8(b) and Figure 3.8(d) show that with the moisture transfer and phase change, the temperature on the air side can be higher than the boundary condition inlet temperature (306 K) over a significant region of the exchanger. Furthermore, even in the solution side the temperature can exceed both the inlet air temperature of 306 K and the air temperature for $y^* > 0.8$ and $x^* < 0.4$. This means that the liquid is actually heating the air at this part of the exchanger even though the inlet temperature of the liquid is less than the inlet temperature of the air. The air side temperature distributions differ significantly with and without moisture transfer. On the solution side, the contours are similar in shape but the temperature magnitudes differ significantly.

The operating conditions in this example are such that moisture transfer is from the air stream to the liquid desiccant. This transition from a vapour to a liquid results in a release of energy. The net result is that the temperatures in the air and the liquid increase due to the phase change, which is expected.

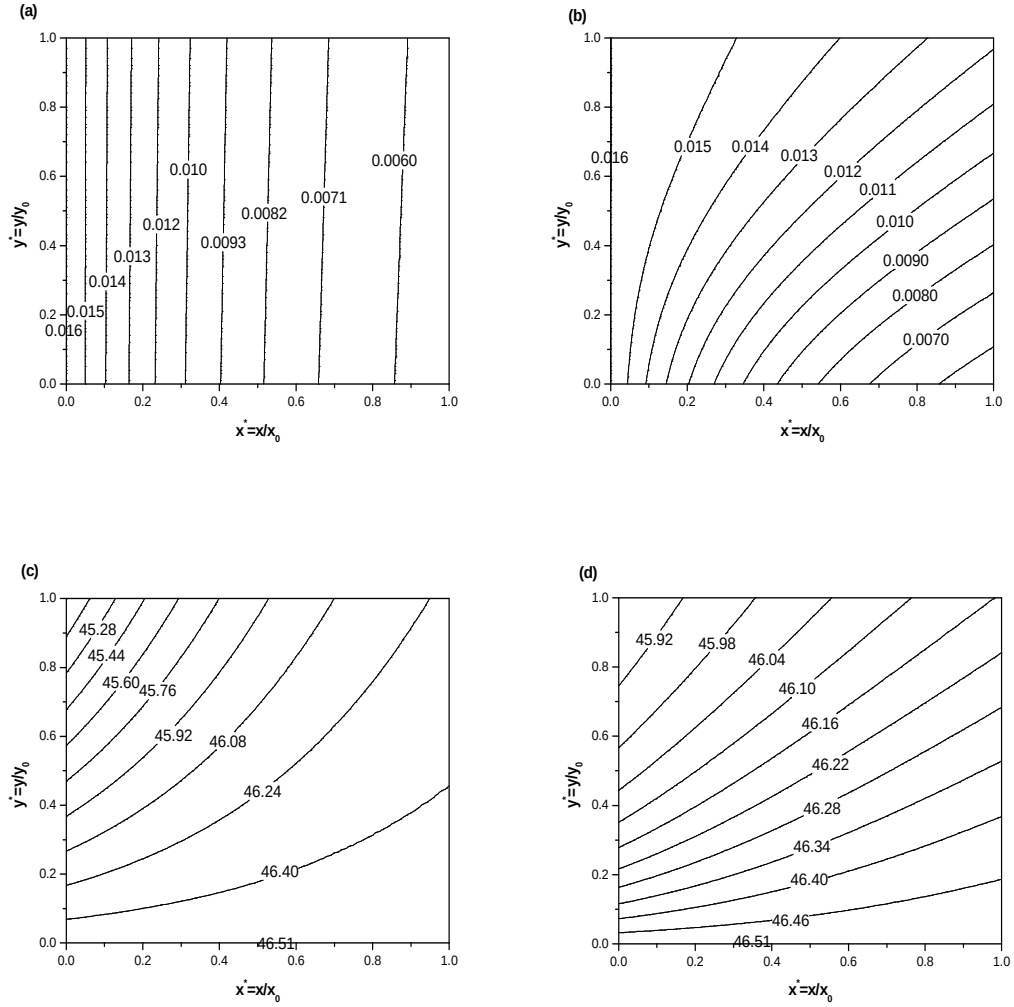

Figure 3.9 *Humidity ratio and salt concentration distributions in one exchanger for air (in positive x-direction) (a) without heat transfer and (b) with heat transfer, and LiBr salt solution(in positive y-direction) (c) without heat transfer and (d) with heat transfer*

Figure 3.9(b) and Figure 3.9(d) show that with heat transfer, both the contour and the magnitudes of the moisture contents of the air differ significantly. On the solution side, however, the contour differs only slightly but the magnitudes differ significantly with and without heat transfer. These results demonstrate that the phase change in the exchanger has a great impact on the performance of the exchanger. For some extreme

cases, the fluid, which is supposed to be cooled, may be actually heated because of the phase change.

To compare with the heat exchanger studied in Chapter 2, the same operating conditions, as shown in Table 3.5, are selected for the heat and moisture exchanger. Also, the same *NTU* and *Cr* value are chosen to simulate the heat and moisture exchanger. The results are presented in Figure 3.10, Figure 3.11 and Figure 3.12.

Table 3.5 *Operating conditions of the single heat and moisture exchanger for NTU and Cr study*

Inlet temperature of the air stream ($T_{Air,in}$)	$308.15\,K$ $(35\ ^{\circ}C)$
Inlet humidity ratio of the air stream($W_{Air,in}$)	$17.5\,g/kg$
Inlet temperature of the liquid stream($T_{Sol,in}$)	$297.15\,K$ $(24\ ^{\circ}C)$
Inlet concentration of the liquid stream($X_{Sol,,in}$)	$1.5\,kg/kg(40\%)$

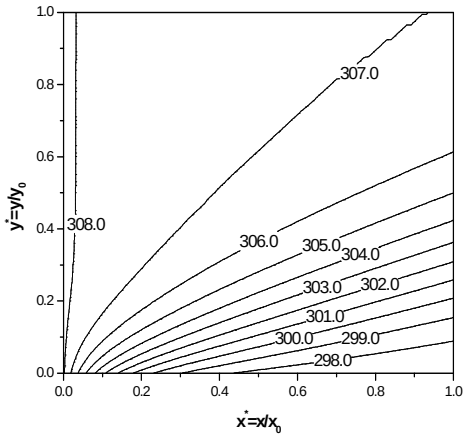

a. $T_{Air}(x^*, y^*)$ (K), air side

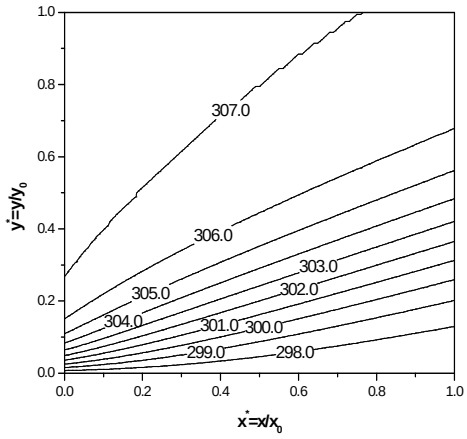

b. $T_{Sol}(x^*, y^*)$ (K), liquid side

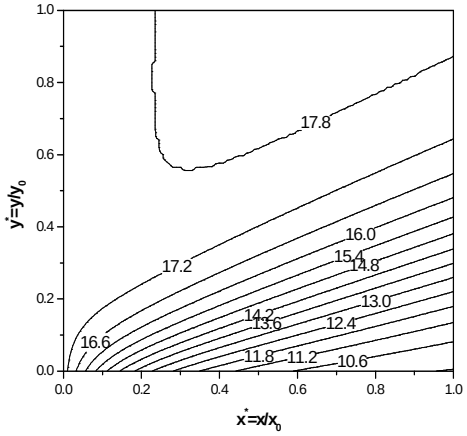

c. $W_{Air}(x^*, y^*)$ (g/kg), air side

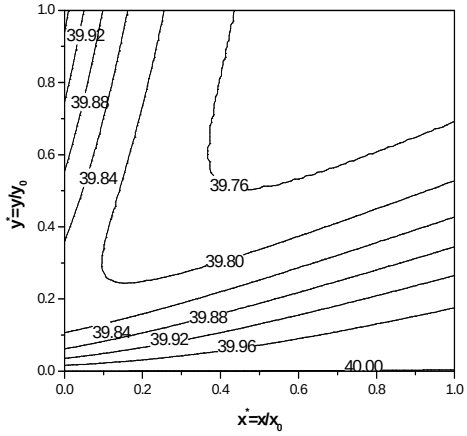

d. $C_{Salt}(x^*, y^*)$ (%), liquid side

Figure 3.10 *Temperature and moisture distributions in one exchanger for NTU=6 and Cr=1(air flow in positive x-direction and liquid flow in positive y-direction).*

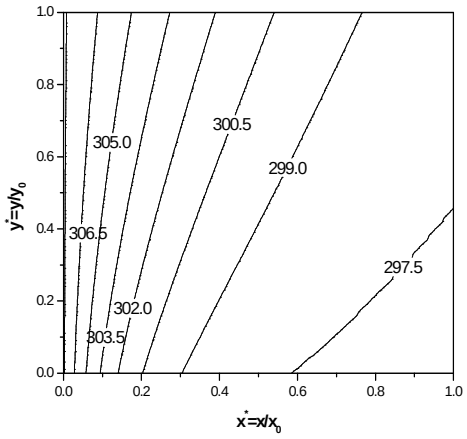

a. $T_{Air}(x^*, y^*)$ (K), air side

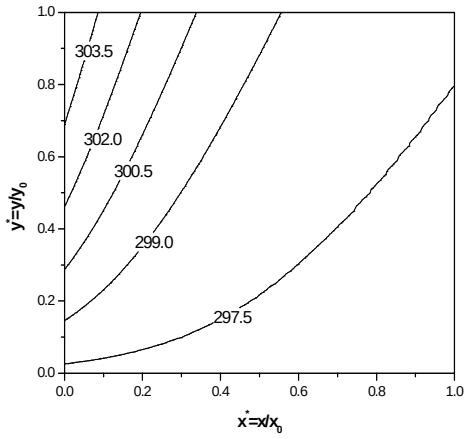

b. $T_{Sol}(x^*, y^*)$ (K), liquid side

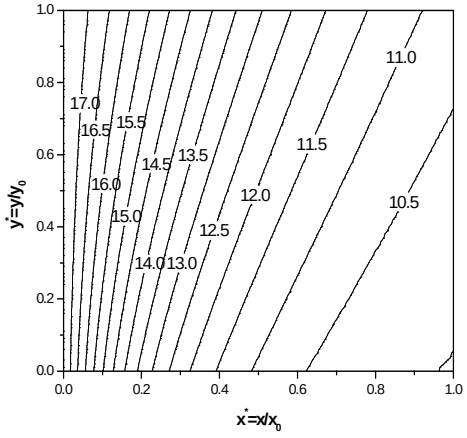

c. $W_{Air}(x^*, y^*)$ (g/kg), air side

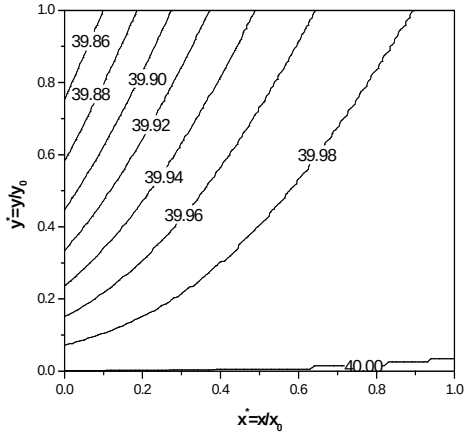

d. $C_{Salt}(x^*, y^*)$ (%), liquid side

Figure 3.11 *Temperature and moisture distributions in one exchanger for NTU=6 and Cr=0.1, (C_{Air}<C_{Sol}, air flow in positive x-direction and liquid flow in positive y-direction)*

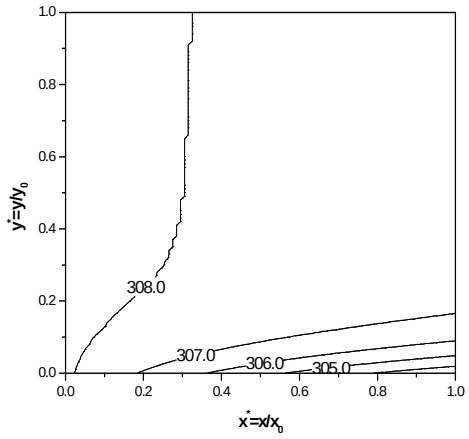

a. $T_{Air}(x^*, y^*)$ (K), air side

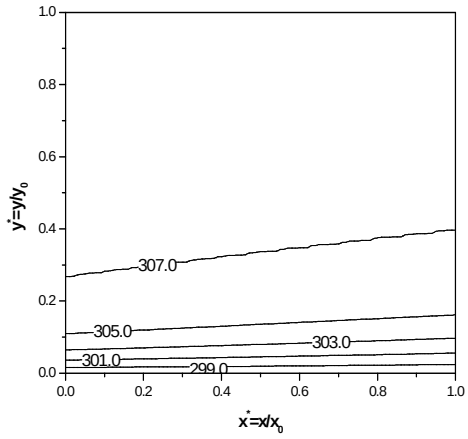

b. $T_{Sol}(x^*, y^*)$ (K), liquid side

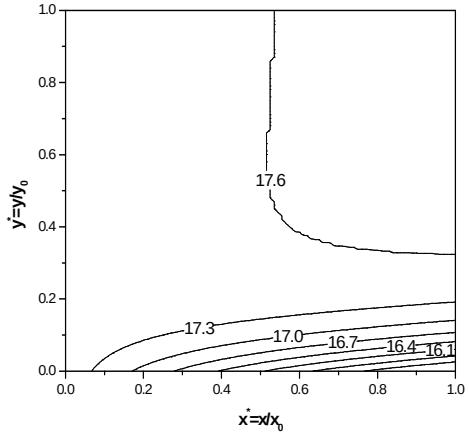

c. $W_{Air}(x^*, y^*)$ (g/kg), air side

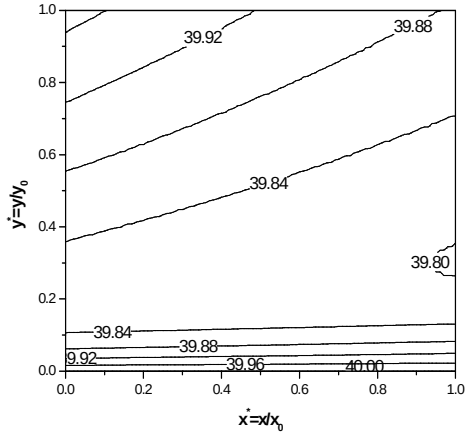

d. $C_{Salt}(x^*, y^*)$ (%), liquid side

Figure 3.12 *Temperature and moisture distributions in one exchanger for NTU=6 and Cr=0.1, (C_{Air}>C_{Sol}, air flow in positive x-direction and liquid flow in positive y-direction).*

From Figure 3.10, Figure 3.11 and Figure 3.12, it can be seen that the distributions of the isothermal temperature lines in the heat and moisture exchanger are

quite different from those presented in Chapter 2 (Figures 2.8-2.10) for a heat exchanger. This indicates that the moisture transfer and the phase change have a great effect on the distribution of the temperature in the exchangers. Thus the moisture transfer and phase change will affect the performance of the exchangers. The phase change also means that the magnitude of the sensible heat flux from the air to the liquid, $q(z)_A$, does not equal the magnitude of the sensible heat flux from the liquid to the air, $q(z)_L$. The balance of the heat transferred in the exchanger is as follows:

$$\begin{aligned} &\frac{1}{x_0 \cdot y_0} C_A \frac{\partial T_{Air}}{\partial x^*} = q(z)_A(x^*, y^*) \\ &= q(z)_L(x^*, y^*) + \dot{m} h_{fg} = \frac{1}{x_0 \cdot y_0} C_L \frac{\partial T_{Sol}}{\partial y^*} + \dot{m} h_{fg} \end{aligned} \quad . \tag{3.47}$$

Equation (3.47) indicates that the moisture transfer term, $\dot{m} h_{fg}$, affects the gradients of temperature ($\frac{\partial T_{Air}}{\partial x^*}$ and $\frac{\partial T_{Sol}}{\partial y^*}$) and plays an important role in determining the distribution of the temperature in the exchanger. Also it can be seen from the above figures that the salt solution may release moisture in part of the heat and moisture exchanger and absorb moisture in another part of the heat and moisture exchanger. This is due to the dramatic temperature change in the exchanger caused by the phase change.

Since the number of mass transfer units (NTU_m) is one of the dimensionless parameters in the dimensionless governing equations, the performance of the exchanger will not only depend on the number of heat transfer units, *NTU*, and the heat capacity ratio, *Cr*, but also the number of mass transfer units, NTU_m, and the mass flow ratio, M_{Salt}/M_{Air}. The temperature and moisture content distributions in the exchanger for

NTU_m=6, and various values of M_{Salt}/M_{Air} (0.1, 1 and 10) are presented in Figure 3.13, Figure 3.14 and Figure 3.15. It is important to note that, for a given exchanger and testing conditions, there is a direct relationship between NTU_m and NTU and between Cr and M_{Salt}/M_{Air}. For the exchanger (Table 3.2) and operating conditions (Table 3.5) studied here, $NTU_m = 6$ and $M_{Salt} / M_{Air} = 0.1$ corresponds to $NTU = 1.5$ and $C_{Sol} / C_{Air} = 0.6$, $NTU_m = 6$ and $M_{Salt} / M_{Air} = 1$ corresponds to $NTU = 9$ and $C_{Sol} / C_{Air} = 6$, and $NTU_m = 6$ and $M_{Salt} / M_{Air} = 10$ corresponds to $NTU = 9$ and $C_{Sol} / C_{Air} = 60$. Therefore, the results in Figure 3.13-3.15 are not unrelated to the results in Figures 3.10-3.12, but are presented for completeness.

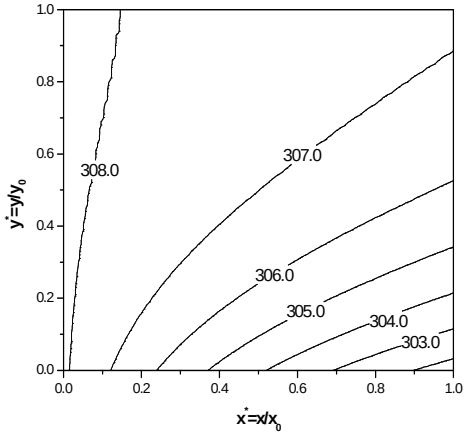

a. $T_{Air}(x^*, y^*)$ (K), air side

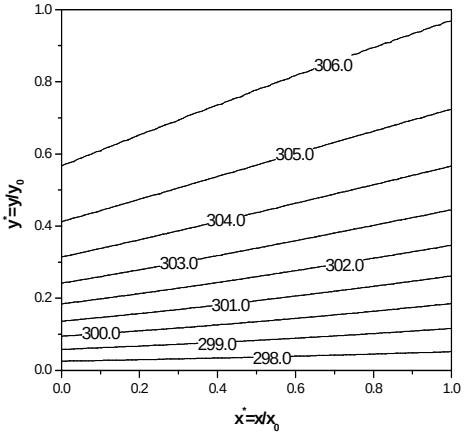

b. $T_{Sol}(x^*, y^*)$ (K), liquid side

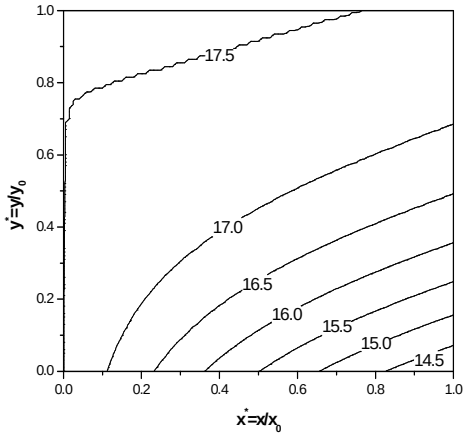

c. $W_{Air}(x^*, y^*)$ (g/kg), air side

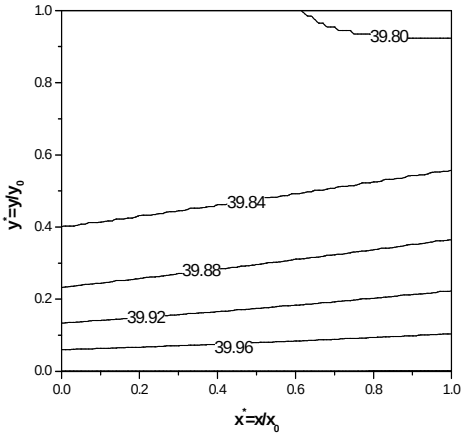

d. $C_{Salt}(x^*, y^*)$ (%), liquid side

Figure 3.13 *Temperature and moisture distributions in one exchanger for NTU_m=6 and M_{Salt}/M_{Air} =0.1(air flow in positive x-direction and liquid flow in positive y-direction).*

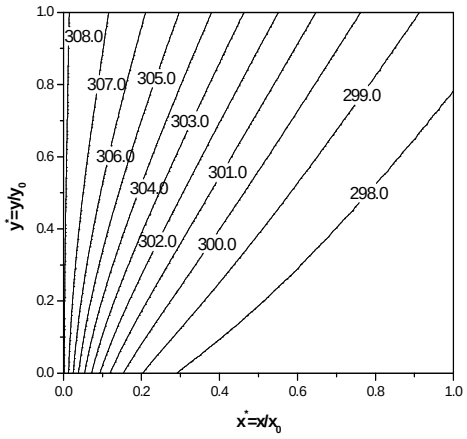

a. $T_{Air}(x^*, y^*)$ (K), air side

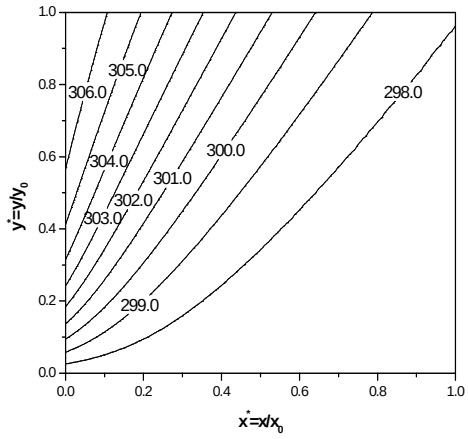

b. $T_{Sol}(x^*, y^*)$ (K), liquid side

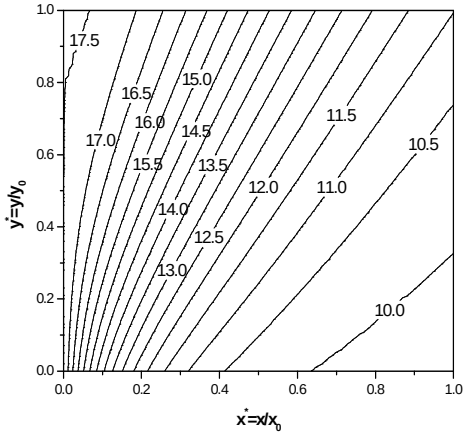

c. $W_{Air}(x^*, y^*)$ (g/kg), air side

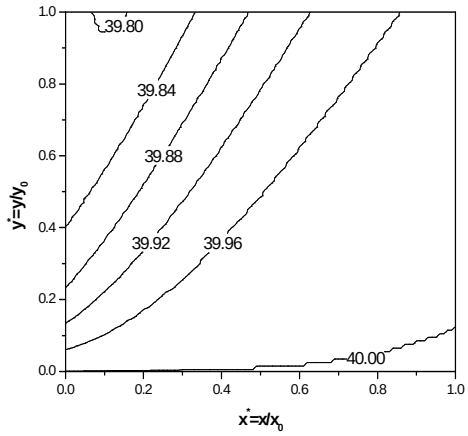

d. $C_{Salt}(x^*, y^*)$ (%), liquid side

Figure 3.14 *Temperature and moisture distributions in one exchanger for NTU_m=6 and M_{Salt}/M_{Air} =1(air flow in positive x-direction and liquid flow in positive y-direction).*

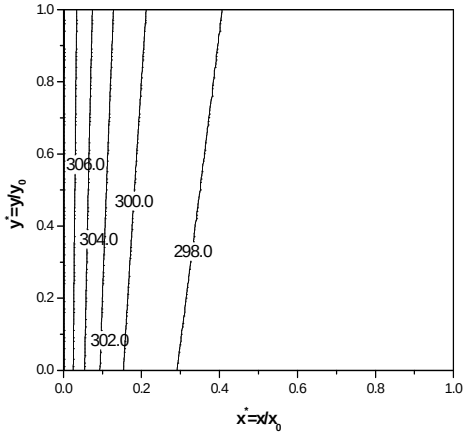

a. $T_{Air}(x^*, y^*)$ (K), air side

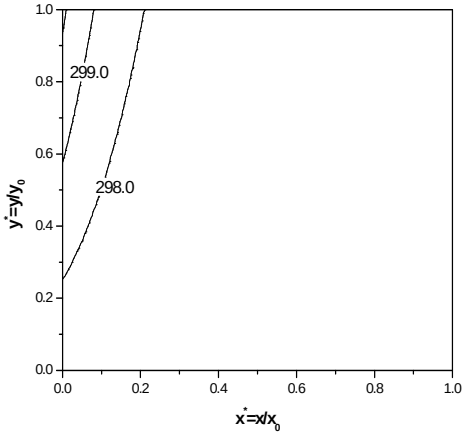

b. $T_{Sol}(x^*, y^*)$ (K), liquid side

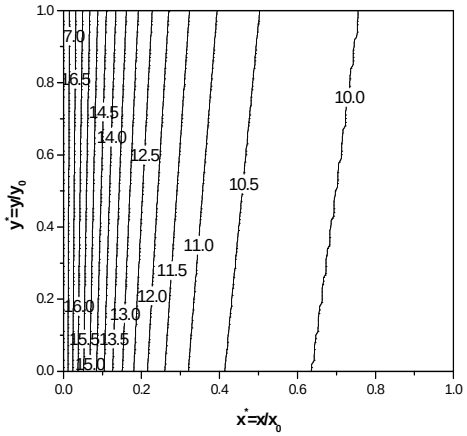

c. $W_{Air}(x^*, y^*)$ (g/kg), air side

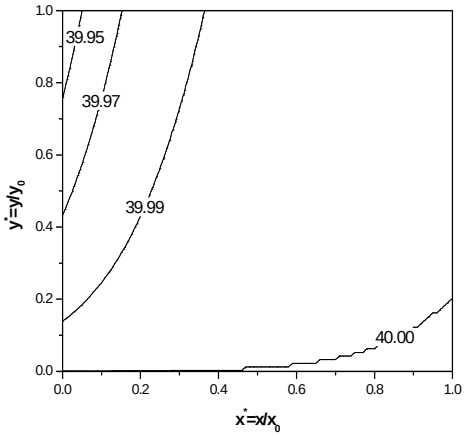

d. $C_{Salt}(x^*, y^*)$ (%), liquid side

Figure 3.15 *Temperature and moisture distributions in one exchanger for NTU_m=6 and M_{Salt}/M_{Air} =10(air flow in positive x-direction and liquid flow in positive y-direction).*

Figures 3.13, 3.14 and 3.15 show that the distributions of temperature and moisture content in the exchanger depend on the mass flow rate ratio of the pure salt and dry air for a specific NTU_m value. That is the distribution of the temperature and moisture content varies with the variation of the mass flow rate ratio of the salt and air, M_{Salt}/M_{Air}. Similarly as the distance between isothermal lines corresponds to the temperature gradient, the distance between equal moisture content lines corresponds to the moisture content gradient. The moisture transfer rate from the air per unit area at any point is

$$\dot{M}(z)_{Air}(x^*, y^*) = \frac{1}{x_0 y_0} M_{Air} \frac{\partial W_{Air}}{\partial x^*}, \tag{3.48}$$

the moisture transfer rate from the salt solution per unit area at any point is

$$\dot{M}(z)_{Sol}(x^*, y^*) = \frac{1}{x_0 y_0} M_{Salt} \frac{\partial X_{Sol}}{\partial y^*} \tag{3.49}$$

For the mass balance of the exchanger, we have

$$\frac{1}{x_0 y_0} M_{Salt} \frac{\partial X_{Sol}}{\partial y^*} = \frac{1}{x_0 y_0} M_{Air} \frac{\partial W_{Air}}{\partial x^*} \tag{3.50}$$

Figures 3.13 to 3.15 show that the equal moisture content lines of the air become closer as M_{Salt}/M_{Air} increases and the equal moisture content lines of the salt solution become further apart as M_{Salt}/M_{Air} increases. Because the variation of distribution of the temperature and moisture contents indicate a change in the outlet conditions of the exchanger, the effectiveness of the exchanger will also change as M_{Salt}/M_{Air} changes.

Thus the effectiveness of the exchanger will be different for different value of NTU_m and M_{Salt}/M_{Air}.

With the numerical model, it is possible to study how the effectiveness changes due to changes in all four dimensionless parameters (NTU_m and M_{Salt}/M_{Air}, and NTU and C_{Salt}/C_{Air}) of the heat and moisture exchanger. The results are shown in Figures 3.16 to 3.19.

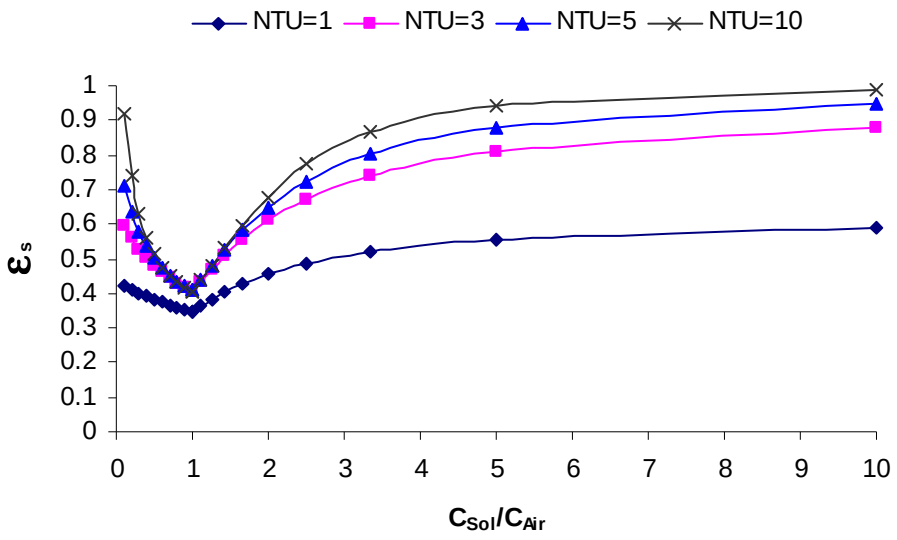

Figure 3.16 *Variations in* ε_s *with* C_{Sol}/C_{Air} *for a single heat and moisture exchanger.*

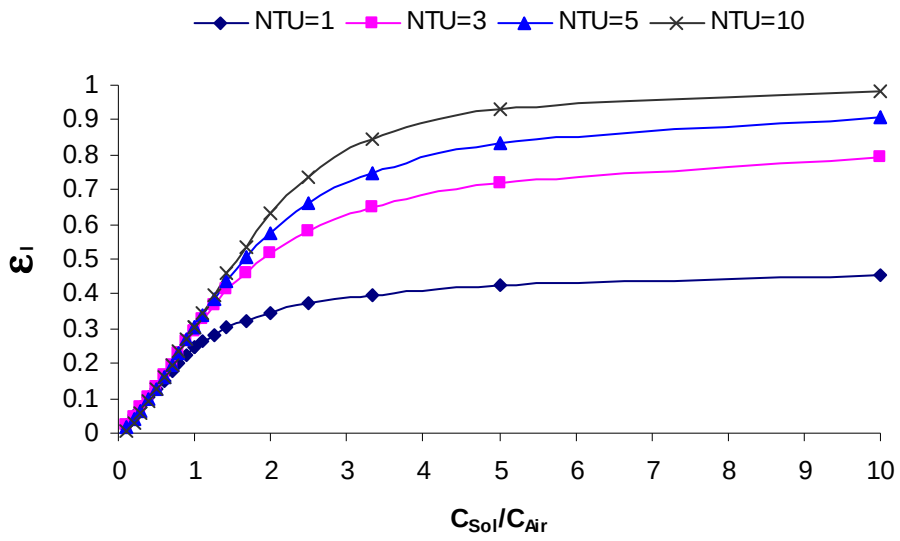

Figure 3.17 *Variations in* ε_l *with* C_{Sol}/C_{Air} *for a single heat and moisture exchanger.*

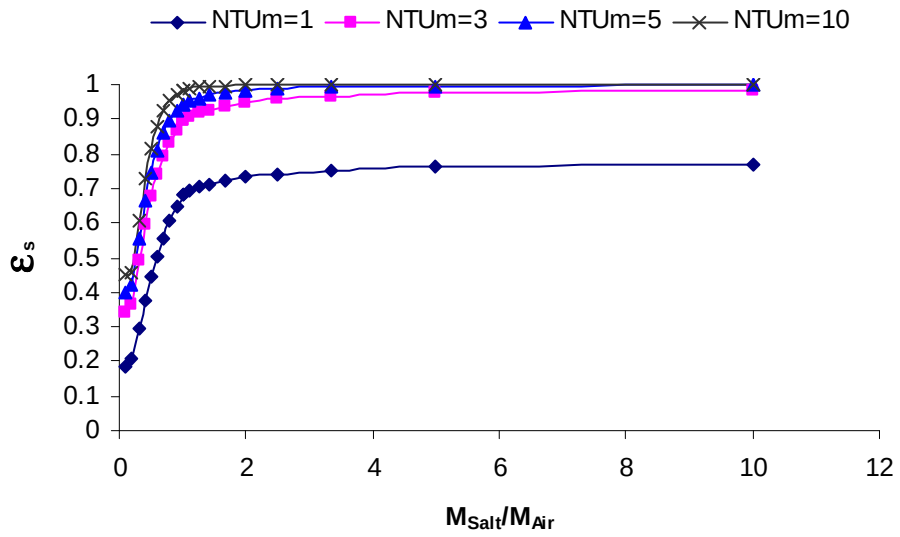

Figure 3.18 *Variations in* ε_s *with* M_{salt}/M_{air} *for a single heat and moisture exchanger.*

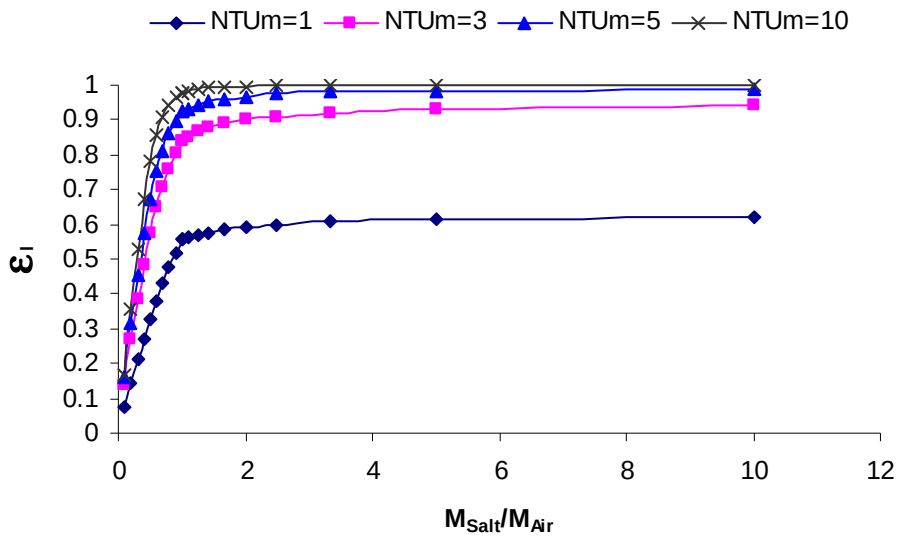

Figure 3.19 *Variations in* ε_l *with* M_{salt}/M_{air} *for a single heat and moisture exchanger.*

From Figure 3.16 and Figure 3.17, it can be seen that the sensible effectiveness of the exchanger is minimum at $C_{Sol}/C_{Air}=1$ and increases as C_{Sol}/C_{Air} increases or decreases from 1. This is similar to the response of sensible heat exchangers presented in Chapter 2 and those reported in the literature. The latent effectiveness, on the other hand, simply increases as C_{Sol}/C_{Air} increases. Figure 3.18 and Figure 3.19 show a similar response for both sensible and latent effectiveness to changes in M_{salt}/M_{air}. In these figures, ε_s and ε_l increase as M_{salt}/M_{air} increases when $M_{salt}/M_{air}<1$, but ε_s and ε_l are nearly constant when $M_{salt}/M_{air}>1$, especially for large value of NTU_m.

Chapter 4

RUN-AROUND HEAT AND MOISTURE RECOVERY SYSTEM

4.1 Introduction

A run-around heat and moisture recovery system is comprised of two or more liquid-to-air heat and moisture exchangers that are coupled by an aqueous desiccant salt solution as shown in Figure 4.1. The system is different from the traditional run-around heat recovery system presented in Chapter 2 in that it can transfer both heat and moisture with the heat and moisture exchangers. The coupling liquid, which is typically a desiccant (e.g. LiBr or LiCl) and water mixture and is running cross-flow to the exhaust and supply airflow, can regenerate itself through moisture exchange with the supply and exhaust air and thus transport moisture from exhaust air to supply air or vice-versa. In some cases, it may be beneficial to configure the system to include external sourced sinks of heat and moisture (e.g. waste heat) to improve performance. In this configuration, the heat and moisture transfer at the supply exchanger may not equal the heat and moisture transfer at the exhaust exchanger due to the external sources of heat and moisture. Investigation of this configuration will be left to future studies. In all configurations, the liquid circulating pump can adjust the flow rate of the salt solution to

control the heat and moisture transfer rates between the supply and exhaust air, which may be necessary as the outdoor conditions change.

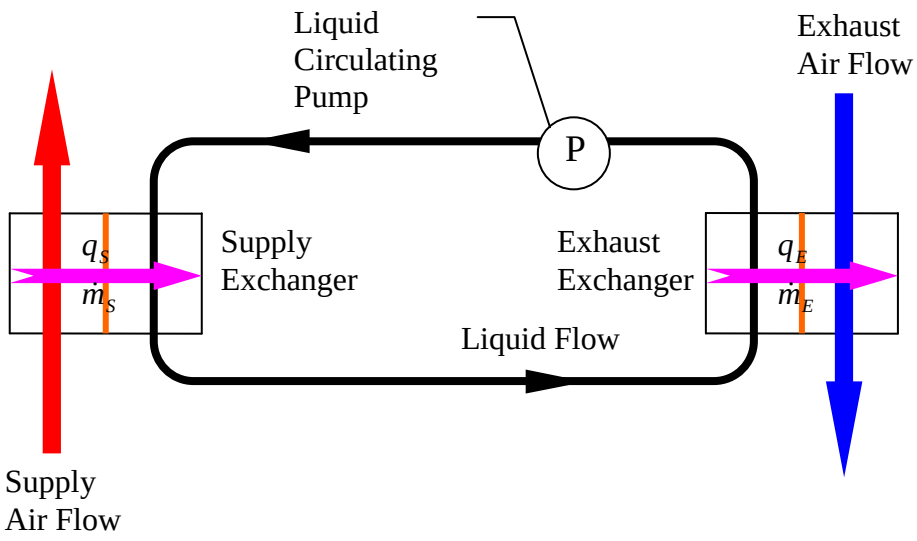

Figure 4.1 *Run-around heat and moisture recovery system*

4.2 Theoretical Model

The steady-state operating condition for the run-around heat and moisture recovery system that will be investigated in this thesis is when the total heat and mass transfer rates in the exhaust exchanger balance the rates in the supply exchanger. When this occurs, energy and water do not need to be added or removed from the system during operation, except for the small amount of pumping energy required to circulate the coupling fluid and the fan energy required to cause a flow of air through the exchangers. Since these external energy inputs are assumed to not alter the performance

of the exchangers for heat and mass transfer, the modeling of the system in this simulation is based on this energy and mass balance between the supply and exhaust exchangers. The assumptions used in this analysis are the same as for the individual exchangers in each air stream (see Section 3.1) plus two new assumptions.

1. Heat and mass transfer occurs only within each exchanger (i.e., no heat and mass transfer between the exchangers or connecting piping and ambient air).

2. The bulk mean coupling fluid temperature and water concentration at the exit of one exchanger can be used for the entrance to the downstream exchanger.

Basic Equations

For the Run-Around system shown in Figure 4.2, it is assumed that the inlet air temperatures of the supply and exhaust side air, $T_{AS,in}$ and $T_{AE,in}$, and the inlet humidity ratio of the supply and exhaust side air, $W_{AS,in}$ and $W_{AE,in}$, are known. To start the simulation, we define an arbitrary inlet condition of the supply side liquid, $T_{LS,in}$ and $X_{LS,in}$. Then using the algorithm to start iterating the thermo-physical properties, all the parameters of the inlet and outlet conditions for each exchanger and the imbalance of heat and water vapour flows in the run-around system can be calculated for any iteration.

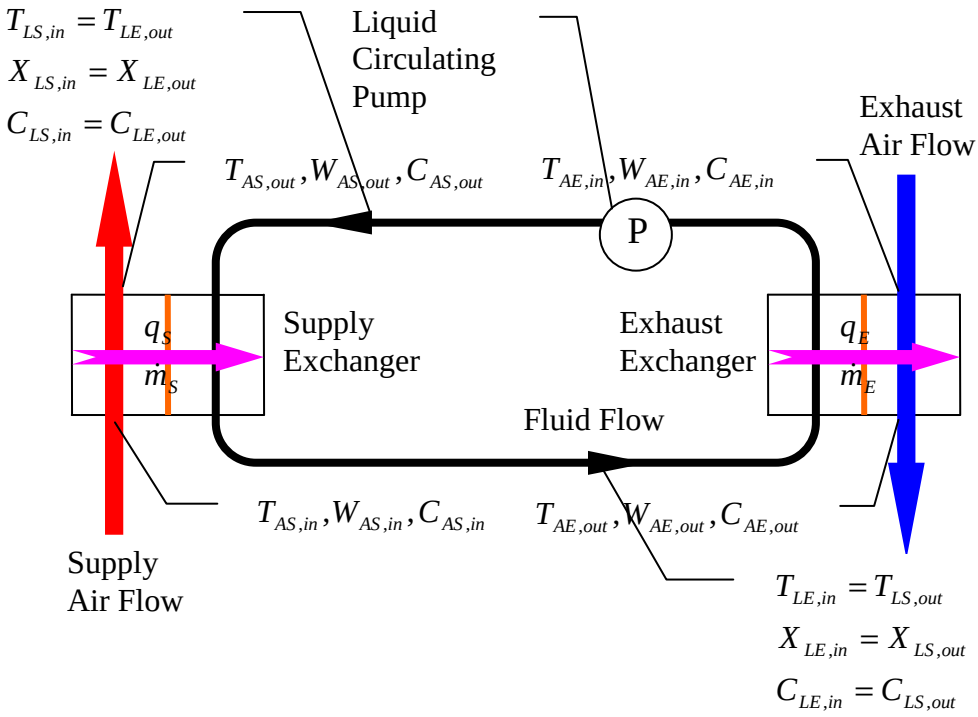

Figure 4.2 *Thermal Circuit of Run-Around System with Enthalpy Exchangers*

The equations for energy and mass rate are as follows:

For the supply exchanger, the energy transfer rate between the air and liquid is

$$q_S = C_{AS,in}T_{AS,in} - C_{AS,out}T_{AS,out} + \dot{m}_S \cdot h_{fg} = C_{LS,out}T_{LS,out} - C_{LS,in}T_{LS,in}, \qquad (4.1)$$

and the mass transfer rate between the air and liquid is

$$\dot{m}_S = M_{Salt}(X_{LS,out} - X_{LS,in}) = M_{Air}(W_{AS,in} - W_{AS,out}). \qquad (4.2)$$

For the exhaust exchanger, the energy transfer rate between the air and liquid is

$$q_E = C_{AE,out}T_{AE,out} - C_{AE,in}T_{AE,in} + \dot{m}_E h_{fg} = C_{LE,in}T_{LE,in} - C_{LE,out}T_{LE,out}, \qquad (4.3)$$

and the mass transfer rate between the air and liquid is

$$\dot{m}_E = M_{Salt}(X_{LE,in} - X_{LE,out}) = M_{Air}(W_{AE,out} - W_{AE,in}). \quad (4.4)$$

The outlet bulk mean outlet temperatures of the air and the salt solution fluid are calculated by the following equations. The outlet temperature of the air is

$$T_{A,out} = \frac{1}{m_A Cp_A} \cdot \int_y M_A Cp_A T_A dy. \quad (4.5)$$

and the outlet temperature of the liquid is

$$T_{L,out} = \frac{1}{m_L Cp_L} \cdot \int_x M_L Cp_L T_L dx. \quad (4.6)$$

The outlet bulk mean outlet moisture contents of the air and the salt solution fluid are calculated by the following equations. The outlet humidity ratio of the air is

$$W_{A,out} = \frac{1}{y_0} \cdot \int_y W_A dy, \quad (4.7)$$

and the outlet concentration of the liquid is

$$X_{L,out} = \frac{1}{x_0} \cdot \int_x X_L dx. \quad (4.8)$$

For no heat and mass gain or loss in the connecting pipes, the inlet properties of the supply exchanger should be equal to the outlet properties of the exhaust exchanger

and the inlet properties of the exhaust exchanger should be equal to the outlet properties of the supply exchanger. The inlet temperature of the liquid in the supply exchanger is

$$T_{LS,in} = T_{LE,out}\,, \tag{4.9}$$

and the inlet temperature of liquid in the exhaust exchanger is

$$T_{LE,in} = T_{LS,out}\,. \tag{4.10}$$

The inlet concentration of the liquid in the supply exchanger is

$$X_{LS,in} = X_{LE,out}\,, \tag{4.11}$$

and the inlet concentration of the liquid in the exhaust exchanger is

$$X_{LE,in} = X_{LS,out}\,. \tag{4.12}$$

Based on the mass and energy balance, that is $\dot{m}_S = \dot{m}_E$ and $q_S = q_E$, we can get the steady state inlet and outlet conditions of the run-around system by adjusting the liquid properties for each iterative calculation of the system. Using these steady state inlet and outlet conditions, the overall effectiveness of the system is calculated for each operating condition for the inlet air.

As mentioned in Chapter 2, the effectiveness of any type of heat exchanger can be expressed as:

$$\varepsilon = \frac{Actual\ heat\ transfer\ rate}{Maximum\ possible\ heat\ transfer\ rate\ of\ an\ exchanger\ with\ an\ infinite\ heat\ transfer\ area\ and\ the\ same\ operating\ conditions} \tag{4.13}$$

Following equation (4.13), the sensible effectiveness of the run-around system with coupled heat and moisture exchange and equal supply and exhaust air mass flow rates (i.e. $m_{AE} = m_{AS}$ as shown in Figure 4.3) is:

$$\varepsilon_s = \frac{T_{AS,in} - T_{AS,out}}{T_{AS,in} - T_{AE,in}} = \frac{T_{AE,out} - T_{AE,in}}{T_{AS,in} - T_{AE,in}}, \tag{4.14}$$

where the inlet and outlet conditions are shown in Figure 4.3. Similarly, the latent effectiveness of the run-around system with coupled heat and moisture exchange is:

$$\varepsilon_l = \frac{W_{AS,in} - W_{AS,out}}{W_{AS,in} - W_{AE,in}} = \frac{W_{AE,out} - W_{AE,in}}{W_{AS,in} - W_{AE,in}}, \tag{4.15}$$

and the total effectiveness of the run-around system with coupled heat and moisture exchange is:

$$\varepsilon_t = \frac{H_{AS,in} - H_{AS,out}}{H_{AS,in} - H_{AE,in}} = \frac{H_{AE,out} - H_{AE,in}}{H_{AS,in} - H_{AE,in}}. \tag{4.16}$$

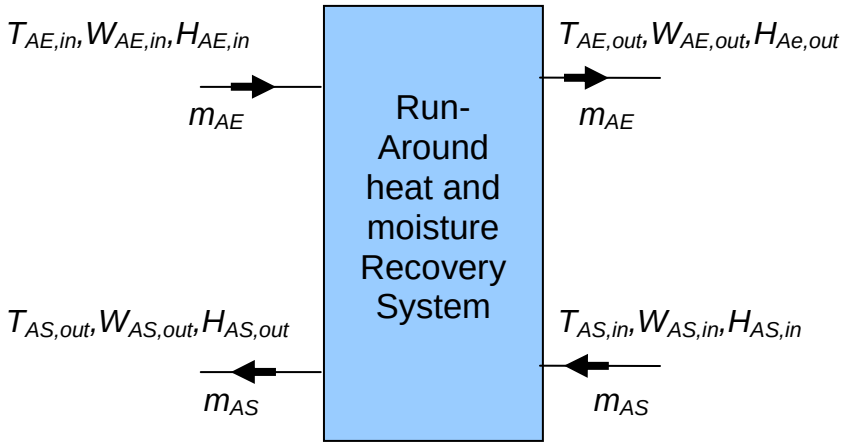

Figure 4.3 *Schematic of the inlet-outlet conditions of the run-around heat and moisture recovery system*

The numerical model for run-around heat recovery system was verified in Chapter 2 with Mason's (Kern and Kraus, 1972) analytical solution and $\varepsilon - NTU$ correlations. Since heat and mass transfer are analogous, there is significant confidence in the results generated from the numerical model for the run-around heat and moisture recovery system.

4.3 Numerical Solution Method and Results

In this section, the run-around heat and moisture recovery system is assumed to be composed of two cross-flow flat-plate heat and moisture exchangers having the same parameters and properties as the exchanger described in Table 3.3—one as the supply exchanger and the other the exhaust exchanger. The performance of the run-around system operating under ARI summer and winter test conditions (ANSI/ARI Standard

1060, 2001) (as shown in Table 4.1) with LiBr and LiCl salt solutions as the coupling fluid is presented.

Table 4.1 *Operating conditions of the run-around system in the model in Chapter 4.*

Summer	Inlet temperature of the supply air stream ($T_{AS,in}$)	$308.15\,K$ $(35\,^{\circ}C)$
	Inlet humidity ratio of the supply air stream ($W_{AS,in}$)	$17.5\,g/kg$
	Inlet temperature of the exhaust air stream ($T_{AE,in}$)	$297.15\,K$ $(24\,^{\circ}C)$
	Inlet humidity ratio of the exhaust air stream ($W_{AE,in}$)	$9.3\,g/kg$
Winter	Inlet temperature of the supply air stream ($T_{AS,in}$)	$274.85\,K$ $(1.7\,^{\circ}C)$
	Inlet humidity ratio of the supply air stream ($W_{AS,in}$)	$3.5\,g/kg$
	Inlet temperature of the exhaust air stream ($T_{AE,in}$)	$294.15\,K$ $(21\,^{\circ}C)$
	Inlet humidity ratio of the exhaust air stream ($W_{AE,in}$)	$7.1\,g/kg$
Salt Solution	Initial inlet temperature of the liquid stream ($T_{L,in}$)	$297.15\,K$ $(24\,^{\circ}C)$
	Initial inlet concentration of the liquid stream ($X_{L,in}$)	$1.5\,kg/kg(40\%)$

The numerical solution method of the run-around system with moisture transfer is about the same as the solution for the sensible run-around system. The difference is that, for the run-around system with moisture transfer, the mass transfer has to be balanced as well as the heat transfer. An initial inlet operating condition of the coupling liquid is selected, iterating until the heat and moisture is balanced. The solution is considered converged when the difference in heat rate, q, and difference in the moisture transfer rate, $\dot{m}$, are all less than 10^{-4}. That is, the difference in the heat rate:

$$\frac{q_S - q_E}{(q_S + q_E)/2} < 10^{-4}, \tag{4.17}$$

and the difference in the mass transfer rate:

$$\frac{\dot{m}_S - \dot{m}_E}{(\dot{m}_S + \dot{m}_E)/2} < 10^{-4}. \tag{4.18}$$

The detailed algorithm for the run-around heat and moisture recovery system is given in Appendix C. With the numerical model developed above and the definition of the effectiveness, the performance of the run-around system can be simulated and the results (Figure 4.4) compared with the sensible run-around system in Chapter 2 (Figure 2.16).

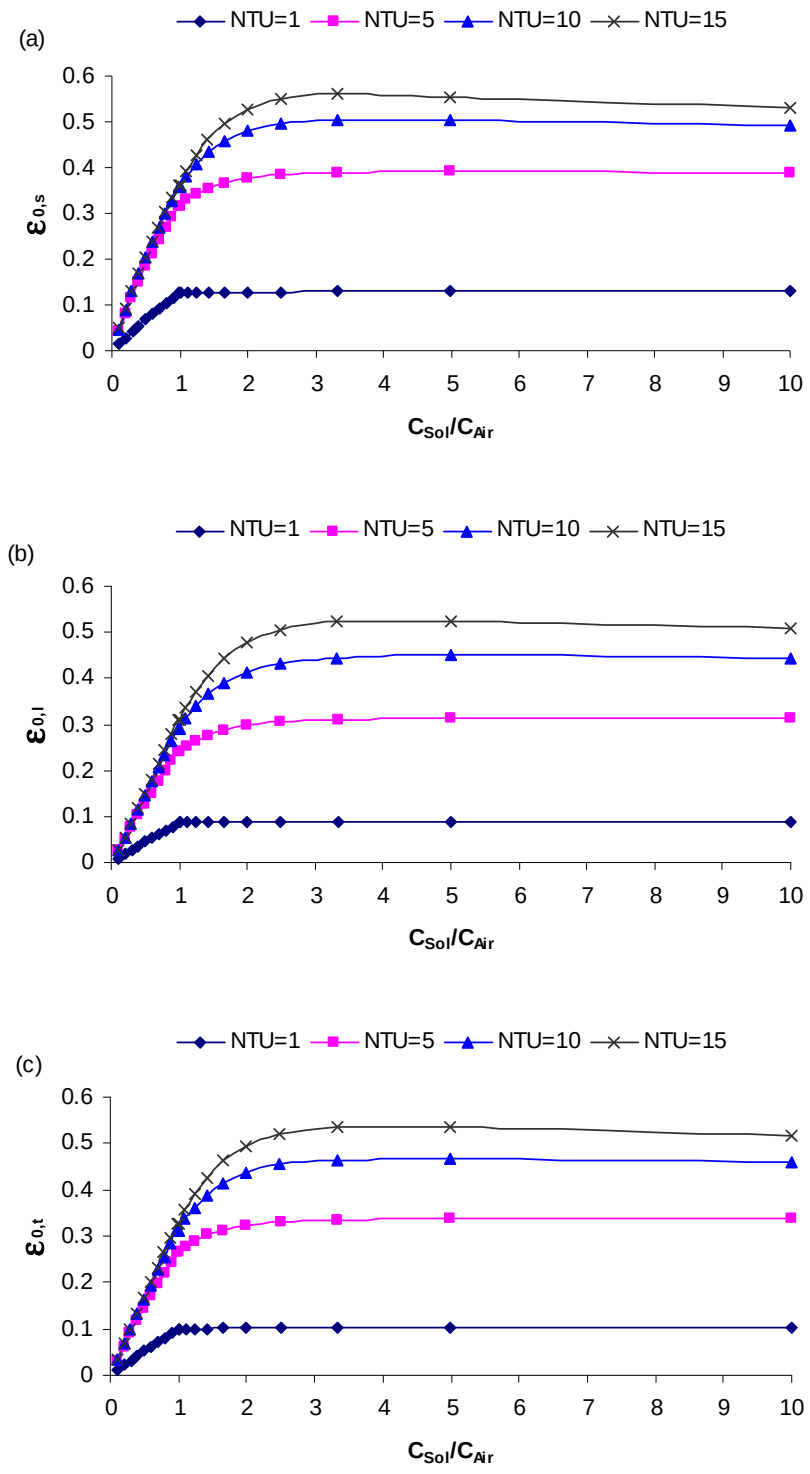

Figure 4.4 *Variation of the overall (a)sensible, (b)latent, and (c)total effectiveness of the run-around system as a function of* C_{Sol}/C_{Air} *with NTU as a parameter (LiBr solution, ARI summer condition).*

Comparing Figure 4.4 with Figure 2.16 shows that the run-around system with moisture transfer performs very differently from the sensible run-around system. For the sensible run-around heat recovery system, the optimum effectiveness occurs approximately at the heat capacity ratio of coupling fluid to air, $C_L / C_A = 1$. Though for lower *NTU* values, the maximum effectiveness shifts a little bit from $C_L / C_A = 1$, but the change is so trivial that it can be neglected. For the run-around heat and moisture recovery system, however, the maximum effectiveness occurs approximately at a heat capacity ratio of coupling salt solution to air, $C_{Sol} / C_{Air} = 3$, especially for high *NTU*. This means that the pumping rate of the coupling fluid must be kept at a higher level for total energy transfer than for sensible heat transfer only. The heat capacity rate of the coupling fluid should be 3 times larger than that of the air. This difference between the run-around heat and moisture recovery system and sensible run-around heat recovery system is believed to be caused by the phase change accompanying the moisture transfer. When there is phase change, a large amount of heat is released or absorbed and the magnitude of this heat may be similar to the magnitude of the sensible heat exchanged in the exchangers. Since the heat of phase change is delivered to or taken from the salt solution, this phase change alters the optimal heat capacity rate of the solution. As a result, the performance of the exchangers changes and thus the performance of the run-around system also changes. This is expected because Figures 3.10-3.12 showed that the magnitude of both the temperature and moisture content in the air side increase as the heat capacity of the coupling fluid increases.

The moisture transfer in the exchangers is determined not only by the temperature change in the exchangers but also by the concentration change of the salt

solution. Thus it may be helpful to analyze the performance of the run-around heat and moisture recovery system using the number of mass transfer units, NTU_m, and mass flow rate ratio of pure salt in the coupling fluid to dry air, M_{salt} / M_{Air}. In addition, different salt solutions may result in different effectiveness so LiBr and LiCl are studied as the coupling fluid. The results are shown in Figure 4.5 and Figure 4.6.

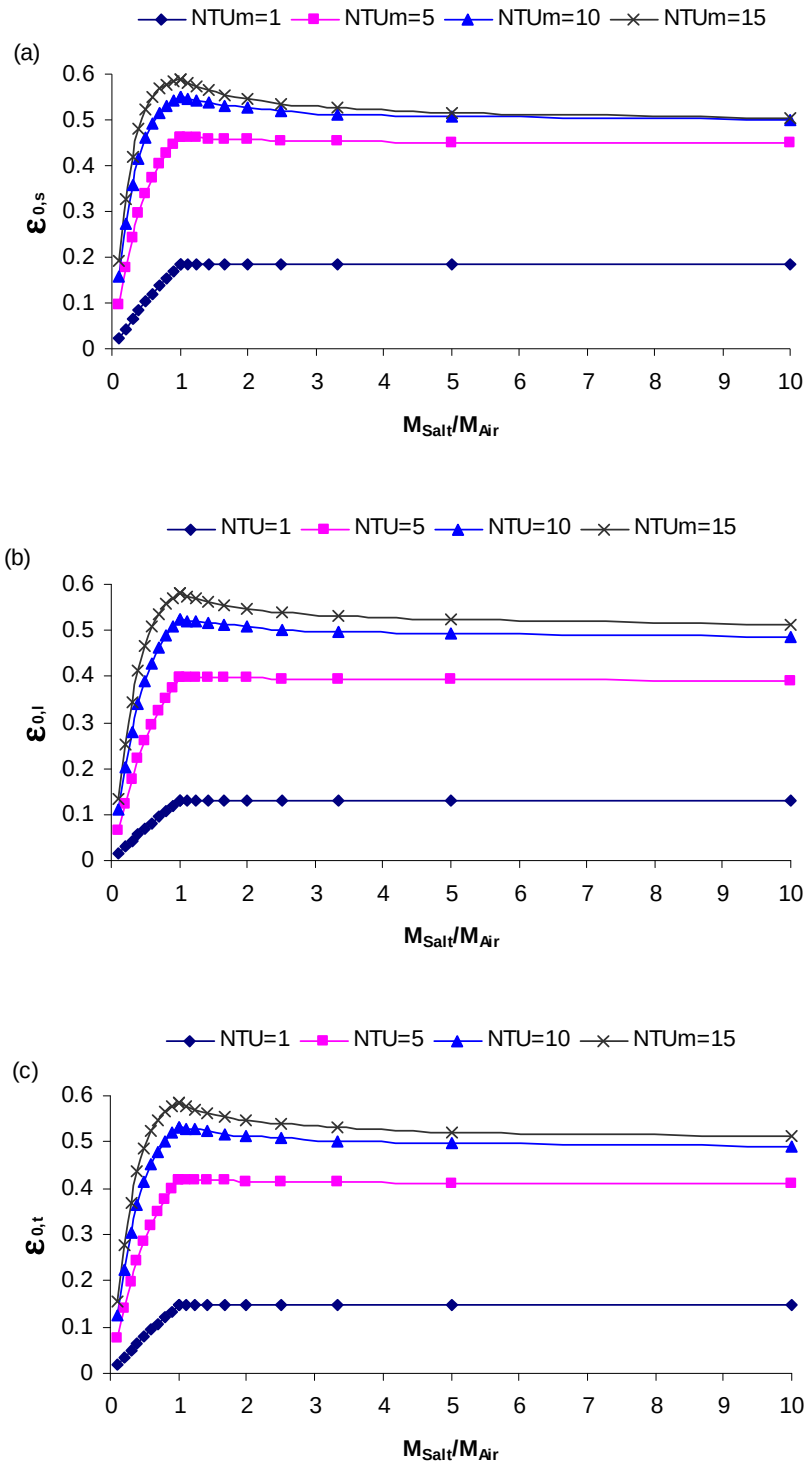

Figure 4.5 *Variation of the overall (a)sensible, (b)latent, and (c)total effectiveness of the run-around system as a function of* M_{Sol} / M_{Air} *with* NTU_m *as a parameter (LiBr solution, ARI summer condition).*

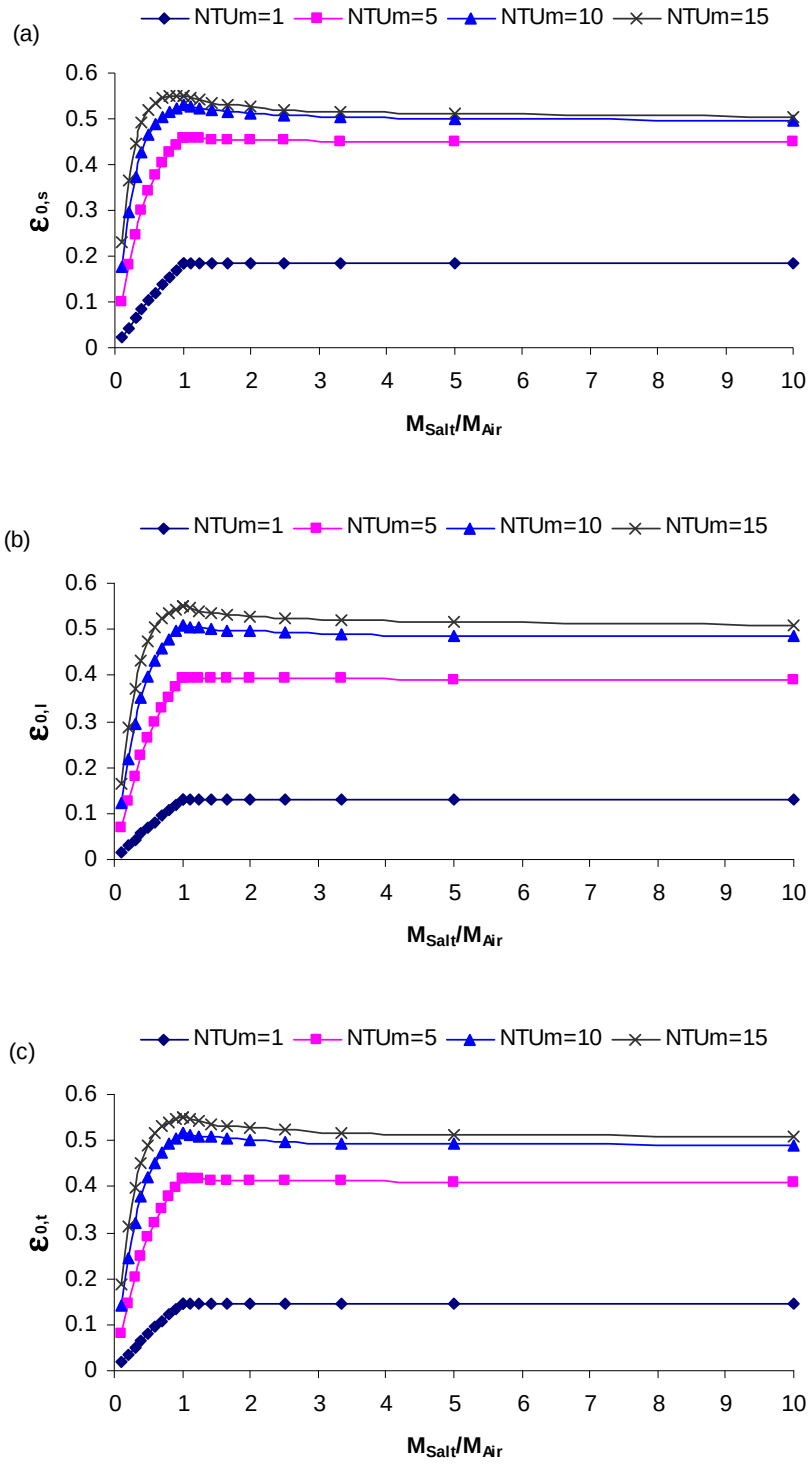

Figure 4.6 *Variation of the overall (a)sensible, (b)latent, and (c)total effectiveness of the run-around system as a function of* M_{Sol} / M_{Air} *with* NTU_m *as a parameter (LiCl solution, ARI summer condition).*

Figure 4.5 and Figure 4.6 show that the effectiveness of the run-around heat and moisture recovery system increases with increasing NTU_m. The maximum effectiveness of the system occurs approximately at $M_{salt} / M_{Air} = 1$. The effectiveness of the system is very sensitive to the mass flow rate of pure salt in the coupling fluid when $M_{salt} / M_{Air} < 1$, but doesn't change much with mass flow rate of pure salt in the coupling fluid when $M_{salt} / M_{Air} > 1$. This means that in the practical operation of the run-around system, the pumping rate of the coupling fluid should be kept at a value so that the mass flow rate of the pure salt in the fluid is about same as or a little higher than the mass flow rate of dry air. Comparing the effectiveness values in Figures 4.5 and 4.6 shows that the run-around system has a better performance with LiBr solution as the coupling fluid than with LiCl solution as the coupling fluid. Another advantage of the LiBr solution is that the equilibrium concentration is higher than LiCl for these operating conditions. Therefore, the total solution flow rate (salt + water) and pumping energy will be slightly lower for LiBr than for LiCl.

To investigate the effect of the operating temperature and humidity, the effectiveness of the run-around heat and moisture recovery system operating at ARI winter test conditions is shown in Figure 4.7 and Figure 4.8.

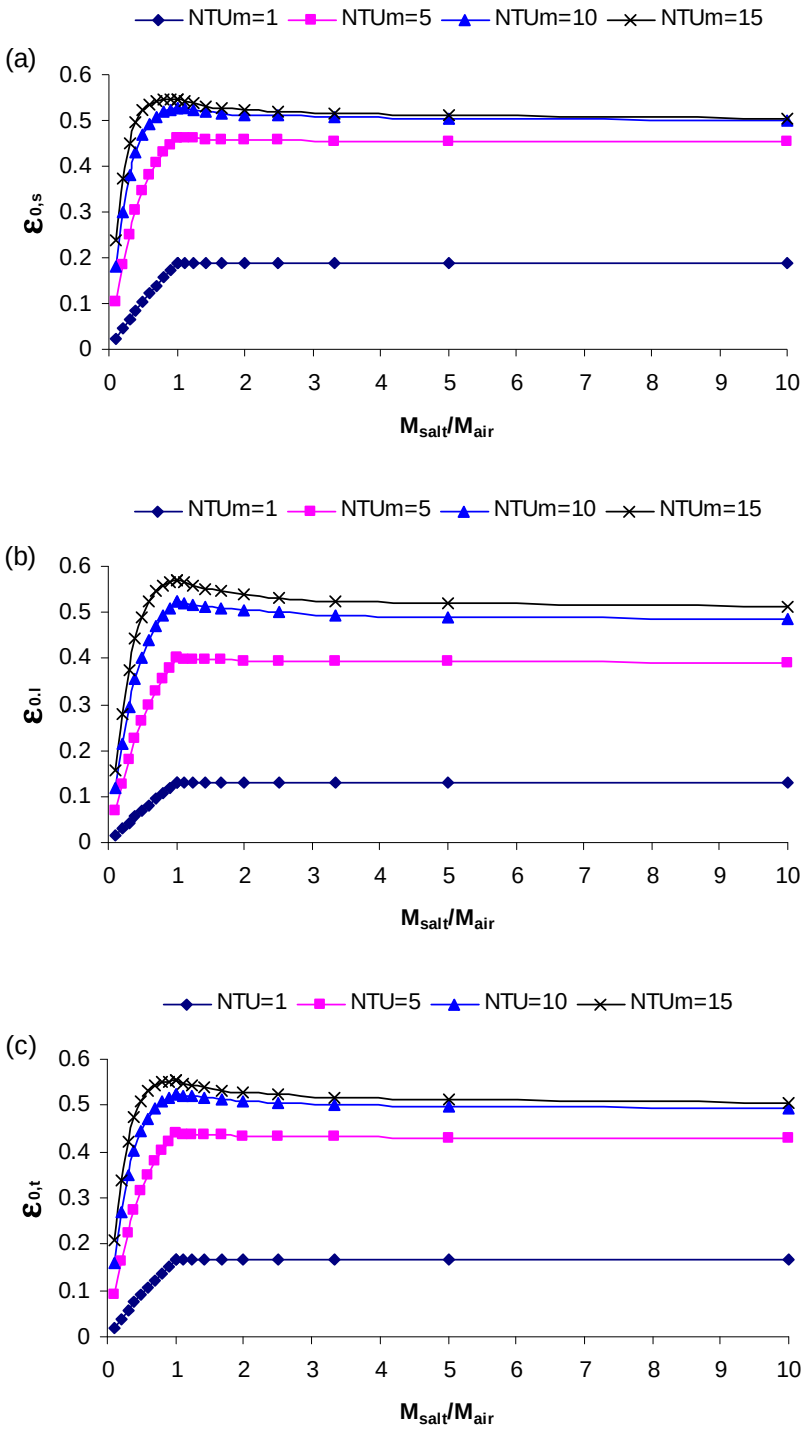

Figure 4.7 *Variation of the overall (a)sensible, (b)latent, and (c)total effectiveness of the run-around system as a function of* M_{Salt} / M_{Air} *with* NTU_m *as a parameter (LiBr solution, ARI winter condition).*

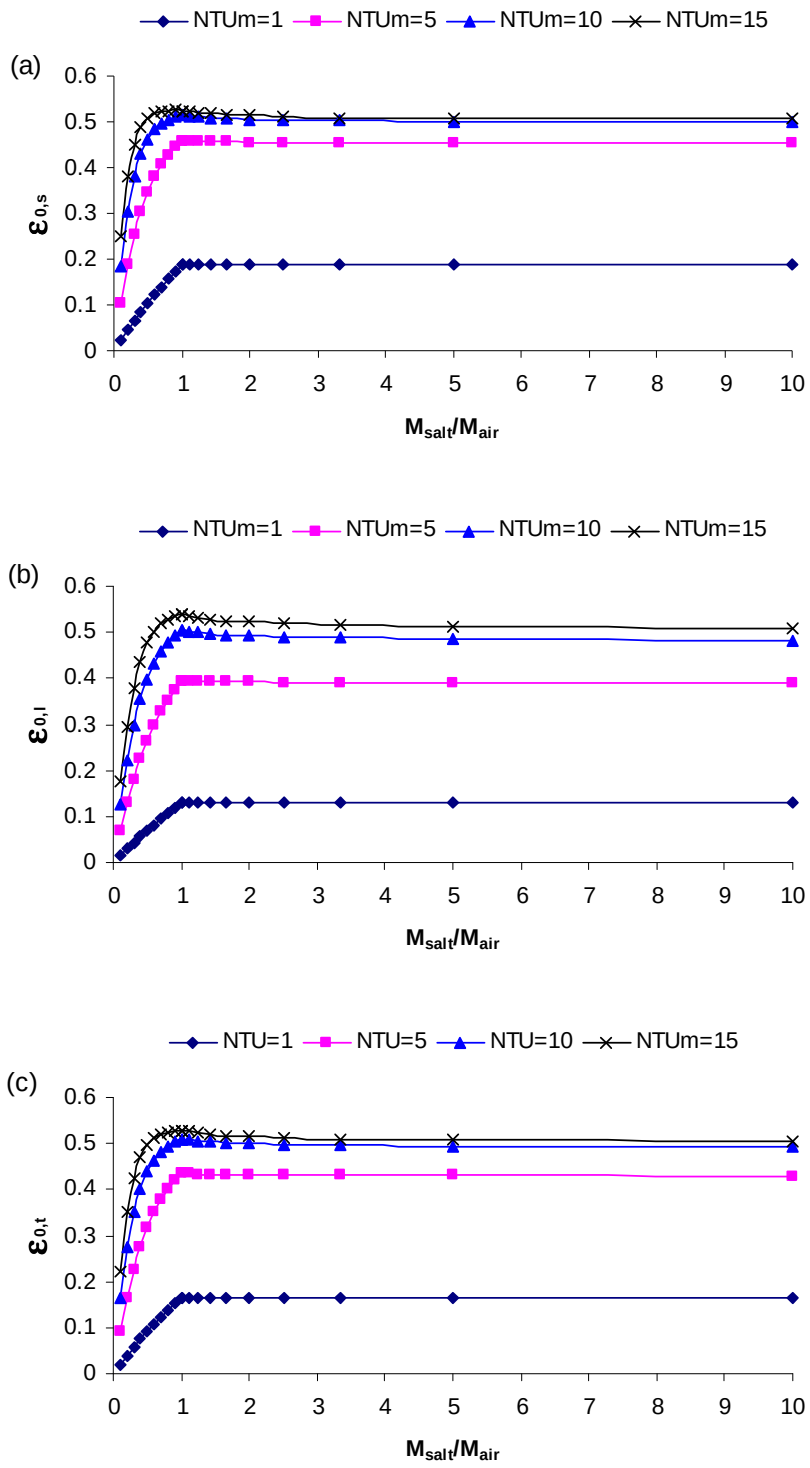

Figure 4.8 *Variation of the overall (a)sensible, (b)latent, and (c)total effectiveness of the run-around system as a function of* M_{Salt} / M_{Air} *with* NTU_m *as a parameter (LiCl solution, ARI winter condition).*

Comparing Figures 4.5 and 4.6 with Figures 4.7 and 4.8, it can be seen that the run-around system performance is similar under ARI winter and summer test conditions. The effectiveness is only slightly higher at ARI summer than at ARI winter conditions. The different performance in the summer than in the winter is likely due to the fact that the desiccant salt solutions have different properties such as vapour pressure and heat capacity at different temperatures and concentrations.

Chapter 5

SENSITIVITY STUDIES AND ANALYSIS

The purpose of the simulations presented in this chapter is to show the effect of certain assumptions and parameters on the predicted performance of the exchanger and the run-around system. These studies help to verify the model partially, check the validity of the assumptions, and demonstrate the performance of the system under different situations. The parameters investigated in this chapter include the heat and mass transfer coefficients, the channel size, the pumping rate of the coupling liquid, thermal entry length, and the axial conduction in the exchanger.

5.1 Heat and Mass Transfer Coefficients

In the development of the numerical model, the number of transfer units and the number of mass transfer units are defined as,

$$NTU = 2 \cdot \frac{U \cdot x_0 \cdot y_0}{C}, \text{ and} \tag{5.1}$$

$$NTU_m = 2 \cdot \frac{U_m \cdot x_0 \cdot y_0}{m}. \tag{5.2}$$

The overall heat transfer coefficient between the air and salt solution is:

$$U = \left[\frac{1}{h_{Sol}} + \frac{\delta}{k} + \frac{1}{h_{Air}} \right]^{-1}. \tag{5.3}$$

The overall mass transfer coefficient between the air and salt solution is:

$$U_m = \left[\frac{1}{h_{m,Sol}} + \frac{\delta}{k_m} + \frac{1}{h_{m,Air}} \right]^{-1}. \tag{5.4}$$

The studies in Chapter 4 show that the effectiveness of the run-around system varies with the change of the NTU and NTU_{m} for specific values of C_{Sol}/C_{Air} and M_{Salt}/M_{Air}. So from equations (5.1)-(5.3), it can be seen that the effectiveness of the run-around system should be sensitive to the convection heat and mass transfer coefficients (h, h_m) of the air and salt solution and the heat and mass conductivities (k, k_m) of the membrane. For $M_{Salt}/M_{Air} = 1$, the variation of the overall effectiveness of the run-around system with the heat and mass conductivities is presented in Figure 5.1 and Figure 5.2.

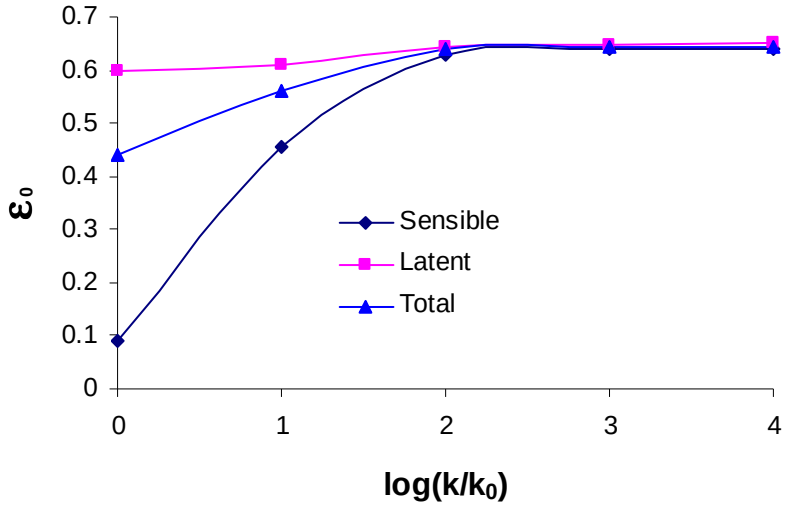

Figure 5.1 *Overall effectiveness* (ε_0) *versus log(k/k₀) [* $k_0 = 3.34\times10^{-4}\, W/(m\cdot K)$ *].*

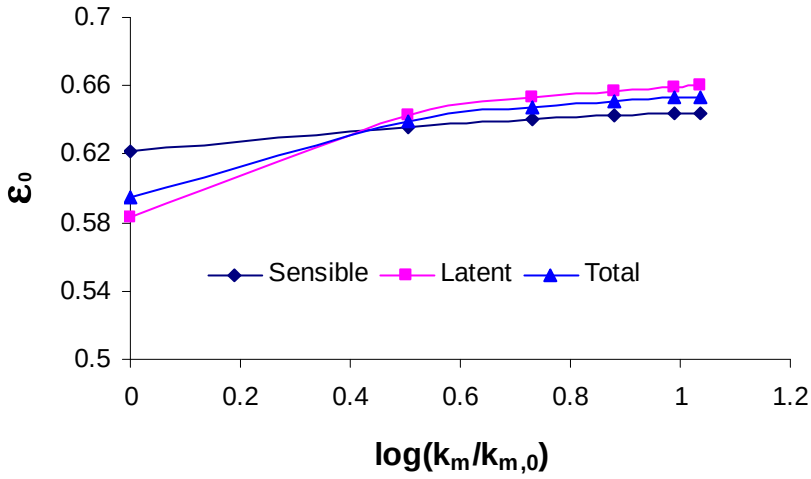

Figure 5.2 *Overall effectiveness* (ε_0) *versus log(kₘ/kₘ,₀) [* $k_{m,0} = 9.1\times10^{-6}\, kg/(m\cdot s)$ *].*

Figure 5.1 and Figure 5.2 show that the overall effectiveness of the run-around system is not sensitive to the heat and mass conductivities in certain range of the value of k and k_m. For the membrane material chosen in this research, the heat and mass

conductivities are in this insensitive range. Also, it can be seen that the overall sensible effectiveness is less sensitive to k_m and more sensitive to k than the overall latent effectiveness.

The convection heat transfer coefficient is determined by the Nusselt number (Nu) and the hydraulic diameters (D_h) of the channels of the exchangers:

$$h = \frac{Nu \cdot k_f}{D_h}, \tag{5.5}$$

and the mass transfer coefficient (h_m) can be determined from the heat transfer coefficient (h) using the heat and mass analogy. The hydraulic diameter (D_h) is determined by the channel size of the exchangers which is investigated in Section 5.2. In this section, the effect of Nusselt number (Nu) is investigated. For laminar flow in parallel pates, the Nusselt number is a specific value. In previous studies, constant wall heat fluxes in the exchangers is assumed, that is $Nu = 8.24$ (Kays and Crawford, 1993). The performance of the run-around system is simulated with Nu varied from 7.54 (constant wall temperature) to 8.24 (constant wall heat fluxes), and the results are shown in Figure 5.3.

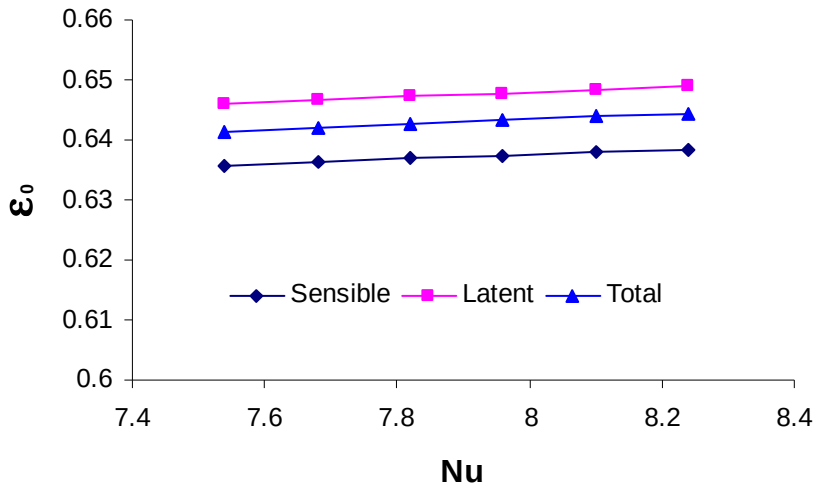

Figure 5.3 *Overall effectiveness* (ε_0) *versus Nu.*

It can be seen from Figure 5.3 that the overall effectiveness of the run-around system is not very sensitive to *Nu* in the range of 7.54 to 8.24 and the biggest difference in ε_0 is less than 0.3%.

5.2 Channel Size

Equation 5.4 shows that the channel sizes of the exchanger, d_A and d_L, have great impact on the effectiveness of the run-around system. The variation of the overall effectiveness of the run-around system with channel size (d_A and d_L) are shown in Figure 5.4 and Figure 5.5.

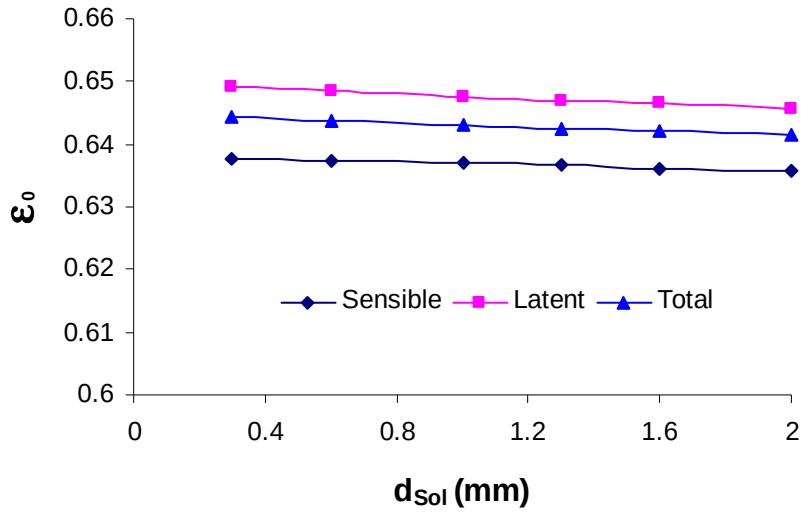

Figure 5.4 *Overall effectiveness* (ε_0) *versus diameter of the liquid channel* (d_{Sol}).

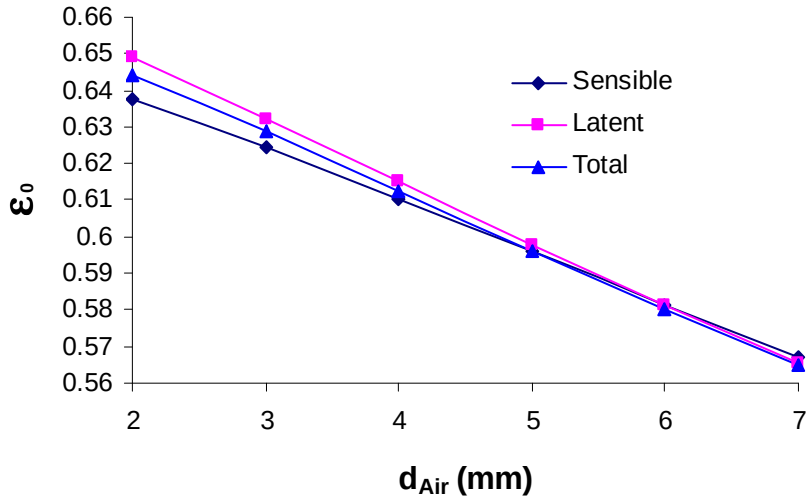

Figure 5.5 *Overall effectiveness* (ε_0) *versus diameter of the air channel* (d_{Air}).

Figure 5.4 and Figure 5.5 show that the overall effectiveness of the run-around system is less sensitive to the channel size of the liquid flow than to the channel size of the air flow. The overall effectiveness of the run around system decreases with the increase of channel size of the exchangers. This indicates that the channel sizes of both

the liquid and air flow should be kept at a practical small value to achieve a better performance of the run-around system.

5.3 Pumping Rate

The previous studies show that the pumping rate of the coupling liquid has great impact on the performance of the run-around system. For the run-around system without moisture transfer, the pumping rate of the coupling liquid should be kept so that the thermal capacity rate ratio of the air and liquid equals 1 (i.e. $Cr = 1$). But for the run-around system with moisture transfer, the pumping rate of the coupling liquid should be kept so that the mass flow rate ratio of the air and pure salt equals 1 (i.e. $M_{Air} / M_{Salt} = 1$). So it may be interesting to investigate the effectiveness variation with the variation of the pumping rate of the coupling liquid for a specific mass flow rate of the air. The results are presented in Figure 5.6 and Figure 5.7 for a run-around system with and without moisture transfer.

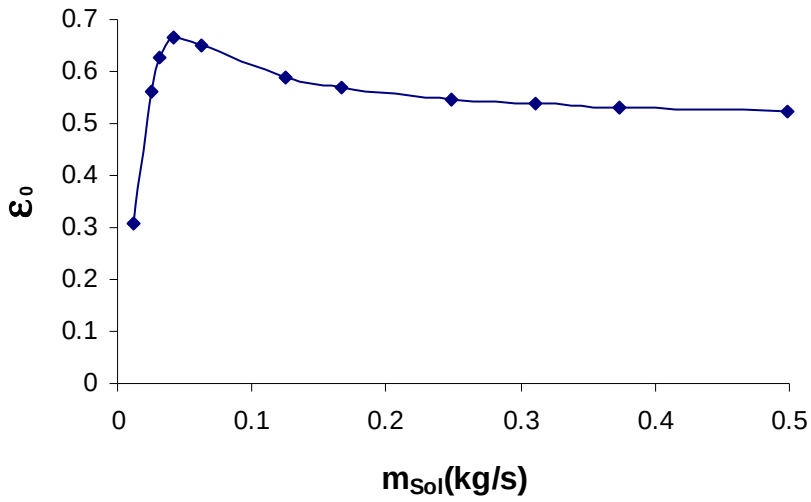

Figure 5.6 *Overall effectiveness* (ε_0) *for the run-around system without moisture transfer versus pumping rate of liquid* (m_{Sol})

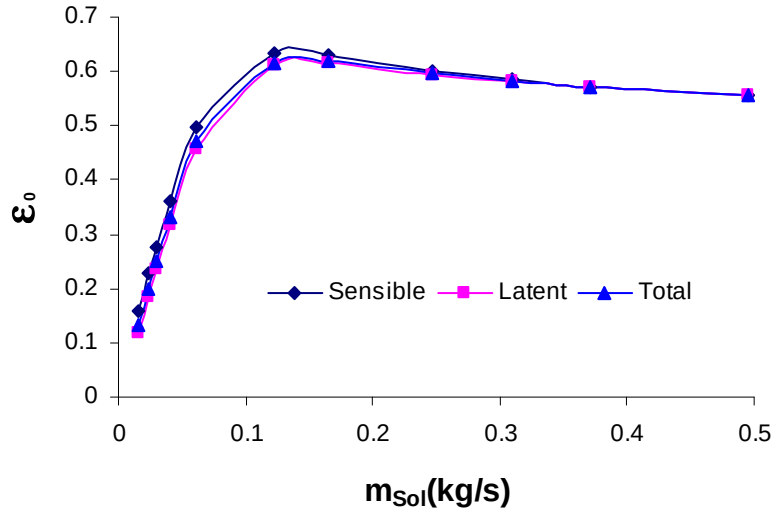

Figure 5.7 *Overall effectiveness* (ε_0) *for the run-around system with moisture transfer versus pumping rate of liquid* (m_{Sol})

Figure 5.6 and Figure 5.7 show that the overall effectiveness (ε_0) of a run-around system increases with an increase in the pumping rate of the coupling liquid to approximately 0.4 kg/s for run-around system without moisture transfer and 1.2kg/s for run-around system with moisture transfer. Then it decreases with increase in the pumping rate of the coupling liquid. This indicates that with moisture transfer, the optimum effectiveness of the run-around system occurs at a larger flow rate of the coupling liquid than without moisture transfer.

5.4 Entry Length

The previous results do not include the increased heat and mass transfer in the hydrodynamic and thermal entry length region for the air and liquid entering each channel of the exchanger. Because the size of the channels of the exchangers is much smaller than the size of the exchangers, the effect of entry length can be neglected. In order to investigate the effect of entry length, simulations are performed where the increased heat and mass transfer coefficients in the thermal entry region are included. For the thermal entry length problem for parallel plates with constant and equal wall heat fluxes, Shah and London (1978) recommended following approximate equations to determine the Nusselt numbers for laminar flow:

$$Nu = \begin{cases} 2.236(x^+)^{-1/3} & for\ x^+ \le 0.001 \\ 2.236(x^+)^{-1/3} + 0.9 & for\ 0.001 < x^+ < 0.01 \\ 8.235 + \dfrac{0.0364}{x^+} & for\ x^+ \ge 0.01 \end{cases} \quad (5.6)$$

where

$$x^{+} = \frac{2x / D_h}{\mathrm{Re} \cdot \mathrm{Pr}}. \tag{5.7}$$

With the above equations included in the model, the performance of the run-around system including the effect of thermal entry length was simulated and compared to the case when entry length effects were neglected. The results are presented in Figure 5.8.

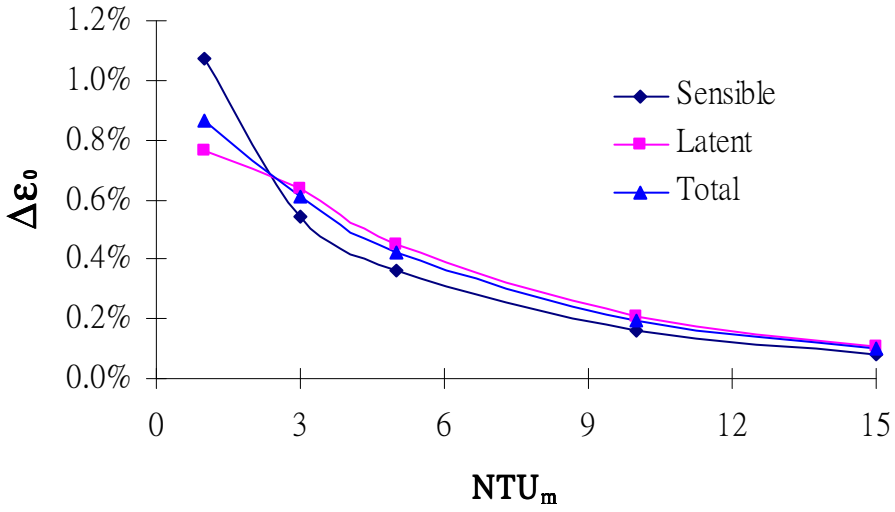

Figure 5.8 *Effect of including the entry region as a function of* NTU_m *of the run-around system* $(\Delta\varepsilon_0 = \varepsilon_{0,\text{including entry length}} - \varepsilon_{0,\text{neglecting entry length}})$.

It can be seen from Figure 5.8 that the difference between the effectiveness of the run-around system including the thermal entry effects and the effectiveness neglecting the thermal entry length effects is very small and can be neglected, especially for high NTU_m. With increasing NTU_m, the difference decreases.

5.5 Axial Conduction Effect

Throughout this thesis, the effect of axial conduction in the exchanger has been neglected, because Luo and Roetzel (1997) have shown that the effect of axial dispersion is negligible for Peclet number greater than 20. In most of the simulations in this thesis, *Pe* is greater than 20, but it is worthwhile to investigate the effect of axial dispersion of both heat and mass. To study the axial dispersion effect of both heat and mass in an exchanger, the model of the exchanger has to be revised to include the axial dispersion terms.

For the air flow, the axial dispersion can be neglected when compared to the liquid flow, because the velocity of air flow is much bigger than the liquid flow,

$$NTU_{m,Air}(W_{Air} - W_{Sol}) = -\frac{\partial W_{Air}}{\partial x^*}, \tag{5.8}$$

$$NTU_{Air}(T_{Air} - T_{Sol}) = -\frac{\partial T_{Air}}{\partial x^*}. \tag{5.9}$$

But for the liquid flow, the axial dispersion cannot be neglected:

$$NTU_{m,Sol}(W_{Air} - W_{Sol}) = \frac{\partial X_{Sol}}{\partial y^*} - \frac{1}{Pe_m} \cdot \frac{\partial^2 X_{Sol}}{\partial y^{*2}}, \text{ and} \tag{5.10}$$

$$NTU_{Sol}(T_{Air} - T_{Sol}) = \frac{\partial T_{Sol}}{\partial y^*} - \frac{1}{Pe} \cdot \frac{\partial^2 T_{Sol}}{\partial y^{*2}} - \frac{2U_m x_0 y_0}{C_{Sol}}(W_{Air} - W_{Sol}) \cdot h_{fg}, \tag{5.11}$$

where:

$$x^* = \frac{x}{x_0}, \tag{5.12}$$

$$y^* = \frac{y}{y_0}, \tag{5.13}$$

$$Pe = \frac{U \cdot D_h}{\alpha} = \mathrm{Re} \cdot \mathrm{Pr}, \tag{5.14}$$

$$Pe_m = \frac{U \cdot D_h}{D_{AB}} = \mathrm{Re} \cdot Sc. \tag{5.15}$$

With the above modified model, the performance of the exchanger including axial dispersion effect can be simulated and the results are presented in Figure 5.9.

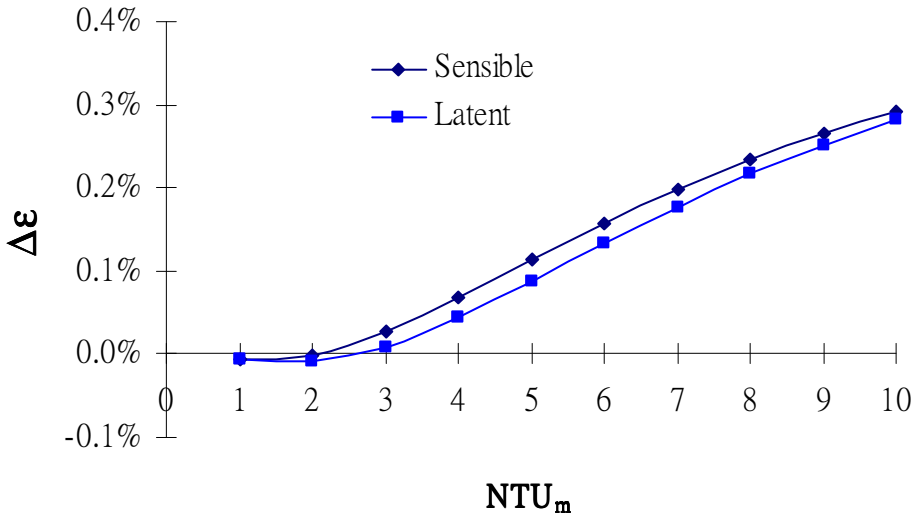

Figure 5.9 *Effect of including the axial dispersion as a function of* NTU_m *of the exchanger* $(\Delta\varepsilon = \varepsilon_{0,neglecting\ axial\ dispersion} - \varepsilon_{0,including\ axial\ dispersion})$.

Figure 5.9 shows that the difference of the effectiveness of the exchanger with and without axial dispersion is very small, less than 0.4% for $NTU_m = 10$. This indicates that the effect of axial dispersion can be neglected.

5.6 Summary

In this chapter, the sensitivity of various assumptions and property data on the numerically predicted effectiveness of the run-around system has been investigated and justified. It was found that the effectiveness of the run-around system is not sensitive to the heat and mass conductivities in the practical range of the values of them. The channel size of the air flow in the exchangers has greater impact on the performance of the run-around system than the channel size of the liquid flow. To get a better performance of the system, the channel size of the air flow should be kept at a practical small value. The pumping rate of the coupling liquid is an important parameter to be considered in the design of a run-around system, because the effectiveness of the system is very sensitive to the pumping rate of the coupling liquid. The thermal entry length of the exchangers can be neglected in a run-around heat and moisture recovery system. The axial conduction has very little effect on the performance of the run-around system and can be neglected.

Though many parameters and properties have been investigated in this chapter, there are still several more properties that should be addressed in future work to manufacture a practical and workable run-around heat and moisture recovery system. Since the performance is very sensitive to the channel size of the air flow, non-uniform channel size due to pressure variations within the exchanger or manufacturing variations

should be addressed in the future research. The effect of adding screens or other spacers in the channel should also be investigated.

Chapter 6

SUMMARY, CONCLUSIONS AND RECOMMENDATIONS

The main objectives of this thesis are to investigate the feasibility of a run-around heat and moisture recovery system made of semi-permeable membranes and to find the design characteristics of such a system. To achieve these objectives, a mathematical/numerical model was developed, validated for the case of no moisture transfer with accepted analytical solutions, and applied to investigate the optimal operating conditions of the single exchanger and the whole coupled system. This research demonstrates that the run-around heat and moisture recovery system is feasible and that high effectiveness (up to 60%) is possible for well designed systems. In this chapter, a summary of the work completed is presented followed by conclusions and recommendations for future work.

6.1 Summary

A numerical model of the single cross-flow plate heat exchanger and sensible run-around heat recovery system was developed and validated with analytical solutions and correlations from the literature in Chapter 2. Using the model, the optimal pumping rate for the coupling liquid was investigated and the temperature distribution in the heat exchanger was studied, which explains why the optimal pumping rates are different for the single exchanger and the run-around heat recovery system.

Moisture transfer and phase change were introduced into the model of single individual sensible heat exchangers and a coupled heat and moisture transfer model was developed for a heat and moisture exchanger in Chapter 3. The effect of phase change in the exchanger was studied and new parameters, the number of mass transfer units, NTU_m, and mass flow rate ratio, M_{Salt}/M_{Air}, were introduced to study the optimal operating conditions of a single heat and moisture exchanger.

In Chapter 4, two heat and moisture exchangers were coupled to form the model of a run-around heat and moisture recovery system. The performance of the system was studied under ARI summer and winter test conditions with both LiBr and LiCl salt solutions as the coupling fluid. Results were compared with the sensible system and optimal pumping rate of the coupling salt solution was investigated.

Sensitivity studies were performed in Chapter 5. In these sensitivity studies, the sensitivity of the effectiveness to the heat transfer coefficients, the channel size, the pumping rate of the coupling liquid, and the thermal entry length of the exchanger was investigated. Also, the axial conduction effect was addressed in this chapter.

6.2 Conclusions

The following conclusions can be made from the research presented in this thesis:

1. The run around heat and moisture recovery system envisioned and investigated in this thesis, which consists of two cross-flow heat and moisture exchangers constructed with a water vapour permeable membrane and coupled with an aqueous salt solution, is feasible. Overall sensible, latent and total effectiveness of 60% are possible for a well designed, practical system.

2. The numerical model for sensible heat exchangers and run-around heat recovery systems, developed in this thesis, provide reliable effectiveness data. This conclusion is based on a comparison on the numerical data and analytical data from the literature which shows differences of less than 1.1%.
3. For a single cross-flow plate heat exchanger, the temperature distribution in the exchanger is determined by number of transfer units, *NTU*, and heat capacity ratio, *Cr*, of the exchanger. The temperature distribution can be related to the effectiveness of the exchanger.
4. For a run-around heat recovery system with cross-flow plate heat exchangers, the optimum effectiveness occurs when the heat capacity ratio of the coupling fluid and the air are nearly equal ($C_L / C_A = 1$) for high value of *NTU* ($NTU \geq 10$). For lower values of *NTU* ($NTU < 10$), the optimal effectiveness shifts slightly from $C_L / C_A = 1$. The heat capacity of the coupling fluid should be kept in the range of $0.8C_A < C_L < 1.2C_A$ for the highest effectiveness and maximum heat transfer rate. This recommendation is a little different from the recommendation of $0.95C_A < C_L < 1.2C_A$ by London and Kays (1951).
5. The temperature and moisture content distributions in a single heat and moisture exchanger are complex. Because the heat and moisture transfer in the exchanger are coupled by the phase change associated with the moisture transfer, the moisture content distribution affect the temperature distribution in the exchanger and the effectiveness of the exchanger. Thus the factors that may affect the distribution of the temperature and moisture content in the exchanger and the effectiveness of the exchanger are the inlet temperature and humidity ratio of the air, *NTU* and

C_{Sol}/C_{Air}, NTU_m and M_{Sol}/M_{Air}, and the inlet temperature and concentration of the salt solution. Both the sensible and latent effectiveness increase as *NTU*, C_{Sol}/C_{Air}, NTU_m and M_{Sol}/M_{Air} increase for all combinations, except for sensible effectiveness and C_{Sol}/C_{Air}. In this case, the sensible effectiveness is a minimum for $C_{Sol}/C_{Air}=1$ and increases as C_{Sol}/C_{Air} increases or decreases from 1.

6. For ARI summer and winter test conditions, the maximum effectiveness of a run-around heat and moisture recovery system occurs approximately at $C_{Sol}/C_{Air}=3$, which is three times higher than the capacity ratio for a run-around heat recovery system in conclusion 4. This difference is due to the heat of phase change associated with the moisture transfer in these exchangers. For $C_{Sol}/C_{Air}>3$, the effectiveness of the system is neatly independent of C_{Sol}/C_{Air}.
7. The maximum effectiveness of a run-around heat and moisture recovery system occurs at $M_{Sol}/M_{Air}\approx 1$. Increasing M_{Sol}/M_{Air} between 0 and 1 increases the effectiveness significantly, but increasing M_{Sol}/M_{Air} above 1 does not have a large effect on the effectiveness. This mean that in the practical operation of the run-around system, the pumping rate of the coupling fluid should be controlled so that the mass flow rate of the pure salt in the fluid is equal to or slightly higher than the mass flow rate of dry air for maximum performance. The mass flow rate of the salt solution should reduced when the heat and moisture transfer rates need to be reduced during moderate outdoor conditions.

8. The effectiveness of the run-around heat and moisture recovery system is sensitive to the desiccant salt solution used, and the temperature and humidity of the supply and exhaust air streams.

6.3 Recommendations for Future Work

Though many topics were covered in this research, there are still many other topics that should be addressed in the future. In particularly, emphasis should be placed on constructing a real, workable run-around heat and moisture recovery system. The recommended future research work is listed below:

1. Although the model was partially verified with the sensitivity study and known analytical correlations for sensible heat transfer in the literature, it should be validated with experimental data in the future. The first step would be to test a single exchanger that is constructed in the laboratory and then a run-around system. The numerical results in the thesis should be used to guide the design and construction of the heat and moisture exchangers.
2. In this thesis, all the exchangers had uniform channel sizes (i.e., membrane spacing) and the same flow rate through each channel. In practice, however, ideally uniform channel sizes and flow rates are not possible, because of manufacturing limitations and pressure variations which may cause the plates to be deformed. A study on the effect of maldistributed fluid flows due to variations in the plate spacing on the performance of a run-around system is recommended.
3. In order to maintain uniform spacing between the membranes in the exchanger it is likely necessary to add a screen or other spacers. The effect of adding screens into the channel is not included in this study, but it should be addressed in future studies.

4. Investigation of frosting and fouling on the exchanger performance is recommended. The moisture transfer rate of the exchanger depends on the permeability of the membrane plates. Frosting and fouling may change the permeability of the membrane and should be investigated.
5. Only steady state data were presented in this thesis, because operating conditions in HVAC systems typically change slowly. However, it was found that it took a many iterations for the numerical model to determine the steady state solution for the run-around system. This may indicate a slow transient response of the heat and moisture exchangers or a slow convergence scheme, and should be studied further.
6. The effectiveness of the run-around heat and moisture recovery system depend on many dimensionless heat and moisture transfer parameters. It was found that the relationship between the effectiveness of the run-around system and the mass transfer parameters (number of mass transfer units, NTU_m, and mass flow rate ratio, M_{Salt} / M_{Air}) is quite different from relationship between the effectiveness and the heat transfer parameters (NTU and C_{Sol} / C_{Air}). Future work should aim to develop correlations between these parameters and the effectiveness of the run-around system.
7. In the research, it was found that the effectiveness of the run-around system was sensitive to the salt solution used. Investigation on systems using different salt solutions or the combination of different salt solutions is recommended.
8. Johnson et al. (1995) investigated the life-cycle cost (LCC) of a run-around heat recovery system. But the LCC for a run-around heat and moisture recovery system will be different from a sensible run-around system. Thus a LCC study for a run-

around heat and moisture recovery system is recommended because is may show unique possibilities and advantage.

REFERENCES

ANSI/ARI Standard 1060, 2001. *Standard for Rating Air-to-Air Exchangers for Energy Recovery Ventilation Equipment*, Air-Conditioning & Refrigeration Institute, Arlington.

Arpaci, V.S. and Larsen, P.S., 1984. *Convection Heat Transfer*, Prentice-Hall, Inc., New Jersey.

ASHRAE, 2001. *ASHRAE Handbook-Fundamentals*, American Society of Heating, Refrigerating, and Air-Conditioning Engineers, Atlanta.

ASHRAE, 2004. *ASHRAE Handbook-HVAC System and Equipment*, American Society of Heating, Refrigerating and Air Conditioning Engineers, Atlanta.

Bennett, I.J.D., Besant, R.W. and Schoenau, G.J., 1994a. Validation of a run-around heat recovery system model, *ASHRAE Transactions*, **100**(1), p 230-237.

Bennett, I.J.D., Besant, R.W., Schoenau, G.J. and Johnson, A.B., 1994b. Procedure for optimizing coils in a run-around heat exchanger system, *ASHRAE Transactions*, **100**(1), p 442-451.

Cisternas, L. A. and Lam, E. J., 1991. An Analytical Correlation for the Vapor Pressure of Aqueous and Non-aqueous Solutions of Single and Mixed Electrolytes. Part II. Application and Extension, *Fluid Phase Equilibrium*, **62**, p 11-27.

Forsyth, B.I. and Besant, R.W., 1988a. The design of a run-around heat recovery system, *ASHRAE Transactions*, **94**(2), p511-531.

Forsyth, B.I. and Besant, R.W., 1988b. The performance of a run-around heat recovery system using aqueous glycol as a coupling liquid, *ASHRAE Transactions*, **94** (2), p532-545.

Incropera, F. P.and Dewitt, D. P., 1996. *Fundamentals of Heat and Mass Transfer, 4th Edition*, John Wiley & Sons Inc., New York.

Johnson, A.B., Besant, R.W. and Schoenau, G.J., 1995. Design of multi-coil run-around heat exchanger systems for ventilation air heating and cooling, *ASHRAE Transactions*, **101**(2), p 967-978.

Kays, W.M. and Crawford, M.E., 1990. *Convective Heat and Mass Transfer, 3rd Edition,* McGraw-Hill, New York.

Kays, W.M. and London, A.L., 1984. *Compact Heat Exchangers, McGraw-Hill,* Toronto.

Kern, D.Q. and Kraus, A.D., 1972. *Extended Surface Heat Transfer,* McGraw-Hill, New York.

London, A.L. and Kays, W.M., 1951, The liquid-coupled indirect-transfer regenerator for gas-turbine plants, ASME Transactions, **73**.

Lou, X. and Roetzel, W., 1998. Theoretical investigation on cross-flow heat exchangers with axial dispersion in one fluid, *Revue Générale de Thermique*, **37**(3), p 223-233.

Mason, J.L., 1955. *Proc. Second U.S. Congr. Applied Mechanics,* ASME, **801**.

Mishra, M., Das, P.K. and Sarangi, S., 2004. Transient Behavior of Crossflow Heat Exchangers with Longitudinal Conduction and Axial Dispersion, *Journal of Heat Transfer,* ASME, **126**, p 425-433.

Niu, J.L. and Zhang, L.Z., 2001. Membrane-based Enthalpy Exchanger: Material considerations and clarification of moisture resistance, *Journal of Membrane Science,* **189**(2), p 179-191.

Shah, R. K., 1981. *Thermal Design Theory for Regenerators.* In *Heat Exchangers: Thermal-Hydraulic Fundamentals and Design*, ed. S. Kakaç, A.E. Bergles and F. Mayinger. Hemisphere, New York, p. 721-763.

Shah, R.K. and London, A.L., 1978. *Laminar Flow Forced Convection in Ducts,* Academic Press, New York.

Simonson, C.J. and Besant, R.W., 1997. Heat and moisture transfer in desiccant coated rotary energy exchangers: Part I - Numerical model. *Int. J. HVAC&R Research,* **3**(4), p325-350.

Simonson, C.J. and Besant, R.W., 1999. Energy wheel effectiveness: Part I - development of dimensionless groups, *International Journal of Heat and Mass Transfer,* **42**(12), p 2161-2170.

Simonson, C.J., 1998. *Heat and moisture transfer in energy wheels,* Ph. D. Thesis, University of Saskatchewan, Saskatoon, Canada.

Welty, J. R., Wicks, C. E., Wilson, R. E. and Rorrer, G., 2001. *Fundamentals of Momentum, Heat and Mass Transfer, 4th Edition,* John Wiley & Sons Inc., New York.

Zaytsev, I.D. and Aseyev, G.G., 1992. *Properties of Aqueous Solutions of Electrolytes*, CRC Press, Inc.

Zeng, Y.Y., 1990. *A study of the performance of run-around heat recovery system using aqueous glycol/air as the coupling fluid,* M.Sc thesis, University of Saskatchewan, Saskatoon, Canada.

Zeng, Y.Y., Besant, R.W. and Rezkallah, K.S., 1992. The effect of temperature-dependent properties on the performance of run-around heat recovery systems using aqueous-glycol coupling fluids, *ASHRAE Transactions*, **98**(1), p551-562.

Zhang, L.Z. and Niu, J.L., 2002. Effectiveness correlations for heat and moisture transfer processes in an enthalpy exchanger with membrane cores, *Journal of Heat Transfer*, ASME, **124** (5), p 922-929.

Appendix A Salt Solution Properties

This appendix contains the properties of the salt solutions required in the numerical model. These properties include: specific heat capacity, density, viscosity, and thermal conductivity.

Specific Heat Capacity:

The specific heat capacity of a multi-component solution can be calculated using the following correlation (Zaytsev and Aseyev, 1992):

$$Cp_{Sol} = Cp_w + \sum_i (B_{1i} + B_{2i} c_i^{'} + B_{3i} t + B_{4i} t^2) c_i \,. \qquad \text{(A-1)}$$

Where Cp_{Sol} is the specific heat capacity of a multi-component solution in J/(kg·K); Cp_w is the specific heat capacity of water in J/(kg·K); B_{ni} are coefficients; $c_i^{'}$ is the mass fraction of the i^{th} component in a binary isopiestic solution; and c_i is the mass fraction of the i^{th} component in a multi-component solution. The $c_i^{'}$ value is calculated by the following correlation:

$$c_i^{'} = E_i^{-1} \cdot \sum_j (E_j c_j)\,, \qquad \text{(A-2)}$$

where E_i are the empirical coefficients (Zaytsev and Aseyev, 1992).

The specific heat capacity of pure water can be calculated with the following correlation (Zaytsev and Aseyev, 1992):

$$Cp_w = 134225.4 \cdot (T/100)^{-6.5} + 3490 \cdot (T/100)^{0.14} \quad (0 \le t \le 100^{\circ}C). \qquad \text{(A-3)}$$

Density:

The density of a multi-component solution can be calculated using the modified Ezrokhi equation (Zaytsev and Aseyev, 1992):

$$\log \rho_{Sol} = \log \rho_w + \sum_i (A_i c_i). \qquad \text{(A-4)}$$

Where ρ_{Sol} is the density of multi-component solution in kg/m^3; ρ_w is the water density in kg/m^3; A_i are empirical coefficients; and c_i is the mass fraction of the component in the solution.

The density of water is calculated by the following correlation (Zaytsev and Aseyev, 1992):

$$\rho_w = 1000 - 0.062 \cdot t - 0.00355 \cdot t^2 \quad (0 \le t \le 100^{\circ}C). \qquad \text{(A-5)}$$

The coefficients A_i in (A-4) are calculated from the empirical equation (Zaytsev and Aseyev, 1992):

$$A_i = b_{0i} + b_{1i} \cdot t + b_{2i} \cdot t^2. \qquad \text{(A-6)}$$

Viscosity:

Dynamic viscosity coefficients can be calculated using the modified Ezrokhi equation (Zaytsev and Aseyev, 1992):

$$\lg \mu_{Sol} = \lg \mu_w + \sum_i (D_i c_i) . \quad \text{(A-7)}$$

Where μ_{Sol} is the viscosity of a multi-component solution in $Pa \cdot s$; μ_w is the viscosity of water in $Pa \cdot s$; D_i are coefficients; and c_i is the mass fraction of the component in the solution.

The viscosity of water can be determined from the Slott formula (Zaytsev and Aseyev, 1992):

$$\mu_w = 0.59849 \cdot (43.252 + t)^{-1.5423} \quad (0 \le t \le 100^{\circ}C). \quad \text{(A-8)}$$

The D_i coefficients in (A-7) are calculated using the empirical equation (Zaytsev and Aseyev, 1992):

$$D_i = d_{0i} + d_{1i} \cdot t + d_{2i} \cdot t^2 . \quad \text{(A-9)}$$

Thermal Conductivity:

Thermal conductivity of solutions can be calculated using the following correlation (Zaytsev and Aseyev, 1992):

$$k_{Sol} = k_w \cdot [1 - \sum_i (\beta_i c_i)] . \quad \text{(A-10)}$$

Where k_{Sol} is the thermal conductivity of the solution in $W/(m \cdot K)$; k_w is the thermal conductivity of water in $W/(m \cdot K)$; β_i are empirical coefficients; and c_i is the mass fraction of the component in the solution.

Thermal conductivity of water is approximated by a polynomial (Zaytsev and Aseyev, 1992):

$$k_w = 0.5545 + 0.00246 \cdot t - 0.00001184 \cdot t^2 \ (0 \le t \le 100^{\circ}C). \qquad \text{(A-11)}$$

Appendix B Development of Equations for Numerical Solution

A control volume method was employed to develop the governing equations for the heat and moisture exchanger using the coordinate system shown in Figure B.1.

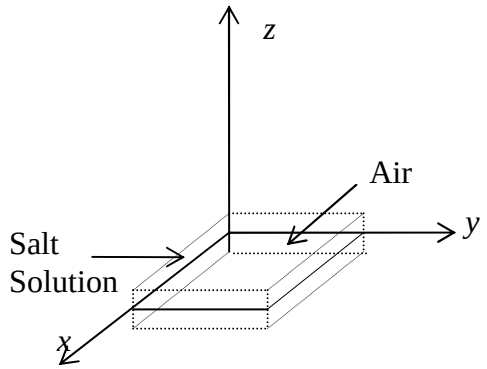

Figure B.1 *The coordinate system of the exchanger*

B.1 Mass Transfer Equation

B.1.1 Air Side

Cutting out a stationary infinitesimal control volume of unit depth within the air side of the heat exchanger as shown in Figure B.2 and assuming no mass diffusion in the *x* and *y* directions (diffusion only in the *z* direction) and steady state conditions, the mass transfer equation can be developed.

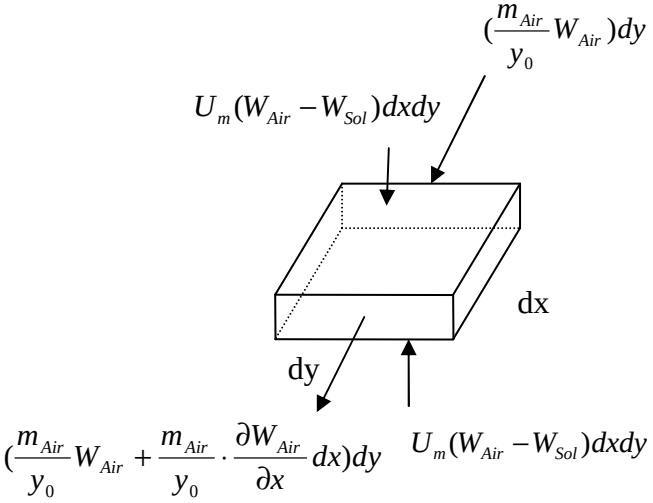

Figure B.2 *Control volume of the air flow*

The principle of conservation of mass for water gives:

$$(W_{Air}\frac{m_{Air}}{y_0})dy = 2U_m(W_{Air}-W_{Sol})dxdy + (W_{Air}\frac{m_{Air}}{y_0}+\frac{m_{Air}}{y_0}\cdot\frac{\partial W_{Air}}{\partial y}dx)dy \quad \text{(B-1)}$$

which can be simplified to:

$$\frac{2U_m y_0}{m_{Air}}(W_{Air}-W_{Sol}) = -\frac{\partial W_{Air}}{\partial x}. \quad \text{(B-2)}$$

Letting $y^* = y/y_0$ yields:

$$\frac{2U_m x_0 y_0}{m_{Air}}(W_{Air}-W_{Sol}) = -\frac{\partial W_{Air}}{\partial x^*}, \quad \text{(B-3)}$$

where

$$U_m = \left[\frac{1}{h_{m,Air}}+\frac{\delta}{k_m}+\frac{1}{h_{m,Sol}}\right]^{-1}, \quad \text{(B-4)}$$

$$W_{Sol} = f(X_{Sol}, T_{Sol}), \tag{B-5}$$

$$W_{Air} = \frac{massH_2O}{MassAIR} = f(\phi_{Air}, T_{Air}), \text{ and} \tag{B-6}$$

m_{Air} is the mass flow rate of the dry air through a single channel.

Introducing

$$2U_m x_0 y_0 / m_{Air} = NTU_{m,Air}, \tag{B-7}$$

gives:

$$NTU_{m,Air}(W_{Air} - W_{Sol}) = -\frac{\partial W_{Air}}{\partial x^*}. \tag{B-8}$$

B.1.2 Liquid Side

Cutting out a stationary infinitesimal control volume of unit depth within the liquid side of the heat exchanger as shown in Figure B.3 and assuming no mass diffusion in *x* and *y* directions (diffusion only in z direction) and steady state conditions, the mass transfer equations can be developed.

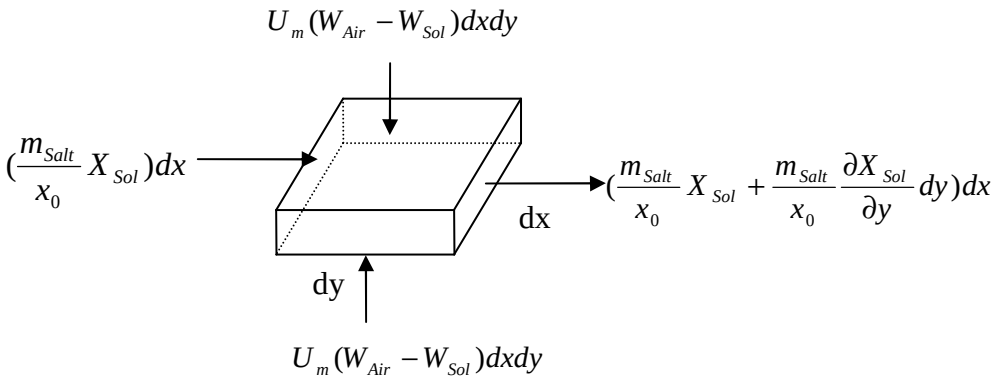

Figure B.3 *Control volume of the liquid flow*

The principle of conservation of mass for water gives:

$$\begin{aligned}&(X_{Sol}\frac{m_{Salt}}{x_0})dx + 2U_m(W_{Air} - W_{Sol})dxdy \\ &= (X_{Sol}\frac{m_{Salt}}{x_0} + \frac{m_{Salt}}{x_0}\cdot\frac{\partial X_{Sol}}{\partial y}dy)dx\end{aligned}, \tag{B-9}$$

which can be simplified to:

$$\frac{2U_m y_0}{m_{Salt}}(W_{Air} - W_{Sol}) = \frac{\partial X_{Sol}}{\partial x}. \tag{B-10}$$

Letting $x^* = x/x_0$ gives:

$$\frac{2U_m x_0 y_0}{m_{Salt}}(W_{Air} - W_{Sol}) = \frac{\partial X_{Sol}}{\partial y^*}, \tag{B-11}$$

where

$$U_m = \left[\frac{1}{h_{ms}} + \frac{\delta}{k_m} + \frac{1}{h_{me}}\right]^{-1}, \tag{B-12}$$

$$W_{Sol} = f(X_{Sol}, T_{Sol}), \tag{B-13}$$

$$X_{Sol} = \frac{MassH_2O}{MassPureSalt}, \text{ and} \tag{B-14}$$

m_{Salt} is the mass flow rate of the pure salt trough a single channel.

Introducing

$$2U_m x_0 y_0 / m_{Salt} = NTU_{m,Sol}, \tag{B-15}$$

gives:

$$NTU_{m,Sol}(W_{Air} - W_{Sol}) = \frac{\partial X_{Sol}}{\partial y^*}. \tag{B-16}$$

B.2 Energy Equations

The energy equations can be developed by following a similar analysis as presented in Section B.1 fro mass transfer. The resulting equations are:

$$NTU_{Air}\left(T_{Air}-T_{Sol}\right)=-\frac{\partial T_{Air}}{\partial x^{*}}\text{, and} \tag{B-17}$$

$$NTU_{Sol}\left(T_{Air}-T_{Sol}\right)=\frac{\partial T_{Sol}}{\partial y^{*}}-\frac{2U_{m}x_{0}y_{0}}{C_{Sol}}\left(W_{Air}-W_{Sol}\right)\cdot h_{fg}\text{.} \tag{B-18}$$

Where C_{Air} and C_{Sol} are heat capacities of the air and salt solution,

$$NTU_{Air}=\frac{Ux_{0}y_{0}}{C_{Air}}, \tag{B-19}$$

$$NTU_{Sol}=\frac{Ux_{0}y_{0}}{C_{Sol}}\text{, and} \tag{B-20}$$

$$U=\left[\frac{1}{h_{Sol}}+\frac{\delta}{k}+\frac{1}{h_{Air}}\right]^{-1}\text{.} \tag{B-21}$$

B.3 Governing Equations and Boundary Conditions

The final governing equations and boundary conditions for the air and liquid are summarized in this section.

B.3.1 Air side

$$2NTU_{m,Air}\left(W_{Air}-W_{Sol}\right)=-\frac{\partial W_{Air}}{\partial x^{*}}\text{, and} \tag{B-22}$$

$$2NTU_{Air}\left(T_{Air}-T_{Sol}\right)=-\frac{\partial T_{Air}}{\partial x^{*}}\text{.} \tag{B-23}$$

$$T_{Air}\left|_{x^{*}=0}=T_{Air,in}\right.\text{, and} \tag{B-24}$$

$$W_{Air}\left|_{x^{*}=0}=W_{Air,in}\right.\text{.} \tag{B-25}$$

B.3.2 Liquid side

$$2NTU_{m,Sol}(W_{Air} - W_{Sol}) = \frac{\partial X_{Sol}}{\partial y^*}, \text{ and} \tag{B-26}$$

$$2NTU_{Sol}\left(T_{Air} - T_{Sol}\right) = \frac{\partial T_{Sol}}{\partial y^*} - \frac{2U_m x_0 y_0}{C_{Sol}}(W_{Air} - W_{Sol}) \cdot h_{fg}. \tag{B-27}$$

$$T_{Sol}\,|_{y^*=0} = T_{Sol,in}, \text{ and} \tag{B-28}$$

$$X_{Sol}\,|_{y^*=0} = X_{Sol,in}. \tag{B-29}$$

B.4 Discretization of the Governing Equations:

The governing equations in Section B.3 are discretized using upwind differencing scheme and the results are listed below:

$$(2NTU_{m,Air} \cdot \Delta x^* + 1) \cdot W_{Air}^{n,i} - (2NTU_{m,Air} \cdot \Delta x^*) \cdot W_{Sol}^{n,i} - W_{Air}^{n,i-1} = 0, \tag{B-30}$$

$$(2NTU_{Air} \cdot \Delta x^* + 1) \cdot T_{Air}^{n,i} - (2NTU_{Air} \cdot \Delta x^*) \cdot T_{Sol}^{n,i} - T_{Air}^{n,i-1} = 0, \tag{B-31}$$

$$X_{Sol}^{n,i} - X_{Sol}^{n,i-1} - 2NTU_{m,Air} \cdot \Delta y^* \cdot (W_{Air}^{n,i} - W_{Sol}^{n,i}) = 0, \text{ and} \tag{B-32}$$

$$\begin{aligned}&(2NTU_{Sol} \cdot \Delta y^* + 1) \cdot T_{Sol}^{n,i} - (2NTU_{Air} \cdot \Delta y^*) \cdot T_{Air}^{n,i} \\ &- T_{Sol}^{n,i-1} - \frac{2U_m \cdot x_0 \cdot y_0}{C_{Sol}} \cdot h_{fg} \cdot \Delta y^* \cdot (W_{Air}^{n,i} - W_{Sol}^{n,i}) = 0.\end{aligned} \tag{B-33}$$

Appendix C The Computer Program Algorithm

This appendix shows the basic algorithm of the exchanger and run-around system computer models using flow charts. The actual program is included on a disk with this thesis. The computer program is written in C++ and run on Microsoft Visual Studio.NET 2003.

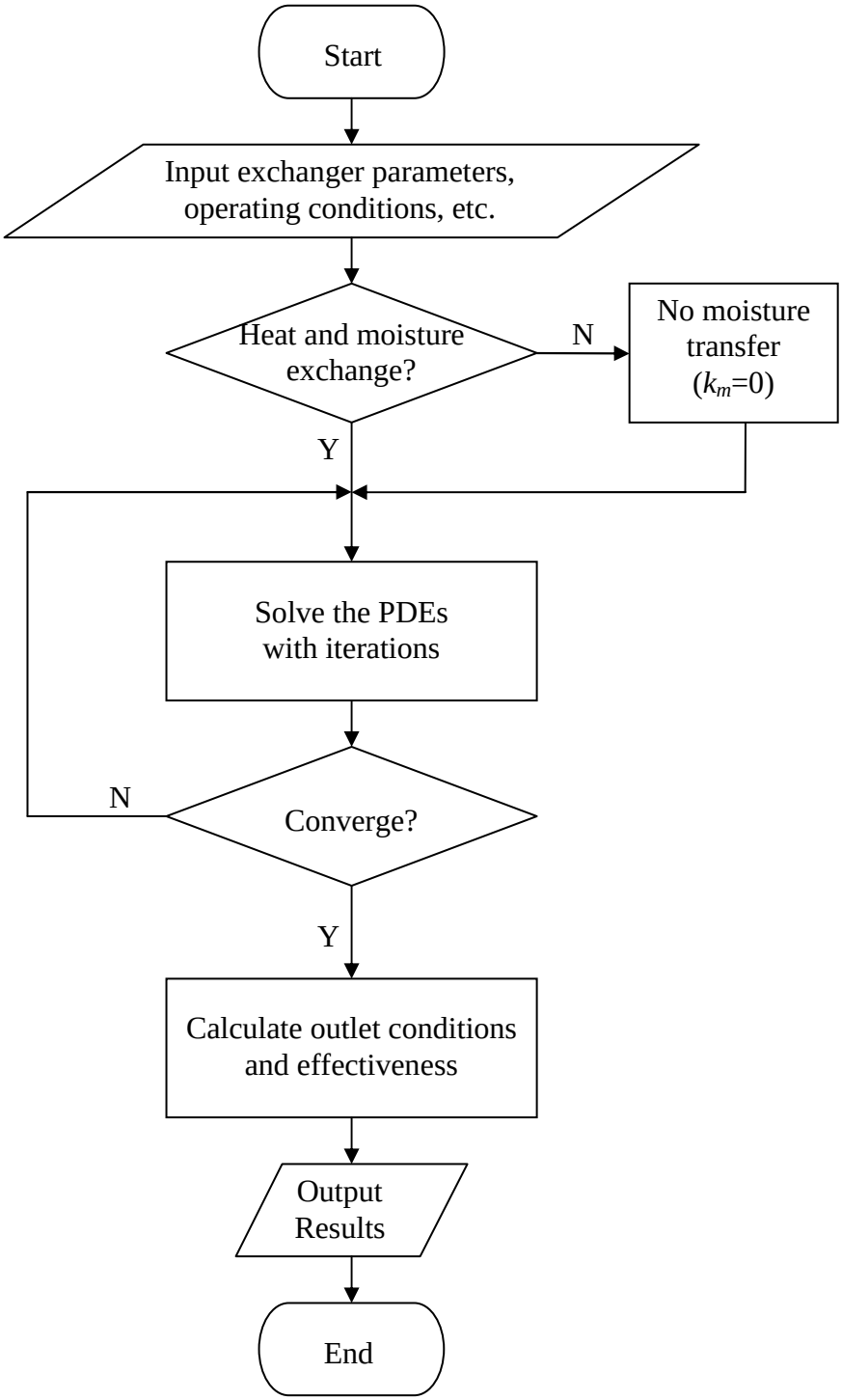

Figure C.1 Flowchart 1 shows the algorithm for a single exchanger.

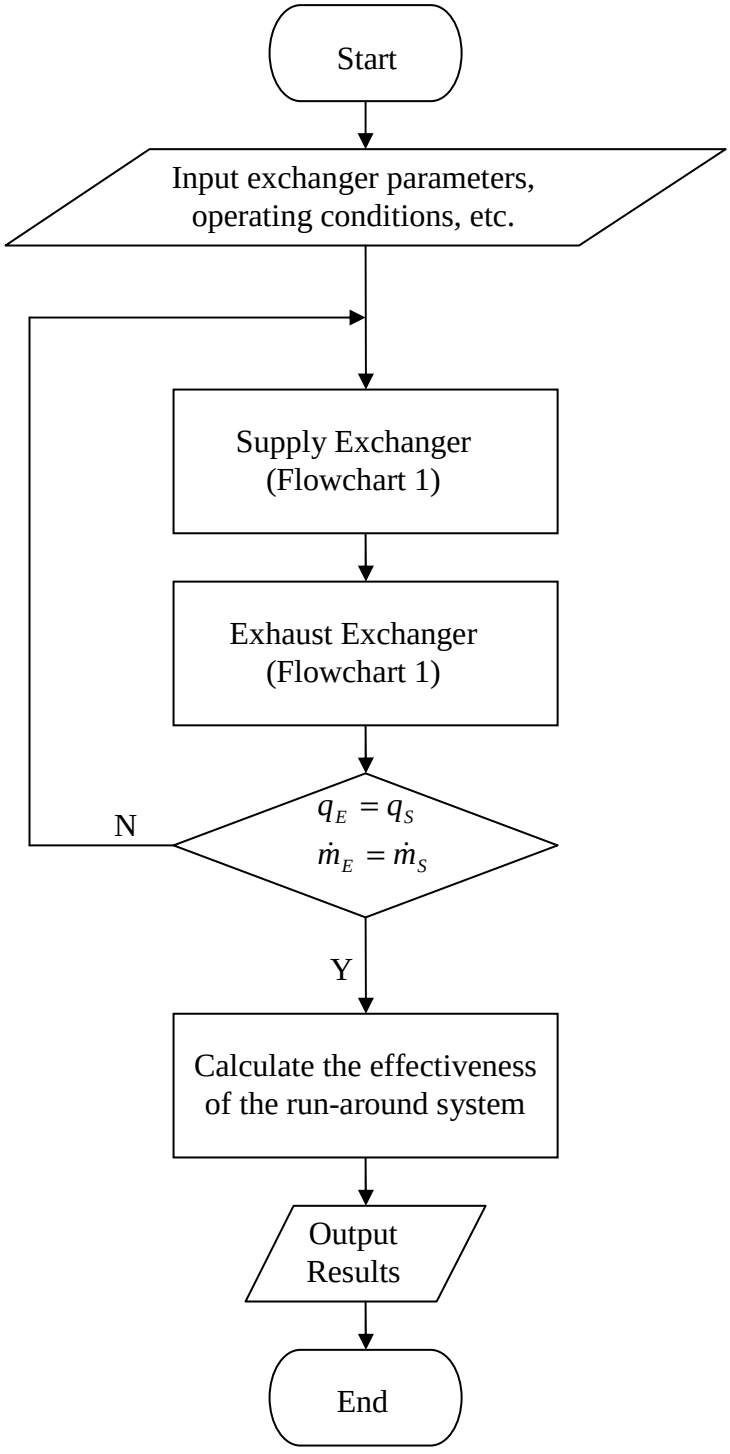

Figure C.2 Flowchart 2 shows the algorithm for the run-around system

Appendix D Temperature Distribution of the Fluids Within a Flow Channel of the Heat Exchanger

For the air flow, the bulk mean temperature is by definition:

$$T_A = \frac{1}{M_A Cp_A} \int_{-\frac{1}{2}d_A}^{\frac{1}{2}d_A} \rho u CpT \cdot dz \,, \tag{D-1}$$

where the mass flow rate of air per unit width of air flow:

$$M_A = \int_{-\frac{1}{2}d_A}^{\frac{1}{2}d_A} \rho u \cdot dz \,. \tag{D-2}$$

The mean value of air density at (x, y):

$$\rho_A = \frac{1}{u_A d_A} \int_{-\frac{1}{2}d_A}^{\frac{1}{2}d_A} \rho u \cdot dz \,. \tag{D-3}$$

If we assume constant properties of the air flow, then Cp and ρ are constant everywhere in the air flow for all values of $0 < x < x_0$ and $0 < y < y_0$. Then we can calculate the mean bulk velocity as:

$$u_A = \frac{1}{\rho_A d_A} \int_{-\frac{1}{2}d_A}^{\frac{1}{2}d_A} \rho u \cdot dz \,. \tag{D-4}$$

If $\mu =$ constant and for fully developed flow (Arpaci and Larsen, 1984), then:

$$u = \frac{3}{2} u_A \left[1 - \left(\frac{z}{\frac{1}{2} d_A} \right) \right]. \tag{D-5}$$

When T_W = wall temperature of the heat exchanger at (*x*, *y*), T_A = bulk mean temperature of the air flow at (*x*, *y*), and $\eta = \frac{z}{\frac{1}{2}d_A}$, then for fully developed flow (Arpaci and Larsen, 1984):

$$\frac{T_W - T}{T_W - T_A} = \frac{35}{136}(5 - 6\eta^2 + \eta^4). \tag{D-6}$$

Therefore, we get the temperature distribution in each air channel:

$$T = T_W + (T_A - T_W)\frac{35}{136}(5 - 6\eta^2 + \eta^4). \tag{D-7}$$

For constant heat flux from air to wall,

$$q_W = h_A(T_A - T_W) = const. \tag{D-8}$$

For constant h_A, then $T_A - T_W = \frac{q_W}{h_A}$, and also the Nusselt number based on hydraulic diameter ($D_h = 2d_A$ for air),

$$Nu = \frac{4(35)}{17} \approx 8.24. \tag{D-10}$$

On the liquid side, we will have a similar set of equations, i.e. for fully developed laminar flow, temperature distribution in each liquid channel of the heat exchanger:

$$T = T_W + (T_L - T_W)\frac{35}{136}(5 - 6\xi^2 + \xi^4), \tag{D-11}$$

where $\xi = \frac{z}{\frac{1}{2}d_L}$, T_L = bulk mean temperature of the liquid flow.

Also for $q_W = const.$, if knowing $T_A(x, y)$ and $T_L(x, y)$ from the numerical solution, then $T_W(x, y)$ is

$$T_W = T_A - \frac{q_W}{h_A} = T_L + \frac{q_W}{h_L}. \qquad \text{(D-12)}$$

Appendix E Analytical Solution for a Single Heat Exchanger

Many researchers have determined the effectiveness values for cross flow heat exchanger with both fluids unmixed. Mason (1955) obtained a solution in the form of an infinite series by employing the Laplace transformation. Mason's solution converges more rapidly then those of previous investigators and is more readily adaptable to the computer. The coordinate system used by Mason is shown in Figure D.1. The plate has dimensions x_0 and y_0, and the coordinate directions are designated as x^* and y^*. The temperature of the cold and hot fluids are functions of the length coordinates and can be represented by $t(x^*, y^*)$ and $T(x^*, y^*)$, respectively.

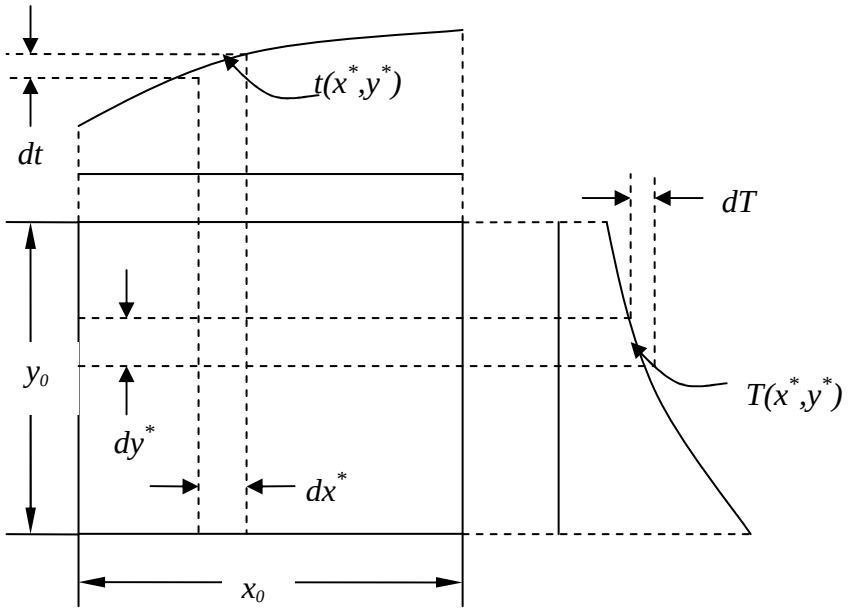

Figure E.1 *Coordinate system for two fluids in cross flow*

At any point in the exchanger, a heat balance can be written as:

$$dq = U(T-t)dx^* dy^*, \tag{E-1}$$

across the elements x_0 and y_0 units in length the energy balances yield

$$dq = -\frac{M \cdot Cp}{x_0} \cdot \frac{\partial T}{\partial y^*} \cdot dx^* dy^*, \text{ and} \tag{E-2}$$

$$dq = \frac{m \cdot c_p}{y_0} \cdot \frac{\partial t}{\partial x^*} \cdot dx^* dy^*. \tag{E-3}$$

Combining equations (E-1) and (E-2) and then equations (E-1) and (E-3) gives

$$\frac{U \cdot x_0}{M \cdot Cp}(T-t) = -\frac{\partial T}{\partial y^*}, \text{ and} \tag{E-4}$$

$$\frac{U \cdot y_0}{m \cdot c_p}(T-t) = \frac{\partial t}{\partial x^*}. \tag{E-5}$$

Differentiating equations (E-4) and (E-5) with respect to x^* and y^* and adding them gives:

$$\frac{U \cdot x_0}{M \cdot Cp} \cdot \frac{\partial (T-t)}{\partial x^*} + \frac{U \cdot y_0}{m \cdot c_p} \cdot \frac{\partial (T-t)}{\partial y^*} = -\frac{\partial^2 (T-t)}{\partial x^* \partial y^*} \tag{E-6}$$

Letting $T - t = \theta^*$, $x = x^* / x_0$, $y = y^* / y_0$ and substituting in equation (E-6) yields:

$$\frac{U \cdot x_0 \cdot y_0}{M \cdot Cp} \cdot \frac{\partial \theta^*}{\partial x} + \frac{U \cdot x_0 \cdot y_0}{m \cdot c_p} \cdot \frac{\partial \theta^*}{\partial y} = -\frac{\partial^2 \theta^*}{\partial x \partial y} \tag{E-7}$$

With $\frac{U \cdot x_0 \cdot y_0}{M \cdot Cp} = NTU_a$, $\frac{U \cdot x_0 \cdot y_0}{m \cdot c_p} = NTU_b$, $\theta_0^* = \theta^*(x^* = 0, y^* = 0)$, and $\theta = \theta^* / \theta_0^*$,

Equation (E-7) becomes

$$NTU_a \cdot \frac{\partial \theta}{\partial x} + NTU_b \cdot \frac{\partial \theta}{\partial y} + \frac{\partial^2 \theta}{\partial x \partial y} = 0. \tag{E-8}$$

If the values of NTU_a and NTU_b are constant, Equation (E-8) can be solved by taking the Laplace transform first with respect to *x* and then with respect to *y*. Let the Laplace transforms be designated as

$$\ell_x[\theta(x,y)] = g_x(r,y), \tag{E-9}$$

$$\ell_y[\theta(x,y)] = g_y(x,s), \text{ and} \tag{E-10}$$

$$\ell_x\ell_y[\theta(x,y)] = g_{xy}(r,s), \tag{E-11}$$

where *r* and *s* are the transform variables.

Transforming Equation (E-8) term by term, using the relationships for the transform of a derivative, gives, for the first term:

$$\ell_x\ell_y[NTU_a \frac{\partial\theta}{\partial x}] = NTU_a[rg_{xy}(r,s) - g_y(0,s)], \tag{E-12}$$

for the second term

$$\ell_x\ell_y[NTU_b \frac{\partial\theta}{\partial y}] = NTU_b[sg_{xy}(r,s) - g_x(r,0)], \tag{E-13}$$

and for the third term

$$\ell_x\ell_y \frac{\partial\theta}{\partial x\partial y} = rsg_{xy}(r,s) - rg_x(r,0) - sg_y(0,s) + \theta(0,0). \tag{E-14}$$

Adding the forgoing as required by Equation (E-8), using $\theta(0,0) = 1$, and rearranging gives:

$$\begin{aligned}&(NTU_a r + NTU_b s + rs)\cdot g_{xy}(r,s)\\ &= (NTU_a + s)\cdot g_y(0,s) + (NTU_b + r)\cdot g_x(r,0) - 1\end{aligned} \tag{E-15}$$

The fluids enter the exchanger at temperature T_1 and t_1. The boundary conditions are obtained from the partial differential equations that are written for each inlet edge of the exchanger.

$$NTU_b \cdot \theta(x,0) = -\frac{\partial}{\partial x}\theta(x,0), \text{ and} \tag{E-16}$$

$$NTU_a \cdot \theta(0,y) = -\frac{\partial}{\partial y}\theta(0,y). \tag{E-17}$$

Again employing the Laplace transform to Equation (E-10) gives

$$NTU_b \cdot g_x(r,0) = -rg_x(r,0) + \theta(0,0) \tag{E-19}$$

and with $\theta(0,0) = 1$

$$g_x(r,0) = \frac{1}{r + NTU_b}. \tag{E-20}$$

A similar result is obtained for Equation (E-11):

$$g_y(0,s) = \frac{1}{s + NTU_a}. \tag{E-21}$$

Equations (E-12) and (E-13) can be substituted into Equation (E-9):

$$(NTU_a r + NTU_b s + rs) \cdot g_{xy}(r,s) = 1 \tag{E-22}$$

Solving for $g_{xy}(r,s)$ gives:

$$g_{xy}(r,s) = \frac{1}{NTU_a r + NTU_b s + rs}. \tag{E-23}$$

The inverse transform of Equation (E-15) is taken with respect to *r* first:

$$g_y(x,s) = \ell_y[\theta(x,y)] = \frac{1}{NTU_a + s} e^{-NTU_b sx/(NTU_a + s)}. \tag{E-24}$$

The exponential containing *s* can be expanded into an infinite series. Inverse transformation term by term then gives

$$\theta(x,y) = e^{-(NTU_a y + NTU_b x)} \sum_{n=0}^{\infty} \left[\frac{NTU_a NTU_b xy}{(n!)^2}\right]^n. \tag{E-25}$$